National Library of Canada
Bibliothèque nationale du Canada

Canadian Theses Service
Service des thèses canadiennes

Ottawa, Canada
K1A 0N4

NOTICE

The quality of this microform is heavily dependent upon the quality of the original thesis submitted for microfilming. Every effort has been made to ensure the highest quality of reproduction possible.

If pages are missing, contact the university which granted the degree.

Some pages may have indistinct print especially if the original pages were typed with a poor typewriter ribbon or if the university sent us an inferior photocopy.

Previously copyrighted materials (journal articles, published tests, etc.) are not filmed.

Reproduction in full or in part of this microform is governed by the Canadian Copyright Act, R.S.C. 1970, c. C-30.

AVIS

La qualité de cette microforme dépend grandement de la qualité de la thèse soumise au microfilmage. Nous avons tout fait pour assurer une qualité supérieure de reproduction.

S'il manque des pages, veuillez communiquer avec l'université qui a conféré le grade.

La qualité d'impression de certaines pages peut laisser à désirer, surtout si les pages originales ont été dactylographiées à l'aide d'un ruban usé ou si l'université nous a fait parvenir une photocopie de qualité inférieure.

Les documents qui font déjà l'objet d'un droit d'auteur (articles de revue, tests publiés, etc.) ne sont pas microfilmés.

La reproduction, même partielle, de cette microforme est soumise à la Loi canadienne sur le droit d'auteur, SRC 1970, c. C-30.

NL-339 (r. 88/04)

Canada

THE UNIVERSITY OF ALBERTA

Geology and Geochemistry Of The Venus Au-Ag-Pb-Zn Vein Deposit, Yukon Territory

by

Lori A. Walton

(C)

A THESIS

SUBMITTED TO THE FACULTY OF GRADUATE STUDIES AND RESEARCH

IN PARTIAL FULFILMENT OF THE REQUIREMENTS FOR THE DEGREE

OF Master of Science

Department of Geology

Edmonton, Alberta

Fall, 1987

Permission has been granted to the National Library of Canada to microfilm this thesis and to lend or sell copies of the film.

The author (copyright owner) has reserved other publication rights, and neither the thesis nor extensive extracts from it may be printed or otherwise reproduced without his/her written permission.

L'autorisation a été accordée à la Bibliothèque nationale du Canada de microfilmer cette thèse et de prêter ou de vendre des exemplaires du film.

L'auteur (titulaire du droit d'auteur) se réserve les autres droits de publication; ni la thèse ni de longs extraits de celle-ci ne doivent être imprimés ou autrement reproduits sans son autorisation écrite.

ISBN 0-315-40935-5

THE UNIVERSITY OF ALBERTA

RELEASE FORM

NAME OF AUTHOR Lori A. Walton

TITLE OF THESIS Geology and Geochemistry Of The Venus Au-Ag-Pb-Zn Vein Deposit, Yukon Territory

DEGREE FOR WHICH THESIS WAS PRESENTED Master of Science

YEAR THIS DEGREE GRANTED Fall, 1987

Permission is hereby granted to THE UNIVERSITY OF ALBERTA LIBRARY to reproduce single copies of this thesis and to lend or sell such copies for private, scholarly or scientific research purposes only.

The author reserves other publication rights, and neither the thesis nor extensive extracts from it may be printed or otherwise reproduced without the author's written permission.

(SIGNED) L. A. Walton

PERMANENT ADDRESS:

#801 10025 - 113 St

Edmonton, Alta.

T5K 2K8 CANADA

DATED May 7 1987

THE UNIVERSITY OF ALBERTA

FACULTY OF GRADUATE STUDIES AND RESEARCH

The undersigned certify that they have read, and recommend to the Faculty of Graduate Studies and Research, for acceptance, a thesis entitled Geology and Geochemistry Of The Venus Au-Ag-Pb-Zn Vein Deposit, Yukon Territory submitted by Lori A. Walton in partial fulfilment of the requirements for the degree of Master of Science.

.....

Supervisor

.....

.....

.....

Date May 1, 87

Dedication

This thesis is dedicated to my parents,

Janet and Edward Walton.

Abstract

The Venus Au-Ag-Pb-Zn vein is hosted in Late Cretaceous, intermediate volcanic rocks of the Mount Nansen Group. The vein consists of quartz, arsenopyrite and pyrite, with lesser amounts of sphalerite and galena. The andesitic to felsic wallrocks are hydrothermally altered to a sericite-carbonate-quartz-pyrite assemblage, with local pods of intense clay alteration.

The paragenesis can be divided into two mineralogically distinct stages: Stage I - early quartz, arsenopyrite and pyrite, and Stage II - later quartz, sphalerite, galena, and gold. Gold and galena occur together as fracture fillings or replacements in earlier deposited arsenopyrite and pyrite. Steeply plunging ore shoots, which are not visually apparent, comprise 20% of the vein and typically contain both Stage I and Stage II mineralization.

Stage I fluid inclusions are characterized by homogenization temperatures of 290°C or greater, moderate CO_2 (17 mole percent), and low salinities (3 to 4 weight percent NaCl equivalent). Relative to Stage I, Stage II fluid inclusions are cooler (260°C), CO_2 depleted and may have been more saline (up to 7.5 weight percent NaCl equivalent). Variable H_2O-CO_2 ratios indicate that sporadic effervescence occurred during Stage II. Influx of Stage II fluid and subsequent base metal-gold precipitation was restricted to open parts of the vein.

Sulphide precipitation and loss of H_2S from sporadic effervescence generated a sulphide deficiency in the fluid, and subsequent breakdown of $Au(HS)_2^-$ complexes. Gold precipitated with galena in the last stages of mineral deposition. Preferential precipitation of gold and galena near pre-existing arsenopyrite and pyrite may be due to electrochemical interaction between sulphide grain surfaces and the hydrothermal ore fluid.

An enrichment of ^{18}O in the Venus quartz depositing fluid (+10 to +14‰), and preliminary δD data (-159‰) suggest a meteoric-hydrothermal origin for the fluid. Pressure estimates from fluid inclusions average between 1000 to 1300 bars, indicating a depth of formation of at least 3 km. The high $\delta^{18}O$ values are probably a function of extensive water-rock interaction at high temperatures and depths.

Acknowledgements

I would like to thank my supervisor, Bruce Nesbitt, for his suggestions, enthusiasm, and perpetual optimism throughout this study. Financial support from the Geology Section of the Department of Indian and Northern Development and from a teaching assistantship provided by the Department of Geology is gratefully acknowledged. Jim Morin is thanked for suggesting the topic. Teresa Potter is thanked for her field assistance.

This project would not have been possible without the support of United Keno Hill Mines Ltd. They provided accomodation at the minesite, allowed unlimited access to the mine, paid laboratory costs, and allowed me to pillage company reports, files and maps. Dennis Prince, in particular, is thanked for his numerous helpful suggestions and for providing summer employment. Mary Armstrong, Bob Stirling, and Holly Plaskett are thanked for their help and encouragement. Donna Hudgeon is thanked for her friendship and support.

Karlis Muehlenbachs is gratefully acknowledged for instigating an interest in isotopes, and for providing much appreciated encouragement and advice. Karlis is also thanked for allowing access to his isotope lab, office, and, in particular, his Macintosh computer. Aileen Freschauf is thanked for her encouragement and support. Jim Murowchick deserves special thanks for his many useful discussions and instruction in fluid inclusion and isotope lab techniques. Marc Dubord is thanked for making my polished mounts and fluid incluison plates. Mike Dufresne deserves special recognition for his long hours spent solving my textform problems. The staff of the Geology Department is thanked for their help and encouragement.

I would like to thank the inhabitants (past and present) of the Economic Geology Research Unit-Chris Sayer, Darrell Fluet, Paul Lhotka, Mike Dufresne, Pierre Maheux, Doug Rucker, Greg Lynch, and Steve Swatton-for their help and friendship. I am indebted to Cheryl Squair for her support and friendship.

I am grateful to a number of people outside the University for their assistance. Barbara Bannerman and Babe and Bruce Laidlaw are thanked for their financial help and encouragement. Jack and Audrey Bannerman are thanked for their support and for letting me

use the 'Deerhunter'. John Biczok deserves very special thanks for his useful suggestions, support, encouragement and long distance phone calls. And finally, a very special thanks to my parents, Janet and Edward Walton, for putting up with me and my chaotic schedule throughout this period.

Table of Contents

Chapter — Page

I. INTRODUCTION 1

A. Purpose of Study 1

B. Location, Access, and Physiography 2

C. Previous Work 4

D. History of the Venus Mine 5

II. REGIONAL GEOLOGY 7

A. Introduction 7

B. Tectonic Setting 7

C. Regional Stratigraphy and Structure 9

Cache Creek Group 9

Lewes River Group 11

Laberge Group 12

Granitic Rocks 12

Mt. Nansen Group 12

Regional Structure 15

D. Regional Precious Metal Vein Mineralization 15

III. LOCAL GEOLOGY 17

A. Introduction 17

B. General Geology and Structure 17

Description of Volcanic Rock Types 17

Structure of the Montana Mountain Volcanic Complex 20

Metamorphism and Alteration 21

C. Evolution of the Montana Mountain Volcanic Complex 22

D. Geological Setting of the Venus Vein 22

E. Precious Metal Veins on Montana Mountain 23

IV. VEIN STRUCTURE, MINERALOGY AND PARAGENESIS 24

A. Introduction 24
B. Vein Structure 24
C. Vein Texture and Mineralogy 25
Ore Shoots 26
D. Wallrock Alteration 29
Oxidation Zone 30
E. Sulphide Petrography 30
Arsenopyrite 30
Pyrite 33
Sphalerite 33
Galena 33
Gold 34
F. Paragenetic Sequence and Discussion 40
V. FLUID INCLUSIONS 43
A. Introduction 43
B. Analytical Technique 45
C. Inclusion Petrography 46
Types of Inclusions 55
D. Phase Changes at Low Temperatures 59
Eutectic Temperature 59
Final Melting Temperature of CO_2 59
Final Melting Temperature for CO_2 Clathrate 61
Final Melting Temperature of Ice 65
E. Heating Measurements 66
F. Fluid Composition and Bulk Density 73
G. Discussion 74
Evidence for Phase Separation 74

Pressure and Depth Estimates 76
H. Summary 81
VI. STABLE ISOTOPE STUDY 82
A. Introduction 82
B. Analytical Technique 82
Oxygen Isotopes 82
Hydrogen Isotopes 83
C. Results of Isotopic Analysis 83
D. Discussion 87
Regional Considerations 93
Summary 93
VII. DISCUSSION AND MODEL 94
A. Summary 94
B. Environment of Ore Deposition 94
C. Controls on Ore Shoot Formation 96
Location of Ore Shoots 96
Gold Precipitation 97
D. Model for Ore Deposition 99
E. Regional Considerations 102
References 104
Appendix 1 111
Appendix 2 112
Appendix 3 113

List of Tables

Table		Page
1.	Table of Formations in south-central Yukon (modified after Roots, 1982).	10
2.	Oxidation zone minerals.	31
3.	Minor opaque minerals (<1%) found in the Venus vein.	32
4.	Occurrences of gold grains (>5μm).	35
5.	Fluid inclusion measurements.	54
6.	Fluid inclusion compositions, bulk densities, and pressures.	72
7.	Average fluid inclusion composition.	75
8.	Oxygen isotope data.	85

List of Figures

Figure — Page

1. Major tectonic elements of southwestern Yukon and northwestern British Colombia, and location of the Montana Mountain Volcanic Complex. 3
2. Regional geology of southwestern Yukon and northwestern British Columbia. 8
3. Geology of the Montana Mountain volcanic complex (modified after Roots, 1982). 18
4. Idealized paragenetic sequence of the Venus vein. 41
5. Types of fluid inclusions. 56
6. Modes of occurrence for fluid inclusions. 57
7. Te and Tmice temperatures from Type 1 inclusions. 60
8. $TmCO_2$ and TmClath temperatures from Type 2 inclusions. 62
9. Salinity (weight percent NaCl equivalent) estimates for Type 1 and Type 2 inclusions. 64
10. CO_2 homogenization temperatures. F=Fades 67
11. Homogenization and decrepitation temperatures. 68
12. Mole % CO_2 vs. Th 77
13. Pressure vs. mole % CO_2 (modified after Takenouchi and Kennedy (1964) and Parry (1986). 78
14. Results of Venus isotope study on a plot of δD vs. $\delta^{18}O$ 88
15. Changes in fluid chemistry and mineralogy with time at the Venus deposit. 95
16. Idealized model of ore shoot formation. 101

List of Plates

Plate — Page

1. The Venus vein (2700' level) showing a quartz core and asymmetrical arsenopyrite-pyrite bands. 27

2. A high grade ore-shoot located on the 2850' level (looking at the north face before drift extension); a) Arsenopyrite-pyrite-quartz (22 cm wide) containing 1.6 oz./ton Au and 9.1 oz./ton Ag. b) Sphalerite-galena-quartz (30 cm wide) containing 0.14 oz./ton Au and 40.10 oz./ton Ag. c) Arsenopyrite-pyrite-quartz (35 cm wide) containing 0.49 oz./ton Au and 13.6 oz./ton Ag. 28

3. Polished block L-84-30 from the 2850' level. Gold and minor galena have infilled microfractures in, and replaced arsenopyrite. 36

4. Polished block L-84-21 from the 2850' level. Galena and gold have replaced arsenopyrite. Gold also occurs at the boundary between quartz and arsenopyrite. 37

5. Polished block L-83-16 from the 2700' level. Galena and gold have infilled corrosion openings in arsenopyrite. 38

6. Polished block L-84-208 from the 2800' level. Tetrahedrite and gold have infilled fractures in arsenopyrite. Gold has replaced arsenopyrite and pyrite. 39

I. INTRODUCTION

A. Purpose of Study

The Venus Au-Ag-Pb-Zn vein is located 120 km south of Whitehorse, Yukon, in a region of late Cretaceous volcanic rocks known as the Montana Mountain volcanic complex (Roots, 1982). The vein is a simple fissure-filling containing massive to crystalline quartz and lesser amounts of arsenopyrite, pyrite, sphalerite and galena. Arsenopyrite and pyrite, the most abundant sulphides, occur in crude bands or lenses on the outer edges of the vein. Sphalerite and galena occur sporadically, usually in pods near the center of the vein or infilling interstitial spaces between quartz crystals.

Gold mineralization at Venus is concentrated in steeply plunging ore shoots within the vein structure. Ore shoots are those parts of the Venus vein that contain a higher concentration of gold and silver relative to the rest of the vein. Ore shoots comprise approximately 20% of the Venus vein (depending on the current price of precious metals) and are defined solely on the basis of assay data.

The purpose of this study was to examine the mineralogy and fluid inclusions in the deposit, and establish physical and chemical controls on the distribution of ore shoots within the Venus vein structure. The major objectives of the study were as follows:

1. Determine petrographically the relationship of gold to the other mineral phases - especially arsenopyrite, pyrite, sphalerite and galena.
2. Determine the composition, temperature and pressure of the mineralizing fluid.
3. Consolidate research data into a model for ore shoot formation.

Fieldwork was carried out over a six week period in the summer of 1984. Each of the five levels in the mine was systematically sampled. The mineralogy, structure, texture,

alteration and other features were noted at each sample site. When the vein could be subdivided on the basis of mineralogy, texture, or some other feature, separate samples were taken from each zone. A number of surface traverses were made to investigate and sample the volcanic host rocks and the outcrop of Venus vein. Visual comparisons with other vein systems in southwestern Yukon and northwestern British Columbia were made during regional exploration.

The mineralogy and paragenesis of vein mineralization were determined using thin sections, polished mounts and polished thin sections. The temperature, pressure and composition of the mineralizing fluids were determined by fluid inclusion analysis of vein quartz and sphalerite. The isotopic nature of the mineralizing fluid was determined by examination of $\delta^{18}O$ and, to a lesser extent, δD values of vein quartz.

B. Location, Access, and Physiography

The Venus deposit, located 120 km by road south of Whitehorse, is hosted by Mount Nansen Group volcanic rocks (Figure 1). In this study, "Montana Mountain area" refers to the region north of the Yukon-British Columbia border and bounded by Bennett Lake on the west and Windy Arm of Tagish Lake on the east. "Montana Mountain volcanic complex" refers to Mt. Nansen Group volcanics, which dominate the region. The Venus mine is situated at latitude 60°01' N and longitude 134°38' W (N.T.S. mapsheet 105D/2) on a steep, southeast facing slope overlooking Windy Arm (elevation 655 m). Access to the minesite is by Klondike highway No. 2.

The Montana Mountain area is an upland plateau containing abrupt changes in topography caused by stream cuts and cirques. Lower slopes show signs of continental glaciation, but upper regions are covered with glacial till. Bedrock exposure is largely confined to stream cuts and steep cliffs.

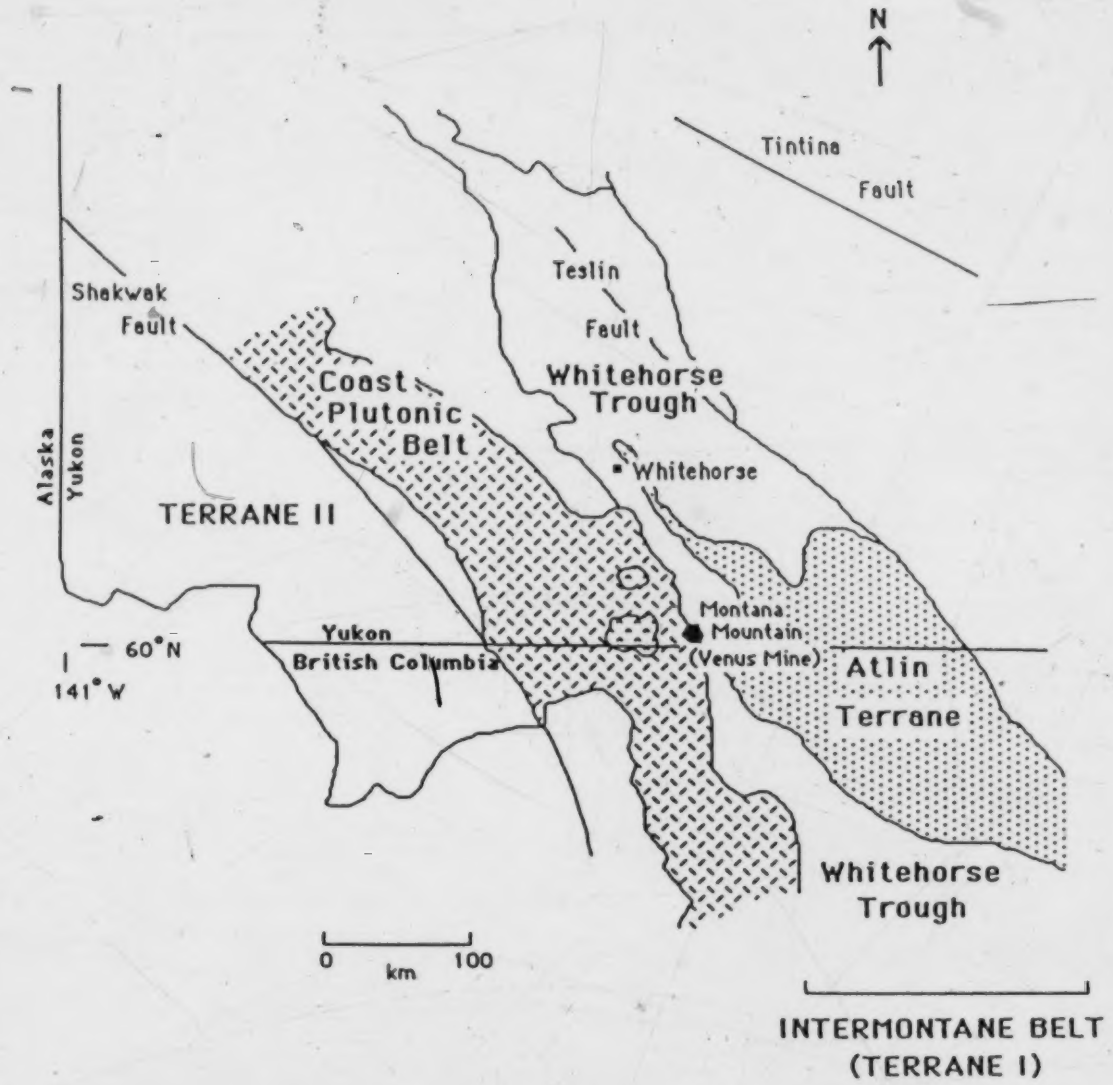

Figure 1. Major tectonic elements of southwestern Yukon and northwestern British Columbia, and location of the Montana Mountain Volcanic Complex.

C. Previous Work

The first published descriptions of the Venus vein were written in the early 1900's by government geologists. McConnell (1906) and Cairnes (1907, 1908, 1917) describe the location, general geology, mine geology and mine development for several of the veins on Montana Mountain, including Venus. A description of precious metal veins in the Wheaton River district and the Windy Arm district is provided by MacLean (1914). An early report on the geology of the Whitehorse area was written by Cockfield and Bell (1929). Wheeler (1961) performed reconnaissance mapping of the Whitehorse mapsheet, and identified major rock units and contacts.

In the late 1960's and early 1970's, renewed activity at Venus by Venus Mines Ltd., generated additional publications. Private company reports (MacDonald, 1967; MacDonald, 1971; Scott, 1974) and government reports (Findlay, 1967, 1969a, 1969b) contain descriptions of the geology of the deposit and mine development during this time period.

In the 1970's, the first detailed studies relating to regional geology were done. Lambert (1974) studied the Bennett Lake caldera, 20 km west of Montana Mountain. The geology, structure and geological history of the Atlin Terrane were described by Monger (1975). Age dating of the "Carcross pluton" in the Montana Mountain area was included in a study of age dating (K-Ar method) of granitic plutons in the Whitehorse map area (Morrison *et al.*, 1979). Tempelman-Kluit (1979) describes the tectonic history of the Yukon.

In the 1980's, Dagenais (1984) studied $\delta^{18}O$ values of granitoid intrusions in the Whitehorse Trough. The Mount Skukum volcanic complex in the Wheaton River district has been mapped by Pride (1983). Current research on the economic geology in the Wheaton River district includes an investigation of the Mount Skukum gold deposit (McDonald *et al.*, 1986) and a regional metallogeny study of the Wheaton River district (Rucker *pers. comm.*, 1986).

The Venus deposit was included in a study of element zoning in Yukon precious metal vein deposits (Morin, 1981), and in a regional study of precious metal vein deposits in the Bennett Lake area (Schroeter, 1986). A B.Sc. thesis on the mineralogy, zoning and alteration

of the Venus vein was done by Ralfs (1975). Roots (1981) described the geological setting of Au-Ag veins on Montana Mountain and did a detailed study of the Montana Mountain volcanic complex (Roots, 1982). The geostatistics of the Venus vein system are currently being studied by T. Stubens (Stubens *pers. comm.*, 1986).

D. History of the Venus Mine

The following history of the Venus Mine is summarized from private company reports (Watson, 1979; Prince, 1984b) and government publications (Cairnes, 1907, 1908, 1917).

Mineralized float was first discovered on the slopes of Montana Mountain by prospectors on the Tagish Lake part of the White Pass Trail to the Klondike gold fields. In 1900, the Venus vein was discovered by two young prospectors, Jack Stewart and Jack Pooly. In 1904, Stewart and Pooly sold the VENUS claims to Colonel J.H. Conrad for $120,000. Colonel Conrad acquired other Au-Ag veins on Montana Mountain and began preliminary development work on the Montana, Joe Petty, Uranus, M & M, Thistle, Humper, Nipper, Float, Red Deer, Mountain Hero and Aurora showings. By 1906, development work concentrated on three properties, The Big Thing, Montana and Venus. The town of Conrad was built on the shore of Windy Arm, and aerial tramways up to 6.4 km long were built to ferry supplies to the minesites. Extensive mining was done on the Venus #2 part of the Venus vein. A 465 m long, double aerial tramway was built to carry ore from Venus #2 to a gravity concentrating mill on Windy Arm. It is estimated (Cairnes, 1917) that from 1905 to 1912, 6,000 tons of ore were taken from Venus. In 1912, Colonel Conrad was forced into bankruptcy after spending $750,000 developing the Windy Arm properties. Development work on Venus and other showings ceased, and by 1913 Conrad became a ghost town.

In 1916, the Harper Syndicate acquired the rights to several of the claims, and produced 2,700 tons of 0.64 oz./ton Au and 68.20 oz./ton Ag until production ceased in 1920 (Prince, 1984b).

Very little production work was done on the deposit until 1966. Between 1919 and 1963, the deposit was investigated by Treadwell Yukon Mines Ltd. in 1919, Hollinger in 1922,

Yukon Gold Mines in 1928, and Giant Yellowknife Mines Ltd. in 1963.

In 1966, Venus Mines Ltd. began development on a different part of the Venus vein, called the Venus Extension. This section of the vein contains the present day mine workings. Two crosscuts were driven, and a gravel road from Carcross to the minesite was completed in 1969. A 300 ton per day mill was built and operated briefly until 1971, when insufficient millfeed, lack of capital, low prices, and environmental problems forced closure of the mine. While in operation, the mill treated 23,500 tons of ore grading 0.08 oz./ton Au, 3.30 oz./ton Ag, 7.4% Pb and 5.0% Zn, and 41,435 tons in 1971 grading 0.22 oz./ton Au, 6.47 oz./ton Ag, 1.6% Pb and 1.1% Zn.

In 1975, the claims were acquired by the Tagish Lake Syndicate, which optioned the property to United Keno Hill Mines Ltd. in late 1978. The company resampled old workings and began an underground and surface exploration program. Construction of a new 100 ton per day mill began in 1980 in response to rising precious metal prices. Mining operations were to begin and the mill was virtually completed when falling precious metal prices forced closure of the mine before the end of 1981. In 1983, a small surface trenching program was designed to examine the surface projection of two strong ore shoots (Prince, 1984a). In 1984, a surface and underground exploration program was carried out. Two drifts, two raises and six subdrifts were completed (Stirling *pers. comm.*, 1984) and new ore shoots were found in the north part of the vein system. Other veins on the property (Uranus, Ruby Silver) were drilled. There has been no work done on the property since 1984.

Current ore reserves now stand at 68,300 short tons grading 0.32 oz./ton Au, 8.9 oz./ton Ag, 2.45% Pb and 1.46% Zn. This includes 15,000 tons grading 0.42 oz./ton Au, 10.6 oz./ton Ag, 2.65% Pb and 1.33% Zn (Prince, 1984b). In addition, a previously mined total of 13,360 short tons of exploration muck averaging 0.17 oz./ton Au, 4.3 oz./ton Ag, 1.29% Pb and 0.72% Zn are currently stockpiled at the Venus minesite. Chip samples were averaged out over a 5 foot mining width. No dilution, stope recoveries or other factors are considered in the figures.

II. REGIONAL GEOLOGY

A. Introduction

The following description of the tectonic setting and history of the Montana Mountain area is based on papers by Tempelman-Kluit (1979) and Monger *et al.* (1982). Emphasis is on using the concept of exotic terranes to describe the geological setting and history of the Whitehorse Trough and Montana Mountain volcanic complex. The regional geology of southwestern Yukon and northwestern B.C. is shown in Figure 2.

B. Tectonic Setting

The Montana Mountain volcanic complex is located on the western margin of a Mesozoic fore-arc basin called the Whitehorse Trough (Wheeler, 1961). The Whitehorse Trough is part of the Intermontane Belt: one of five physiographically distinct belts in the Canadian Cordillera. The Cordillera can also be divided into two large, composite terranes (Terrane I and Terrane II), that consist of smaller, allochthonous terranes (Monger *et al.*, 1982). Terrane I, the inner Terrane, is composed of four smaller terranes that amalgamated in the late Triassic. Terrane II is composed of three smaller terranes that were amalgamated in the late Jurassic, prior to accretion to the ancient North American craton (Monger *et al.*, 1982). Accretion of Terrane I in the mid Jurassic and Terrane II in Cretaceous to Tertiary time, caused tectonic overlap and/or compression of crustal rocks, into two tectonic welts (Monger *et al.*, 1982). The Omineca Crystalline Belt formed after collision of Terrane I with the Mesozoic North American margin. The Coast Plutonic Belt, 10 km west of Montana Mountain, formed after accretion of Terrane II to the new western margin of North America.

In southwestern Yukon and northwestern British Columbia, Terrane I is represented by two smaller terranes. Cache Creek terrane contains Paleozoic oceanic crust and reef complexes that accumulated in a back-arc basin (Monger, 1975). Tempelman-Kluit (1979) suggested that the back-arc basin, called the Anvil Ocean, opened in the Mississippian after rifting and westward movement of the Stikine block from the North American craton. The

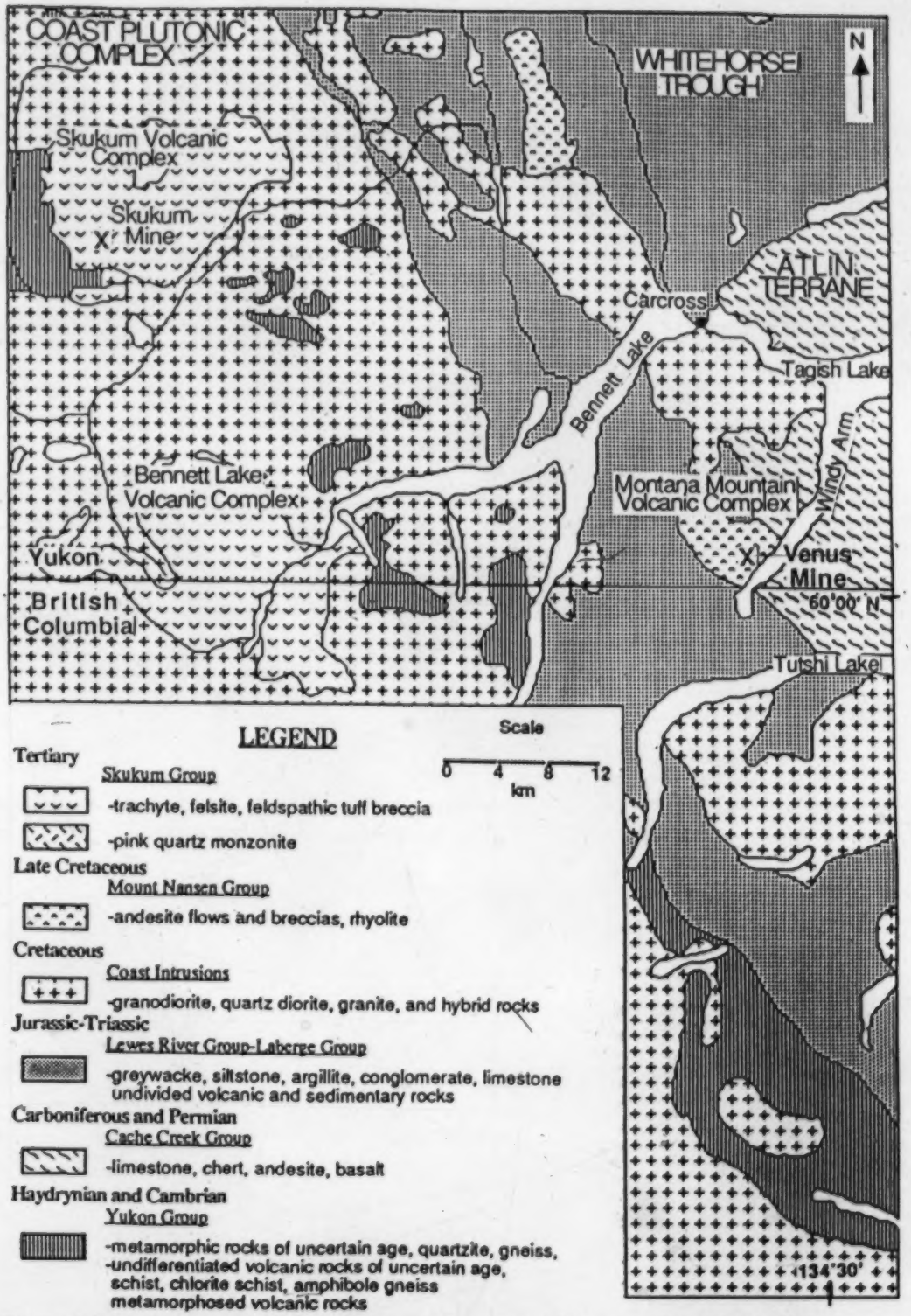

Figure 2. Regional geology of southwestern Yukon and northwestern British Columbia.

Anvil Ocean grew larger until the early Triassic, when westward subduction of oceanic Cache Creek Group rocks under the Stikine block began. The arc system that developed on the Stikine block consisted of Upper Triassic Lewes River Group andesites and basalts and Lower Jurassic Laberge Group sedimentary rocks. Monger *et al.* (1982) suggested that the oceanic Cache Creek terrane and island arc Stikine terrane were stratigraphically linked by the Triassic to form Terrane I.

In the mid Jurassic, Terrane I collided with the Mesozoic North American margin and was obducted over the North American craton (Tempelman-Kluit, 1979). The boundary of this collision is marked by the Teslin suture zone, 90 km east of Montana Mountain. In the late Jurassic, a section of Cache Creek terrane oceanic floor was thrust southwesterly over the Stikine terrane. This portion of the larger Cache Creek terrane is called the Atlin terrane (Monger, 1975), and borders the northeast boundary of the Montana Mountain volcanic complex.

After accretion of Terrane I, Terrane II accreted onto the new west margin of North America. During and after accretion, east-dipping subduction of the Pacific Ocean Plate under the North American continental margin generated a large magmatic island arc called the Coast Plutonic Belt. The Coast Plutonic Belt marks the site of extensive calc-alkaline volcanism and obliterated the existing boundary between Terranes I and II.

Roots (1982) suggested that the Montana Mountain volcanic complex was emplaced on the far west margin of Terrane I during the final stages of the collision between Terrane I and the Mesozoic North America margin.

C. Regional Stratigraphy and Structure

Cache Creek Group

The oldest rocks in the Montana Mountain area are late Paleozoic, Cache Creek Group, mafic volcanic flows in the Atlin Terrane (Table 1). Wheeler (1961) assigned the rocks to the Taku Group, but Monger (1975) suggested that they might be equivalent to

Table 1. Table of Formations in south-central Yukon (modified after Roots, 1982).

ERA	PERIOD or EPOCH		ROCK UNIT	PRINCIPAL ROCK TYPES
CENOZOIC	Pleistocene or Recent			Glacial drift, alluvium
	Unconformity			
	Eocene		Skukum Group	Granite porphyry, rhyolite Ignimbrite, rhyolite, basalt, andesite and dacite, volcanic and granitic breccia
Unconformity				
MESOZOIC	Late Cretaceous		Coast Plutonic Complex	Quartz monzonite, leucogranite, biotite granite, alaskite, hornblende-biotite granodiorite quartz diorite
			Nisling Range Alaskite	Rhyolite, trachyte porphyry felsic dikes and sills
			Carmacks Group	Plateau basalts
			Mount Nansen Group	Andesite, intrusion breccia, ignimbrites, debris flows, andesite and dacite lavas
	Intrusive, locally disconformable contact			
	Lower Jurassic	Whitehorse Trough	Laberge Group	Conglomerate, siltstone, argillite, hornfels
	Disconformity, local angular unconformity			
	Upper Triassic		Lewes River Group	Volcanic greywacke, limestone reefs, volcanic breccia, agglomerate, andesite
Faulted, possible disconformity				
PALEOZOIC	Permian	Atlin Terrane	Atlin Intrusions	Serpentinized gabbro, pyroxenite, dunite
			Cache Creek Group: Horsefeed Formation	Limestone reefs, minor pyroclastic interbeds
	Disconformity			
	Pennsylvanian		Cache Creek Group: Nakina Formation	Amphibolite, breccias, minor chert interbeds

Nakina Formation rocks in the Atlin area. Nakina Formation is considered by Monger (1975) to be among the oldest of five formations in the Atlin terrane. Nakina Formation rocks consist of Mississippian and Pennsylvanian, altered, mafic volcanic rocks with associated ultramafic rocks. Monger (1975) suggested that Nakina Formation rocks formed a basement of oceanic crust in the Mississippian.

In the Montana Mountain area, Nakina Formation rocks in the Atlin terrane are hard, dark grey-green, fine grained amphibolite that has lost any trace of primary texture. Other rock types include metadiorite, bedded chert, carbonate and serpentinite. Mafic volcanic flows are overlain to the north and east of Montana Mountain by bedded carbonates.

Roots (1982) mapped the contact between Nakina Formation rocks and Mount Nansen Group volcanic rocks on Montana Mountain. Roots suggests that the contact exposed south of Pooly Canyon resulted from intrusion of a partly solidified breccia mass. In the north canyon of Pooly Creek, the contact of Mount Nansen Group rocks dips 60° NE beneath Nakina Formation amphibolite (Roots, 1982).

Pods of serpentinized pyroxenite in Nakina Formation rocks were noted by Roots (1982). A plug of ultramafic rock, fault bounded between the volcanic complex and the Carcross pluton, is located 1 km north of Montana Mountain.

Lewes River Group

Upper Triassic, Lewes River Group volcanic rocks do not border the Montana Mountain complex, but are located further east and north along the outer margins of the Whitehorse Trough. In the Montana Mountain area, Lewes River Group volcanic rocks occur as clasts in Lower Jurassic Laberge Group conglomerate. Lewes River Group consists of volcanic flows and breccias, pyroclastic deposits and limestone reef complexes. The most common rock types are purple, grey and green volcanic breccia, volcanic greywacke and lenses of grey and pinkish massive limestone (Wheeler, 1961). Lewes River Group volcanic rocks may be locally confused with Mount Nansen Group volcanic rocks.

Laberge Group

Lower Jurassic, Laberge Group sedimentary rocks occur on the eastern and southern boundaries of the complex. Laberge Group consists of a thick, repetitive succession of deep water facies, greywacke, sandstone, siltstone, shale and conglomerate, and lies disconformably on the Lewes River Group. A narrow strip of the Laberge Group borders the northeastern part of the complex and separates older Nakina Formation rocks from younger volcanic rocks and intrusive rocks. Clastic Laberge Group sedimentary rocks have a characteristic reddish weathering rind (Roots, 1982). On the eastern and southern parts of the Montana Mountain complex, the Laberge Group contains greywacke and finely laminated siltstone with argillite rip-up clasts. Conglomerate layers and lenses that interfinger with greywacke along strike are common in the northwestern part of the complex.

The contact of Laberge Group sedimentary rocks with Nakina Formation mafic volcanic rocks is generally fault bounded, although a poorly exposed contact in Big Thing Creek is disconformable (Roots, 1982).

Granitic Rocks

Pink weathering, medium to coarse grained, granite to granodiorite is exposed north of the volcanic complex. The exposures form the south end of a 22 km long body informally known as the 'Carcross pluton'. Roots (1982) noted a mauve colored altered chlorite granite and a zone of aplite and alaskite bordering the complex and extending into the volcanic rocks. Roots suggests that the Carcross pluton is the granitic equivalent of the Mount Nansen Group volcanic rocks. He also notes that the pluton is more compositionally variable and more granitic than rocks of the Coast Range Batholith 15 km to the west.

Mt. Nansen Group

The Montana Mountain volcanic complex was originally mapped as Hutshi Group by Wheeler (1961). The term Hutshi Group was also used by Bostock and Lees (1938) for volcanic rocks in the Miners range northwest of Whitehorse. Bostock (1936) gave the name

Mount Nansen Group to volcanic rocks in the Carmacks district that he considered equivalent to the Hutshi Group. Tempelman-Kluit (1978) assigned the name Mount Nansen Group to volcanic rocks in the Miners range, and suggested that the Hutshi Group volcanic rocks on Montana Mountain might be part of the Mount Nansen Group volcanic rocks. Roots (1982) mapped the geology of the Montana Mountain volcanic complex and concluded that the complex correlates with Mount Nansen plug domes in south central Yukon and layered Sloko piles in northern Britsh Columbia. The ages of the Hutshi, Mount Nansen and Carmacks Groups were found to be late Cretaceous by Grond *et al.* (1984). They concluded that the three groups of volcanic rocks are contemporaneous and show a typical, subduction related, volcanic arc, calc alkaline to potassic alkaline chemical chemistry. They also suggest that rocks of this late Cretaceous volcanic suite do not correlate in age with younger Skukum and Sloko Group rocks. Since the Hutshi Group also included Upper Triassic, Lewes River Group volcanic rocks, its use has been abandoned.

Description

Mount Nansen Group consists of volcanic flows, breccias, and pyroclastic material ranging from basalt and andesite to rhyolite in composition (Grond *et al.*, 1984). In the Miners Range, Mount Nansen Group volcanic rocks are porphyritic, partly vesicular, calc-alkaline andesite flows and flow breccias intruded by felsic dikes (Grond *et al.*, 1984). Bostock (1936) mapped Mount Nansen Group rocks in the Dawson Range as a heterogeneous assemblage of andesite and basalt flows, breccias and less common tuffs and agglomerates. In the Montana Mountain area, the volcanic complex consists of green and grey-green intermediate volcanic flows and breccias intruded by felsic dikes (Roots, 1982). The volcanic rocks intrude rocks of the older Nakina Formation in the Atlin terrane and Lower Jurassic Laberge Group sedimentary units.

Mount Nansen Group volcanic rocks are distributed throughout southwestern Yukon and northwestern British Columbia. Tempelman-Kluit (1980) interpreted the Mount Nansen volcanic centers as remnants of plug domes and differentiated volcanic piles that were deposited on a erosion surface of considerable relief. Most Mount Nansen Group rock units

are flat-lying, gently dipping and are of lower greenschist facies metamorphic grade.

Age of Mount Nansen Group Volcanics

Mount Nansen Group rocks in the Miners Range were dated at 72.4 ± 2.5 Ma and 69.1 ± 2.6 Ma (K-Ar method) by Grond *et al.* (1984). In the same study, a date of 72.4 ± 2.1 Ma (Rb-Sr method) was assigned to rhyolite from Hutshi Group rocks in northwestern British Columbia. Although the volcanic rocks on Montana Mountain have not been dated directly, they are probably contemporaneous with other late Cretaceous, Mount Nansen Group rocks.

The Carcross pluton, which intruded and metamorphosed the Montana Mountain volcanic complex, has been dated by Morrison *et al.* (1979), at 64.3 ± 2.2 Ma (K-Ar method), but there is some uncertainty about the date. Tempelman-Kluit (1981) suggests the Carcross pluton and associated felsic dikes are equivalent to the Nisling Range alaskite, which is the subvolcanic equivalent and feeder for Mount Nansen Group occurrences in the Dawson Range.

Roots (1982) suggests that intrusion of the Carcross pluton into Mount Nansen Group rocks on Montana Mountain has probably reset the original radioactive ages of the volcanic rocks.

Comparison with Other Volcanic Complexes

The Skukum volcanic complex (Figure 2) is an elliptical, downfaulted area of intermediate to felsic volcanic rock deposited on granitic rocks of the Coast Plutonic Belt and Precambrian Yukon Group schists and gneisses. The complex is Paleocene to Eocene in age and is surrounded by high level rhyolite intrusions dated at 53 ± 1.1 Ma (Rb-Sr method) by Pride and Clark (1985). A dominant structual feature in the complex is a series of north-northeast trending fractures, which host dikes and precious metal veins.

The early Tertiary Bennett Lake caldera was deposited on predominately Cretaceous granitic rocks of the Coast Plutonic Belt. The volcanic complex consists of two cycles of ignimbrite deposits overlain by increasingly mafic breccias and lava flows. The complex was

mapped in detail by Lambert (1974), who suggested that major ash flow eruptions contributed to caldera collapse.

Pride (1983) compared the Skukum volcanic complex to the Bennett volcanic complex and concluded that, although the two structures are related in age and some geological characteristics, each complex represents a distinct structural and geological setting. The Skukum complex has a bimodal suite of extrusive rocks, is structurally complex and shows a wide variety of depositional environments. In addition, the Skukum complex does not show evidence of a major cauldron subsidence.

The Skukum complex and Bennett Lake volcanic complex contrast with Mount Nansen Group rocks on Montana Mountain because they are younger, more felsic and intrude Paleozoic and older rocks west of the trend of Mount Nansen Group volcanic rocks (Roots, 1982).

Regional Structure

The Whitehorse Trough consists of Late Paleozoic and Mesozoic rocks that have been folded into a northwesterly trending synclinorium. The Whitehorse Trough is separated from the Coast Plutonic Belt by the steeply dipping Llewellyn fault system. The Nahlin Fault separates Mesozoic rocks in the Whitehorse Trough from the Paleozoic rocks in the Atlin Terrane. The southwestern part of the Nahlin Fault has been traced for more than 250 miles. It is a vertical or steep, northeast dipping thrust fault, and extends from the southern Yukon southeasterly across British Columbia to the Cassiar Mountains, where it appears to swing south into the Pinchi Lake Fault Zone.

D. Regional Precious Metal Vein Mineralization

The Montana Mountain mining district is one of several precious metal districts in southwestern Yukon and northeastern B.C.

The Wheaton River gold-silver district is located 35 km northwest of Montana Mountain (Figure 2). It is situated on the eastern margin of the Coast Plutonic Belt. The host

rocks are Coast Plutonic Belt intrusive rocks, Upper Triassic Lewes River Group volcanic rocks, Lower Jurassic Laberge Group sedimentary rocks and Pre-Permian rocks of the Yukon Group. The area also contains two large volcanic complexes. The Mt. Skukum volcanic complex is situated on the western side of the district. The Bennett Lake Caldera is located on the southern border. Morin and Downing (1984) list 26 gold-silver deposits and occurrences in the Wheaton River district. There are at least three types of veins in the Wheaton River district, Au-Ag, Sb-Ag and Ag-Pb (Cairnes, 1912).

The Skukum gold deposit, in the Wheaton River District, was found in 1980 by AGIP, and is currently being mined by Mt. Skukum Gold Mines Ltd. Current ore reserves in the main Cirque zone are estimated at 148,980 tonnes of 24.98 g/tonne Au and 20.5 g/tonne Ag (McDonald *et al.*, 1986). The deposit is an epithermal Au-Ag vein system hosted by Tertiary andesites in the Mt. Skukum volcanic complex. The gold occurs in steeply dipping quartz-carbonate-sericite veins associated with major faults and rhyolite dykes. The main vein averages 5 m in width, has a known vertical depth of 80 m and has been traced for 200 m along strike (McDonald *et al.*, 1986). The unusual feature of this deposit is that the gold-bearing veins have little or no sulphides or other indicators of mineralization.

In northeastern British Columbia, several precious metal occurrences are situated in a belt of Mesozoic island arc derived volcanic and sedimentary rocks. Schroeter (1986) suggests that epithermal and mesothermal mineralization in this belt is structurally controlled by north trending fractures and may be genetically related to Cretaceous and Tertiary volcanic and plutonic activity.

III. LOCAL GEOLOGY

A. Introduction

The Montana Mountain volcanic complex encompasses a roughly circular, high standing area approximately 7 km in diameter. Mount Nansen Group volcanic rocks on Montana Mountain consist predominately of medium to dark grey-green to green intermediate volcanic flow rocks and breccias. The northern margin of the complex has been metamorphosed by intrusion of the Carcross pluton. Porphyritic, orange weathering, felsic dikes intrude the volcanic rocks. The geology of the Montana Mountain volcanic complex (Figure 3) was mapped in detail by Roots (1982), and the following chapter is based largely on his work.

B. General Geology and Structure

Description of Volcanic Rock Types

Intrusion Breccias

Intrusion breccias predominate in the northern half of the complex. The breccias are massive, homogeneous bodies of coarse volcanic fragmental rocks, and may have resulted from subterranean stoping and churning (Roots, 1982). He suggests that the lack of extrusive features, the massive nature of the breccias and the presence of intrusive contacts indicate subvolcanic emplacement. The breccias are matrix supported with fine grained or aphanitic rounded to angular clasts up to 2.5 cm across. The volcanic clasts are dark green to light grey and intermediate in composition. Some clasts are porphyritic or banded.

The intrusion breccias are distinguished by irregularly oriented fluidal layering, consisting of coarse to fine laminations that swirl and stream together. Roots suggested that the flow layers are conduits for fluids escaping through the intrusion breccia with more mafic minerals precipitating first, along the walls of the opening and siliceous or volatile rich

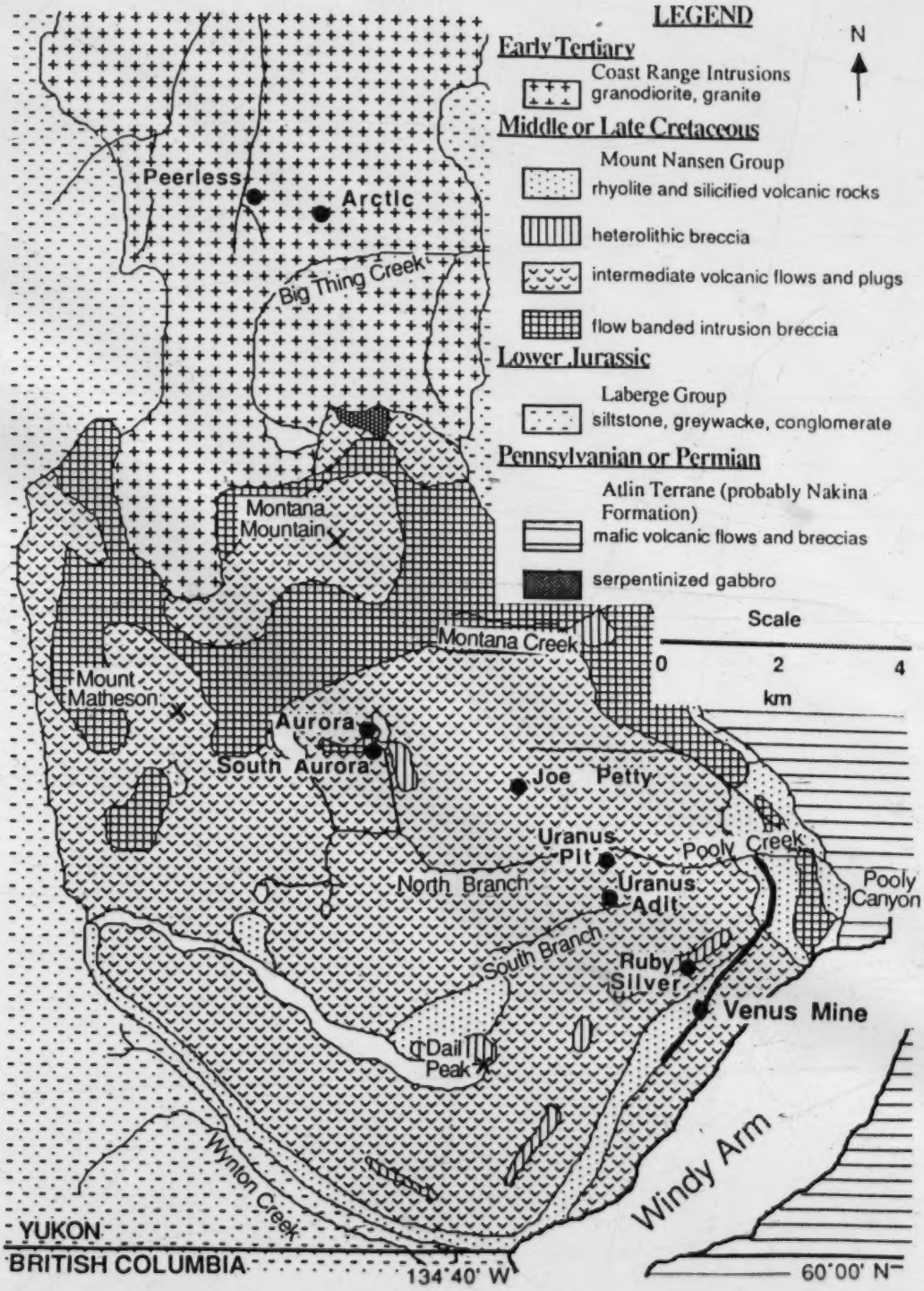

Figure 3. Geology of the Montana Mountain volcanic complex (modified after Roots, 1982).

residues filling the center. The banding in the flow layers developed as the fissure, a zone of weakness, was repeatedly opened and injected with fluids.

Debris Flow Breccias

Dark green and brown, debris flow deposits are found in the central region of the volcanic complex where they occur as beds within lava flow successions, or as thick massive layers. The deposits are composed of coarse, dominantly volcanic fragments suspended in a detrital matrix. The matrix is generally dark green to grey and is composed of small angular chips of andesite, dacite or quartz. The clasts weather light green or maroon, are pebble to boulder sized and are probably derived from andesite and dacite lava flows. The contacts between debris flow deposits are sharp, irregular breaks.

Roots suggests that because the debris flows were once surficial features of the volcanic center, these breccias were greatly influenced by topography at the time of deposition. He suggests that the breccias were derived from an edifice situated to the north of the present complex, and occupy a depression within the center of the complex.

Pyroclastic Breccias

The presence of altered pumice and shards in a breccia suggests a pyroclastic flow deposit, where pyroclastic eruptions have mobilized coarse lithic debris. Roots suggests that the pyroclastic breccias originated from ash and rubble slides originating on the flanks of a volcano or growing dome.

Ignimbrite is exposed in cliffs on the south side of Upper Pooly Creek. The ignimbrite formed from the deposition and consolidation of ash flows, but does not contain abundant lithic blocks. Roots interpreted the ash flow to have erupted late in the sequence. There is also a possibility the ash flow is derived from volcanism at Bennett Lake.

Andesite Plugs

Homogeneous porphyritic andesite comprises large masses, including Mount Matheson and Montana Mountain. The rocks are medium grey or green, fine grained and massive, with no vesicles, foliation or flow structures. The andesite bodies do show regular vertical jointing.

Roots interprets the andesite bodies to be the cores of plug domes.

Volcanic Flow Rocks

Homogeneous, massive, intermediate and mafic volcanic flow rocks dominate the southern part of the volcanic complex. The flows are blocky, dark green, brown and maroon and in places are intercalated with volcanic breccias. Most of the rocks have been partly recrystallized to amphibole and chlorite aggregates, and are aphanitic, dense and relatively soft. The dark green rocks are of andesitic composition (average 55% silica) and the light green rocks are of dacitic composition (64% silica)(Roots, 1982). Vesicules are common in the flow rocks and are frequently filled by calcite, quartz or dark green clay. Some rocks with large and abundant vesicules are maroon or purplish in color; this suggests to Roots that some of the rocks were extruded subaerially.

The contacts between lava flow units are not easily discerned. Roots (1982) suggests that the layers were groups of fluid sheet lavas spread over wide, gently sloped areas. Roots found that lavas and breccias near the edge of the complex are andesitic but upper flows in the central part are dacitic, which indicates the volcanism became more siliceous with time. Compositional cycles of the type observed in the Bennett Lake caldera (Lambert, 1974) do not appear to be present in the Montana Mountain volcanic complex.

Felsic Dikes

Orange weathering quartz latite and trachyte dikes form 5% of the volcanic complex. The dikes are porphyritic, fine to medium grained, and cut all volcanic rock types. They commonly occupy fault zones. Evidence of successive emplacement indicates that the faults must have been recurrent lines of weakness. This theory is supported by observations of slickensides in the walls of quartz veins following the dike swarms.

Structure of the Montana Mountain Volcanic Complex

Roots (1982) suggests that the volcanic complex once extended over a much larger area, as indicated by occurrences of Hutshi Group volcanic rocks mapped southeast of Windy

Arm (Monger, 1975) and 15 km northwest of Carcross (Wheeler, 1961). It is unclear whether the complex is a preserved source area or was derived from vents that are now eroded. Roots suggests that upwards arching of the volcanic complex caused by intrusion of the Carcross pluton may have escalated erosion of the volcanic rocks. Roots interpreted the southern part of the complex to be a remnant of a volcanic edifice, with a broad, dome-like structure, and the northern part to be deeply eroded subvolcanic intrusions.

The volcanic complex has intruded older rocks in the area and is bounded by steeply dipping fault zones. A possible extension of the Nahlin Fault separates Mount Nansen Group rocks from Cache Creek Group rocks in the Atlin terrane. This fault is inferred to cross beneath Windy Arm. In Pooly Canyon, the contact between the two groups is a 1 m wide vertical cleft of protomylonite with lenticles of andesite (Mount Nansen Group) and amphibolite (Cache Creek Group). In the North Canyon of Pooly Creek, the contact of oxidized Mount Nansen rocks dips 60° northeast beneath Nakina amphibolite.

The contact between Mount Nansen Group rocks and Laberge Group sedimentary rocks appears to be gradational in places or is fault bounded.

The contact between Mount Nansen Group volcanic rocks and the Carcross pluton is exposed northwest of Montana Mountain. The contact dips 45° south beneath intrusion breccia, and contains fractured alaskite with abundant tourmaline veinlets, pyrolusite and malachite. Roots suggests that the pluton underlies most of the volcanic complex.

There are three major faults, over 3 km long, as well as numerous smaller ones. The Matheson Fault separates andesite from a debris and lava flow succession. The Dail Peak Fault is marked by a broad shear zone and coincident dike swarms across the south slope of the volcanic complex. The Montana Mountain ridge contains steeply dipping fault traces.

Metamorphism and Alteration

Mount Nansen Group rocks on Montana Mountain are of lower greenschist facies metamorphic grade. Hornfels is found along the northern margin of the volcanic complex, where the Carcross pluton has intruded and metamorphosed the volcanic rocks. Roots found

that alteration and probable devitrification produced the fine grained, homogeneous aphanitic textures seen in the volcanic flow rocks. He also noted that saussuritization by meteoric waters and hydrothermal fluids is common.

C. Evolution of the Montana Mountain Volcanic Complex

The following account of the evolution of the Montana Mountain volcanic complex is summarized from Roots (1982).

Initially, subaerial effusive volcanism generated a broad cone with gentle slopes. Roots estimates the blocky to massive andesitic flows may have extruded more than 20 km from the complex. The volcano probably reached a height of more than 1000 m before internal pressures increased sufficiently to cause eruptions to become more explosive. Pyroclastic and felsic rocks were deposited at the top of the stratified volcanic pile. During development of the cone, one or more periods of subsidence occurred, obliterating the original feeder pipe. Roots suggests that tephra, lava flows and volcaniclastic sediements filled a depression in the central region of the complex.

Andesitic magma and plugs intruded a large (inferred) volcanic structure situated over the northern part of the complex. The magma became more granitic with time and intruded the pre-existing volcanic pile. Felsic dikes intruded and filled zones of weakness (faults, fissures) opened up by upwards arching of the complex. Roots suggests that the volcanic center once extended over the Carcross pluton, which has been exposed by erosion.

D. Geological Setting of the Venus Vein

The Venus vein is situated on the southeast slope of the volcanic complex. The vein partially follows a felsic dike infilling a zone of structural weakness. Roots suggests that the radial and concentric patterns of the veins and the dikes imply that they are related to granitic intrusion and possibly upward arching of the volcanic rocks. Most precious metal veins in the Montana Mountain area are confined to Late Cretaceous Mount Nansen Group rocks. Roots suggests that the quartz veins probably were emplaced after volcanic activity in the complex

ceased, perhaps during structural adjustments.

E. Precious Metal Veins on Montana Mountain

There are over twenty precious metal veins on Montana Mountain. Many of the veins are described by Roots (1981) and are included in a compilation of Yukon precious metal veins by Morin and Downing (1984). The Ruby Silver, Uranus, Joe Petty, Aurora, Arctic and Peerless veins were sampled for this study. Their locations are shown in Figure 3. A brief description of these veins is given in Appendix 1.

IV. VEIN STRUCTURE, MINERALOGY AND PARAGENESIS

A. Introduction

The following chapter summarizes field observations and a petrographic study done on the structure, texture, alteration and mineralogy of the Venus vein. Particular emphasis was placed on identifying gold mineralization and on determining the relationship of gold to vein structure, texture and other mineral phases. Polished mounts were made of representative samples from ore shoots on the vein and from lower grade parts of the vein.

B. Vein Structure

The Venus vein has a known strike length of 2 km. The northern and central parts of the vein strike N 5° E to N 20° E. The extreme southern portion of the vein strikes N 65° E. The vein dips 30° to 50° NW. The change in strike direction in the south part of the mine occurs over less than 15 m, with the dip remaining constant. The known vertical depth of the vein is 400 m. The vein width ranges up to 4 m, but averages 1 m. The vein is wider in the lower levels of the mine, and becomes narrower with increasing elevation. The abrupt northern termination of the Venus vein is at Pooly Canyon. The location of the southern termination of the vein is unknown. The extreme southern part of the vein is oxidized underground and splits into discontinuous, narrow, subparallel veins. There are five levels underground, at elevations of 2600 ft., 2650 ft., 2700 ft., 2800 ft., and 2850 ft.

Normal faults cut the vein at various angles. Fault zones (up to 1 m wide) contain fault breccia, quartz, calcite and oxidized volcanic material. Fault displacement averages 2 cm to 3 m, but some faults have displacements of up to 10 m. The vein contains several strike-slip faults with local shear zones.

Subsidiary veins occur locally, paralleling or crosscutting the main Venus vein. The subsidiary veins are usually narrow (less than 0.5 m wide) and typically contain only quartz, although some contain sulphides. The main Venus vein locally splits into two or three veins, especially in the upper levels of the mine.

C. Vein Texture and Mineralogy

The Venus vein is a fissure filling showing evidence of multiple periods of fluid injections. Movement along slightly curved, planar, surfaces is reflected by the undulatory nature of the vein. Slickensides in the host rock and the presence of clay gouge in the vein are evidence that syndepositional movement along the vein took place. There are no visible marker beds in the volcanic host rocks, so it is difficult to determine the magnitude of fault displacement.

The vein is frequently separated from the hangingwall and footwall by a layer of clay gouge. In other places, the vein-wallrock boundary is poorly defined, due to injection of cross-cutting, late stage quartz stringers and replacement of wallrock by vein material. In the southern part of the vein, parallel quartz veins interbanded with altered host rock are common in the hangingwall and footwall of the main vein. Subsidiary veins and the main Venus vein are often connected by a network of barren quartz stringers.

The Venus vein typically contains ribbons (bands less than 1 cm wide) of clayey, altered wallrock or narrow, parallel veinlets of dark grey arsenopyrite grains. Intercalated altered wallrock in the vein is commonly found as narrow to wide (1 m) bands or as unsupported angular fragments.

Quartz is the dominant mineral in the Venus vein. It varies in its occurrence from milky white grains 1 mm or less in diameter up to well developed, clear, euhedral crystals 15 cm long. The larger quartz crystals often occur in single and multiple layers of irregular comb structures or line vugs located near the center of the vein. Vein quartz is slightly finer grained on upper levels than on lower levels.

Arsenopyrite, pyrite, galena and sphalerite are the four most common minerals after quartz. A quartz-arsenopyrite-pyrite mineral assemblage is the most common. Arsenopyrite and pyrite are ubiquitous, while sphalerite and galena only occur locally. Over an average 1 m vein width, arsenopyrite comprises 8% of the vein, pyrite comprises 6%, and sphalerite and galena together comprise 5%. Quartz was deposited first, followed by arsenopyrite. Pyrite was deposited at the same time or slightly later than arsenopyrite. Arsenopyrite and pyrite often

occur together in crude asymmetrical bands which are concentrated on the outer edges of the vein (Plate 1). More rarely, the center of the vein is sulphide rich with barren quartz concentrated on the outer edges of the vein. Bands of arsenopyrite and pyrite range from less than 1 cm wide to over 1 m wide, and can be monomineralic or consist of narrow, alternating bands of pyrite and arsenopyrite. On upper levels, arsenopyrite occurs locally as large, bladed crystals growing perpendicular to the vein walls. Both sulphide phases occur in hydrothermally altered wallrock as veinlets, disseminated grains and clusters.

Sphalerite and galena are not as common as arsenoypyrite and pyrite. Some parts of the vein show a later quartz-arsenopyrite-pyrite phase crosscutting an earlier quartz-sphalerite-galena phase (Plate 2). Other parts of the vein contain all four major sulphides, where sphalerite and galena are concentrated in massive lenses or pods near the center of the vein. Disseminated anhedral grains of galena and more rarely sphalerite frequently fill interstitial space between euhedral quartz crystals near the center of the vein. Trace amounts of visible tetrahedrite and pyrargyrite occur in galena-sphalerite rich parts of the vein.

The total percentage of sulphides in the Venus vein increases with increasing elevation. In the lower levels of the mine, the vein contains an average of less than 15% sulphides, while on the upper levels, the sulphide content is 30-80% of the vein (estimated visually). The relative proportion of each sulphide in the vein does not change with elevation.

Ore Shoots

At Venus, gold is concentrated in steeply plunging ore shoots of varying size, shape and continuity. Ore shoots have a length to width ratio of 10:1 and comprise 20% of the vein (Prince, 1984b). The strike length of the ore shoots ranges from 7 m up to 30 m. Some shoots are known to extend up to 200 m down the dip of the vein. The highest grade ore shoots occur in wider portions of the vein containing all four sulphides. Sections of ore shoots with flatter dips correspond to higher gold grades (Carlyle, 1984). Gold values and possibly the strike length of ore shoots increase upwards in the vein until the bottom of the surface

Plate 1. The Venus vein (2700' level) showing a quartz core and asymmetrical arsenopyrite-pyrite bands.

Plate 2. A high grade ore-shoot located on the 2850' level (looking at the north face before drift extension); a) Arsenopyrite-pyrite-quartz (22 cm wide) containing 1.6 oz./ton Au and 9.1 oz./ton Ag. b) Sphalerite-galena-quartz (30 cm wide) containing 0.14 oz./ton Au and 40.10 oz./ton Ag. c) Arsenopyrite-pyrite-quartz (35 cm wide) containing 0.49 oz./ton Au and 13.6 oz./ton Ag.

oxidation zone is reached.

D. Wallrock Alteration

An intense hydrothermal alteration envelope 2 m to 10 m wide surrounds the Venus vein. Altered andesitic wallrock in the hangingwall and footwall is light gray-green and silicified. The intensity of alteration increases towards the vein. Small, medium green chlorite clots are common. Local porphyritic and brecciation textures occur where the alteration decreases in intensity, but original mineralogy and textures are largely obliterated. Euhedral pyrite and arsenopyrite occur as veinlets or disseminated veins.

In thin section, altered wallrock near the vein consists of quartz, sericite, carbonate and pyrite, with lesser amounts of arsenopyrite, galena, limonite and feldspar. Quartz and calcite occur separately or together in thin veinlets crosscutting the host rock. Quartz is disseminated throughout the groundmass as small anhedral grains. Sericite is ubiquitous and increases in abundance towards the vein. Chlorite clots consisting of fibrous, radiating crystals are disseminated throughout the altered wallrock.

An zone of intense clay alteration in the hangingwall and footwall of the vein is spatially associated with a ore shoot in the northern part of the vein system. The alteration zone consists of white, soft, clayey material that contains minor pyrite veinlets. The alteration can be traced from surface down to the 2700' level. The main Venus vein changes character in this intense alteration zone. The quartz content in the vein decreases to trace amounts, and all that is left of the vein is a 1 cm to 6 cm wide band of black weathering, massive, sulphide material. Polished block examination of this material shows it to be brecciated arsenopyrite with trace amounts of pyrite. Pyrite veinlets in the bleached wallrock show limonitic replacement. Trace amounts of calcite in veinlets were noted in this altered material on the 2850 ft. level. Assays from the clay alteration zone indicate low precious metal values.

Samples of the white, clayey material in the clay alteration zone have been analyzed using XRD analysis. The main clay mineral present is illite, with trace amounts of chlorite and kaolinite (private company report). Other non-metallic minerals present include ankerite,

quartz, sericite and calcite.

Oxidation Zone

The surface oxidation zone penetrates 75 m to 100 m down dip from the surface (Carlyle, 1984). The southern part of the mine is more oxidized than the northern part, since the south part of the mine is closer to the surface. The wallrock in the oxidized portion of the vein is generally yellow to orange-brown and contains limonite and other iron oxide minerals. Realgar, orpiment and scorodite are visible occasionally underground in the main Venus vein. Yukonite, a rare arsenate, is found in the south end of the 2850 level and in surface workings along the vein. Covellite, malachite and azurite were noted in trace amounts. A list of minerals found in oxidized parts of the Venus vein and wallrock is shown in Table 2.

E. Sulphide Petrography

The following section describes the five most important metallic minerals in the Venus vein. Other metallic minerals present in trace amounts (less than one percent) are listed and described in Table 3.

Arsenopyrite

Arsenopyrite is ubiquitous and occurs as euhedral to subhedral grains, commonly showing rhombic cross sections. Grain size ranges from less than 1 mm up to 3 cm. Arsenopyrite occurs as individual grains disseminated throughout quartz, as single layers parallel to vein walls or as irregular grain aggregates. Where arsenopyrite occurs as thin veinlets, the grains are oriented with their long side parallel to the vein walls. Most arsenopyrite shows varying degrees of cataclastic texture. In most of the polished sections, fracture lines are sharp and angular. In some of the sections, the fractures appear to have been corroded. Where corrosion or oxidation has taken place, the fractures are smooth and wide, with a "worm-like" appearance. Large, thick worm-like fractures do not contain later mineral phases. Intense brecciation and later cementation of arsenopyrite by quartz was

Table 2. Oxidation zone minerals.

Mineral	Formula	Description
Realgar	AsS	Red-orange, found as disseminated grains between quartz crystals. More common in the upper levels of the mine. A large pod of realgar and orpiment is located on the 2850 level.
Orpiment	As_2S_3	Lemon yellow, is associated with realgar (see above)
Scorodite	$FeAsO_4 \cdot 2H_2O$	Pale green or liver brown earthy masses, hydrous ferric arsenate associated with arsenopyrite
Yukonite	$Ca_3Fe_7(AsO_4)_6(OH)_9 \cdot 18H_2O$	Shiny black, amorphous arsenate after arsenopyrite. Rare mineral.
Malachite	$Cu_2CO_3(OH)_2$	Green secondary copper mineral after tetrahedrite or chalcopyrite. Found in trace amounts as small, powdery grains.
Azurite	$Cu_3(CO_3)_2(OH)_2$	Blue secondary copper mineral after tetrahedrite or chalcopyrite. Found in trace amounts as small, powdery grains with malachite.
Covellite	CuS	Covellite replaces tetrahedrite in fracture fillings and interstitial patches. Blue supergene alteration mineral.
Limonite	$FeO \cdot OH \cdot nH_2O$	Reddish-orange, powdery
*Beudantite	$PbFe_3(AsO_4)(SO_4)(OH)_6$	Reddish phosphate or arsenate with sulphate of ferric iron and lead
*Quensledite	$Fe_2(SO_4)_3 \cdot 10H_2O$	White, clayey, iron arsenate sulfate hydrate
*Kankite	$FeAsO_4 \cdot 3.5H_2O$	
Unidentified		Light green-brown radiating crystals found on 2700' level (south end) between large euhedral quartz crystals

* Not seen in this study (included from private company reports)

Table 3. Minor opaque minerals (<1%) found in the Venus vein.

Name	Formula	Description
Tetrahedrite	$(Cu,Fe)_{12}Sb_4S_{13}$	Tetrahedrite is associated with galena as fracture fillings in arsenopyrite and pyrite. It also occurs as blebs within galena, and commonly forms a replacement rim on the outer edges of galena grains and along galena cleavage planes. Electron microprobe analysis indicates tetrahedrite is the silver rich variety (Freibergite), and contains 27.5 % Ag (private company report).
Pyrargyrite	Ag_3SbS_3	Pyrargyrite occurs as rounded blebs located within galena grains. Pyrargyrite replaces galena, tetrahedrite and sphalerite. Electron microprobe analysis indicates a silver content of 59.8% (private company report).
Chalcopyrite	$CuFeS_2$	Chalcopyrite occurs intergrown with sphalerite, forming linear arrays of elongate blebs. Chalcopyrite was also noted as fracture fillings in tetrahedrite.
Jamesonite	$Pb_4FeSb_6S_{14}$	Noted by Ralfs (1975) - is closely related to pyrargyrite.
Pyrrhotite	$Fe_{1-x}S$	Occurs as small blebs within pyrite grains and chalcopyrite grains.
Diaphorite	$Pb_2Ag_3Sb_3S_8$	Identified by microprobe analyses (private company report). Occurs as small blebs in galena.
Electrum (Native Gold)	Au (Ag) Au	Occurs with galena as fracture fillings or replacement blebs in arsenopyrite and pyrite (see text).

observed occasionally. Circular and semi-circular patterns of arsenopyrite grains were observed where arsenopyrite grains infill space surrounding quartz crystals.

Pyrite

Pyrite was deposited at the same time as arsenopyrite or slightly later. It shares simple grain boundaries with arsenopyrite, or replaces it. Pyrite grains are commonly fragmented or shattered, but not as intensely as arsenopyrite grains. Grain size ranges from less than 1 mm to 0.5 cm. Pyrite is not as abundant as arsenopyrite, but it is as widespread. It occurs as euhedral disseminations or as subhedral to anhedral grains in bands with arsenopyrite. Pyrite commonly contains minute rounded blebs of later mineral phases. The mineralogy of these blebs ranges from chalcopyrite and pyrrhotite to chalcopyrite, sphalerite and galena. Pyrite is replaced by sphalerite and galena.

Sphalerite

Sphalerite is less common than arsenopyrite or pyrite, and is usually found in pods near the center of the vein or as disseminated grains infilling space between quartz crystals. Sphalerite is dark brownish red and commonly contains rounded blebs of other minerals including galena, chalcopyrite and tetrahedrite. Chalcopyrite is especially common, occuring as oriented intergrowths in sphalerite. Sphalerite commonly contains galena inclusions.

Galena

Galena was the last of the four main sulphide minerals at Venus to be deposited and is closely associated with sphalerite. Galena replaces arsenopyrite, pyrite and sphalerite and commonly occurs as fracture fillings and corrosion fillings in arsenopyrite and pyrite. It occurs as massive pods, bands, lenses and disseminated grains in wider parts of the vein, but also occurs microscopically in narrower parts of the vein containing arsenopyrite and pyrite. Galena grains commonly have a replacement rim consisting of tetrahedrite and other unidentified minerals. Tetrahedrite replaces galena by penetration along cleavage planes. The

amount of replacement ranges from minor to complete.

Gold

Gold was the last metallic mineral to be deposited at Venus. It shares mutual grain boundaries with, or replaces, arsenopyrite, pyrite, sphalerite, galena, tetrahedrite and pyrargyrite. Gold grains range in color from medium yellow white to deep yellow. A reflectance test at 547 Å on five gold grains indicate a native gold composition; however, an electron microprobe analysis on one gold grain at Venus shows the grain to have a composition closer to electrum (63.4:36.6, private company report). The largest gold grain observed is 110 μm by 110 μm. Grains larger than 80 μm are rare. Most gold grains are in the 10 μm to 40 μm size range.

Table 4 lists the most common type of occurrence for gold grains greater than 5 μm found in the polished mount study. Photomicrographs of gold grains are shown in Plates 3 to 6. Most gold at Venus precipitated with galena from late solutions which penetrated microfractures in, or replaced, earlier deposited arsenopyrite and pyrite. Gold also replaces, or is contemporaneous with tetrahedrite and pyrargyrite. Although gold precipitation was contemporaneous with galena, there is a strong spatial relationship between gold and arsenopyrite. Only one gold grain was found enclosed by quartz, and this was very close to an arsenopyrite grain being replaced by galena and gold. More gold and galena was observed infilling fractures in arsenopyrite than in pyrite. This could be a function of arsenopyrite being more brittle and therefore more susceptible to microfracturing.

The spatial relationship between gold and arsenopyrite-pyrite is so pronounced that gold was not observed in polished mounts composed entirely of massive sphalerite and galena. Gold content is highest in polished mounts that consist of arsenopyrite and pyrite in narrow one to two mm wide veinlets separated by quartz, and infiltrated or replaced by a small amount of late stage sphalerite-galena-gold. Arsenopyrite and pyrite grains in polished blocks that contain a high (five to twenty occurrences) amount of gold are generally euhedral and relatively fresh, with little or no signs of oxidation (i.e. worm texture). Tight microfractures

Table 4. Occurrences of gold grains (>5μm).

Number of gold grains	Occurrence
109	With galena (or more rarely, tetrahedrite or pyrargyrite) as fracture fillings in arsenopyrite or pyrite
61	With galena (or tetrahedrite or pyrargyrite) replacing arsenopyrite and pyrite
40	As a replacement bleb in arsenopyrite or pyrite with galena blebs in the same grain
22	Along grain boundaries between quartz and sulphides, or between two sulphide grains
21	Filling euhedral interstial space between grain boundaries
6	As isolated blebs in arsenopyrite or pyrite
11	Other

Plate 3. Polished block L-84-30 from the 2850' level. Gold and minor galena have infilled microfractures in, and replaced arsenopyrite.

Plate 4. Polished block L-84-21 from the 2850' level. Galena and gold have replaced arsenopyrite. Gold also occurs at the boundary between quartz and arsenopyrite.

Plate 5. Polished block L-83-16 from the 2700' level. Galena and gold have infilled corrosion openings in arsenopyrite.

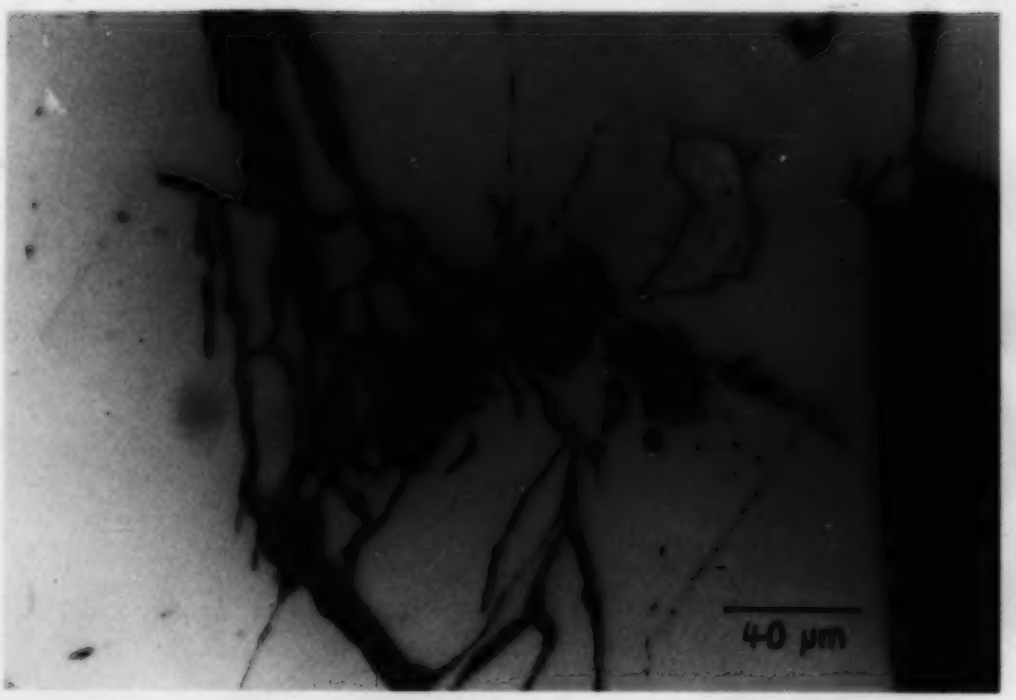

Plate 6. Polished block L-84-208 from the 2800' level. Tetrahedrite and gold have infilled fractures in arsenopyrite. Gold has replaced arsenopyrite and pyrite.

in both minerals are essential for infilling by galena and gold. Many polished mounts fitting the above description were taken from parts of the vein close to massive injections of quartz, sphalerite and galena.

F. Paragenetic Sequence and Discussion

The general depositional sequence at Venus is shown by the idealized paragenetic diagram in Figure 4. The paragenetic sequence can be divided into two stages. Stage I mineral phases were deposited first, and consist of quartz, arsenopyrite and pyrite. Most vein material was deposited during this stage. Stage II was deposited after Stage I, and consists of quartz, sphalerite, galena, gold and other opaque minerals (in trace amounts). The existence of two paragenetically distinct stages does not imply two separate fluids, but instead a gradual evolution from an early mineralizing fluid which deposited quartz, arsenopyrite, and pyrite, to a later, more evolved fluid which deposited quartz, sphalerite, galena, and gold. The sequence of deposition appears to be fairly consistent, although reversals were noted in some parts of the vein, where arsenopyrite and pyrite crosscut sphalerite and galena.

The strong spatial relationship between gold and arsenopyrite-pyrite has been noted previously by Ralfs (1975); however, the paragenetic link between gold and galena is only obvious when gold mineralization is observed directly in polished mounts. For instance, Plate 2 shows assays across arsenopyrite-pyrite rich and sphalerite-galena rich parts of a ore shoot. Gold grades are higher in the arsenopyrite-pyrite portion of the vein, even though gold and galena precipitate together.

Well developed ore shoots, such as the one shown in Plate 2, contain macroscopic arsenopyrite-pyrite and sphalerite-galena. Some parts of the vein contain only typical quartz-arsenopyrite-pyrite on visual examination, but show high gold assay values. Polished mount studies show that Stage II sphalerite-galena-gold mineralization is present in microscopic amounts. Even trace amounts of galena, visible only under high magnification, indicate that gold may also be present. This is relected in scattergrams of Au vs As, and Au vs Pb (Prince *pers. comm.*, 1984). There is a high correlation between Au and As, and a low

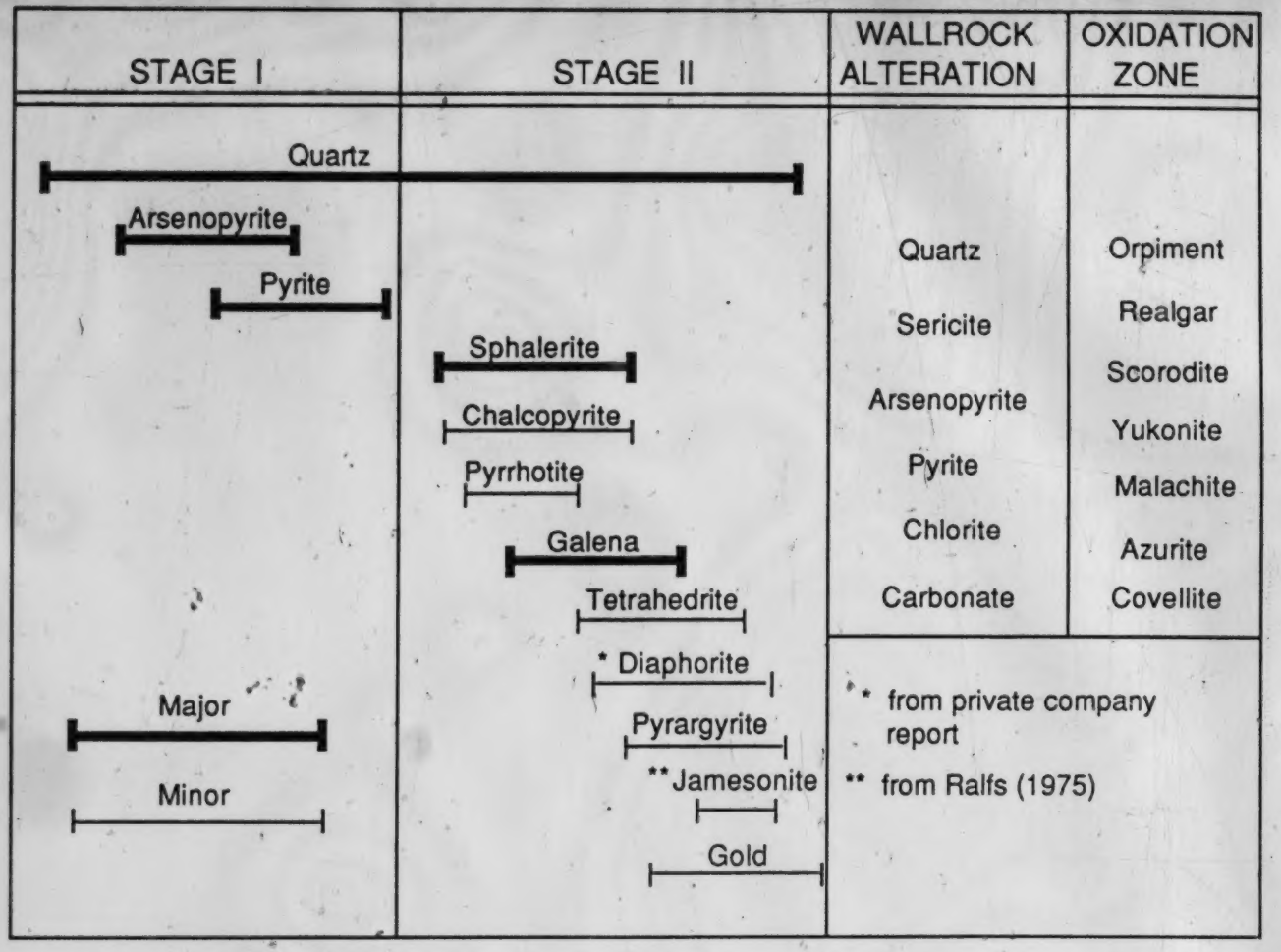

Figure 4. Idealized paragenetic sequence of the Venus vein.

correlation between Au and Pb. The high correlation between gold and arsenopyrite masks the gold-galena relationship found in this study. The implication is that earlier deposited sulphides appear to act as site controls for later gold deposition.

V. FLUID INCLUSIONS

A. Introduction

The object of the fluid inclusion study was to determine the composition, temperature, density and pressure of the fluids responsible for mineral deposition. It was hoped that fluid inclusion analyses of minerals deposited from both paragenetic stages would reveal any spatial or temporal variation in the environment of mineral deposition. Vein quartz and sphalerite samples for fluid inclusion analysis were collected from underground and surface exposures of the Venus vein. A sample location map is shown in Appendix 2. Primary fluid inclusions (defined using the criteria outlined by Roedder, 1984) were found in most of the chips, and were assumed to be representative of the original hydrothermal fluid. Available P-V-T-X data were used in conjunction with temperatures obtained by microthermometry to characterize the physical and chemical environment during mineral deposition. All microthermometric results were interpreted under the assumption that the inclusion has remained a system of constant volume and composition (Roedder and Bodnar, 1980).

The Venus deposit formed in two stages, with gold being deposited late in the second stage. The assignment of a fluid inclusion to any one particular paragenetic stage is therefore critical. The Venus vein formed by multiple fluid injections, and even a single fluid inclusion chip contains evidence for several periods of quartz deposition. To help determine the relationship between the inclusion being studied, and the actual gold depositing fluid, all samples for fluid inclusion analysis were divided into two categories. Stage I inclusions were assumed to contain fluids representative of the early hydrothermal fluid at Venus. The fluid in Stage II inclusions was assumed to be representative of the gold depositing fluid.

The criteria used for assignment of a paragenetic stage to any one field of fluid inclusions were:

1. The mineralogy and assay values of the part of vein from which the sample was taken.

Low grade gold parts of the vein containing quartz, arsenopyrite, and pyrite yielded Stage I inclusions. High grade gold parts of the vein containing quartz, sphalerite, and galena are paragenetically later than Stage I, and contain Stage I and Stage II inclusions.

2. Petrography - the polish on the fluid inclusion chips was of high enough quality so that gold grains could be located using reflected light. The quartz veinlets containing gold grains were assumed to contain Stage II inclusions. In practice, this technique was used only twice, since most gold grains occur as fracture fillings or replacement blebs in arsenopyrite, and it was impossible to trace the related quartz veinlet.

---

3. Inclusions in sphalerite were assigned to Stage II. Most of the gold was deposited later than sphalerite, but inclusion fluids from sphalerite are probably closer in character to the gold depositing fluid than Stage I fluids.

4. Secondary inclusions were analyzed in addition to primary inclusions, since gold was introduced later than the bulk of the quartz.

Abbreviations used in this chapter are:

$TmCO_2$ = final melting temperature of CO_2

Te = eutectic temperature of inclusion brine (first melt)

TmIce = final melting temperature of ice (last melt)

TmClath = final melting temperature of CO_2 clathrate

$ThCO_2$ = homogenization temperature of CO_2

Td = decrepitation temperature

Th = final homogenization temperature (between H_2O and CO_2 or between H_2O and vapor)

B. Analytical Technique

A U.S.G.S. gas-flow heating/freezing stage purchased from Fluid Inc. was used for microthermometry. The stage was slightly modified at the University of Alberta (Murowchick *pers. comm.*, 1986). Descriptions of the U.S.G.S. stage are given by Roedder (1984) and Shepherd *et al.* (1985). The stage operates by passing pre-heated or pre-cooled gas over and around the sample chip, which is held in place by a thin, thermocouple wire. Major temperature corrections are not necessary due to the low thermal mass of the stage. Precise homogenization and melting temperatures can be obtained by quick temperature cycling using an attached pedal.

Petrographic descriptions of the inclusions were made using a Leitz microscope attached to the heating/freezing stage. 10X periplan oculars in combination with 4X, 10X and 32X objectives were used for fluid inclusion observations.

A total of 35 doubly polished fluid inclusion chips, consisting of quartz or quartz and sphalerite were made. Some chips (#12,50,267,279,538) contain inclusions too small for microthermometric analysis. Most of the quartz chips yielded inclusions for examination, but suitable sphalerite hosted inclusions were very difficult to find due to the dark brown color of most sphalerite grains.

A sketch of each chip and a general petrographic description of the inclusions in the chip were made before breaking the chip into smaller pieces. Each smaller chip was used only once in a heating-freezing run, although the phase changes in the inclusions being observed were checked at least twice for reproducibility.

Measurements of all melting and homogenization temperatures were repeated at least twice to test for reproducibility. Replicate measurements for $TmCO_2$ were within ± 1°C. Replicate measurements for Te and TmIce were within ± 3°C, and within ± 2°C for TmClath. $ThCO_2$ was difficult to measure; the reproducibility of measurements was ± 3°C. Reproducibility of final homogenization temperatures for both Type 1 and Type 2 inclusions

was usually better than ±1°C for temperatures between 200°C and 320°C.

All melting measurements during the freezing run were made first. All inclusions were cooled to -120°C, and then slowly heated. When the temperature approached within 10°C of important phase changes, the warming rate was slowed to +0.2 to +0.4°C/min. below the expected Th, and the sample was allowed to equilibrate. The sample was then heated at a constant rate of +0.3 to 0.4°C/min. Any inclusion that showed signs of leakage, either during initial petrographic work, or during heating/freezing runs was ignored. Table 5 lists the melting and heating measurements for all inclusions.

C. Inclusion Petrography

The general nature of the inclusions in each chip was described, and a sketch was made of the field of inclusions to be studied during heating/freezing runs. The inferred origin, type, inclusion length, inclusion width, vapor bubble diameter and the estimated volume percent of each phase (at room temperature and at 40°C) were noted. The method used for volume estimates is discussed in a later section.

Samples of quartz in the fluid inclusion studies ranged from coarse-grained, relatively clear euhedral crystals to crushed or strained quartz containing numerous shears, defined by small secondary fluid inclusions. The shears crosscut grain boundaries and, in some samples, crosscut each other. Identification of primary, secondary and pseudosecondary inclusions was based on the criteria suggested by Roedder (1984). In general, large isolated inclusions were assumed to be primary. Primary inclusions also occur in planar arrays outlining primary growth direction. Most primary inclusions studied are small (averaging 10 x 8 μm) in size. Larger primary inclusions (up to 30 μm long) are generally irregular in shape. Smaller inclusions are often oblate. Large, primary inclusions are commonly located in quartz intergrown with galena or sphalerite.

Useable primary fluid inclusions in sphalerite are very rare and difficult to see, due to the dark brown color of most sphalerite grains. Primary inclusions in sphalerite are generally large (>20 μm) and commonly show a negative crystal shape. Although heating/freezing runs

Table 5. Fluid inclusion measurements.

Sample No./ Chip/ Inclusion	Host	Para. Stage	Origin	Type	Vol. %	Te	Tm CO_2	Tm Ice	Tm Clath	Th CO_2	Th
Surface											
5009-A-1	Q	?	P	2a	7	*	*	*	+8.0	*	+225.7 (H)
5009-A-2	Q	?	P	2a	5	*	*	*	+8.3	*	*
5059-A-2 (VES)	Q	?	P	2a	15	*	*	*	+8.4	*	*
5068-B-1 (UT)	Q	?	P	1a	5 (L)	*	*	*	*	*	+210.7 (L)
5068-B-2	Q	?	S	1b	2 (L)	*	*	*	*	*	+223.2 (L)
5068-B-3	Q	?	S	1b	1 (L)	*	*	*	*	*	+208.4 (L)
5068-B-4	Q	?	S	1b	2 (L)	*	*	*	*	*	+184.3 (L)
5068-B-5	Q	?	S	1b	3 (L)	*	*	*	*	*	+200.1 (L)
5068-B-6	Q	?	S	1b	3 (L)	*	*	*	*	*	+191.8 (L)
5068-B-7	Q	?	P ?	1a	5 (L)	*	*	*	*	*	+229.6 (L)
2850 Level											
38-A-1	Q	II	P	2c	10	*	-56.6	*	+8.0	+28.5 (L) ?	+255.5 ?
38-B-1	Q	II	P ?	2a	30	*	-57.0	*	*	+26.7 (L)	+276.6 (L)
38-B-2	Q	II	PS	1b	2 (L)	*	*	-3.5	*	*	*
89-A-1	Q	I	P	2a	40	*	-56.8	*	+8.5	+26.2 (L)	+270.6 (H)
89-B-1	Q	I	P	2a	25	*	-56.8	*	+8.2	+25.3 (L)	+316.0 (F)
89-B-3	Q	I	S	1a ?	2 (L)	*	*	*	*	*	+291.2 (L)
89-B-5	Q	I	S	2c	8	*	-56.5	*	*	*	+313.0 (L)
96-A-1	Q	II	P	2a	20	*	-56.7	*	+8.6	+27.6 (L)	+242.7 (L)
96-A-2	Q	II	P	2a	20	*	-56.7	*	+8.6	+27.6 (L)	+242.7 (L)
96-A-3	Q	II	P	2a	15	*	*	*	*	*	+292.0 (L)
97-A-1	Q	II	P	2a	15	*	-56.9	*	+8.2	+27.0 (L) ?	+262.0
97-A-2	Q	II	P	2a	10	*	-56.6	*	*	*	+270.1 (L)
97-A-3	Q	II	S	2c	2	*	-56.7	*	*	*	+225.3 (H)

Sample No./ Chip/ Inclusion	Host	Para. Stage	Origin	Type	Vol. %	Te	Tm CO_2	Tm Ice	Tm Clath	Th CO_2	Th
97-A-5	Q	II	P	2a	15	*	-56.6	*	+8.2	+26.2 (L)	*
106-A-1	Q	II	P	2c	20	*	-58.0	*	+9.6	*	+233.3 (H)
106-A-2	Q	II	P	2c	20	*	-59.9	*	+8.2	+25.6 (?)	+252.1 (H)
106-A-3	Q	II	P	2c	20	*	-60.3	*	+9.3	*	+233.8 (F)
115-A-1	S	II	P	3	3 (L)	*	*	-4.6	*	*	*
115-A-2	S	II	P	1a	3 (L)	-26.5	*	-3.3	*	*	*
115-A-3	S	II	P	1b	2 (L)	*	*		*	*	+177.8 (L)
115-A-4	S	II	P	1b	3 (L)	*	*	-3.0	*	*	+184.2 (L)
115-A-5	S	II	P	3	3 (L)	*	*	-3.7	*	*	+172.6 (L)
122-A-1	Q	I	S	1a	5 (L)	*	*	-3.1	*	*	+186.0 (L)
122-A-2	Q	I	S	1a	5 (L)	*	*	-3.0	*	*	+186.1 (L)
122-B-1	Q	I	P	2a	25	*	-57.1	*	+8.6	+25.7 (L)	+280.0 (F)
122-B-2	Q	I	P	2a	25	*	-56.9	*	+8.5	+26.2 (L)	+300.3 (L)
122-B-3	Q	I	P	2a	20	*	-56.8	*	*	+26.3 (L)	+290.6 (L)
122-B-4	Q	I	P	1a	5 (L)	*	*	-3.2	*	*	+212.3 (L)
2800 Level											
217-A-1	Q	II	P	2a	40	*	-56.6	*	*	*	+258.6 (L)
217-A-2	Q	II	P	1b	2 (L)	*	*	-4.0	*	*	*
217-A-3	Q	II	P	2a	25	*	-56.7	*	+8.0	*	+241.3 (H)
217-A-4	Q	II	P	2c	25	*	-56.5	*	+8.0	*	+244.5 (H)
217-A-5	Q	II	P	2a	30	*	-56.4	*	+7.9	+28.8 (L)	+271.6 (H)
217-A-6	Q	II	P	2a	30	*	*	*	*	*	+246.5 (H)
217-A-7	Q	II	P	2c	33	*	*	*	*	*	+243.0 (H)
235-A-2	Q	I	P	2c	15	*	*	*	+8.2	*	+212.8 (H)
235-B-1	Q	I	P	1a ?	15 (L)	*	*	*	*	*	+212.0 (L)
235-C-1	Q	I	P	2a	30	*	-57.2	*	+8.9	+28.2 (F)	+270.2 (L)
235-D-1	Q	I	P ?	1a	10 (L)	*	*	*	*	*	+196.8 (L)

Sample No./ Chip/ Inclusion	Host	Para. Stage	Origin	Type	Vol. %	Te	Tm CO_2	Tm Ice	Tm Clath	Th CO_2	Th
235-D-2	Q	I	S	1b	10 (L)	•	•	•	•	•	+176.0 (L)
253-A-1	Q	I	PS	1a	10 (L)	-20.9	•	•	•	•	+151.4 (L)
253-A-2	Q	I	PS	1a	7 (L)	•	•	-2.0	•	•	+163.2 (L)
253-A-3	Q	I	PS	1a	8 (L)	•	•	-1.1	•	•	+142.7 (L)
253-A-4	Q	I	PS	1a	9 (L)	•	•	-2.0	•	•	+154.1 (L)
253-A-5	Q	I	PS	1a	8 (L)	-16.0	•	•	•	•	+158.3 (L)
253-A-6	Q	I	PS	1a	10 (L)	•	•	-1.4	•	•	•
262-A-1	Q	II	P	2a	15	•	-56.5	•	+7.4	+28.0 (L)	+255.5 (L)
262-A-3	Q	II	PS	2b	50	•	-56.4	•	•	•	+255.0 (L)
262-A-4	Q	II	PS	2c	30	•	-56.5	•	+7.6	+24.5 (L)	+251.9 (H)
262-A-5	Q	II	P	2c	25	•	•	•	+7.7	+27.3 (L)	+235.2 (H)
262-A-6	Q	II	PS	2c	20	•	-56.6	•	+7.5	+26.6 (L)	•
262-A-7	Q	II	PS	2a	15	•	-56.6	•	+7.8	+28.7 (L)	+232.6 (H)
278-A-1	Q	II	P	1a	5 (L)	-17.6	•	•	•	•	•
278-A-2	Q	II	P	2a	15	•	-56.5	•	+7.2	+29.1 (F)	+306.8 (H)
278-A-3	Q	II	P	2a	20	•	-56.8	•	+7.2	•	+265.6 (L)
278-A-4	Q	II	P	2a	15	•	-56.5	•	+7.5	•	+275.3 (H)
278-A-5	Q	II	P	1b	2 (L)	-14.2	•	-3.1	•	•	+163.4 (L)
2700 Level											
435-A-1	Q	I	P	2a	30	•	-56.7	•	•	+25.2 (L)	+291.9 (L)
435-A-3	Q	I	P	2a	25	•	-56.8	•	+8.2	+25.8 (L)	+284.3 (L)
435-B-1	Q	I	S	1b	2 (L)	•	•	•	•	•	+205.0 (L)
435-B-2	Q	I	P	2b	50	•	-56.5	•	+7.9	+26.0 (L)	+266.7 (L)
435-B-5	Q	I	P	2a	35	•	-56.5	•	+8.0	+25.6 (L)	+265.6 (L)
414-A-1	Q	II	P	2a	30	•	-56.5	•	•	+28.9 (L)	+283.5
414-A-3	Q	II	S	1b	5 (L)	•	•	-3.4	•	•	•
414-A-4	Q	II	P	2a	10	•	-56.5	•	•	•	+274.8 (L)

Sample No./ Chip/ Inclusion	Host	Para. Stage	Origin	Type	Vol. %	Te	Tm CO_2	Tm Ice	Tm Clath	Th CO_2	Th
414-B-1	Q	II	P	2a	10	*	-56.4	*	*	+29.2 (L)	*
414-B-2	Q	II	P	2a	8	*	*	*	+7.3	*	+236.7 (H)
414-C-1	Q	II	P	2a	20	*	-56.5	*	+7.9	+28.7 (L)	+231.6
414-D-1	Q	II	P	2a	20	*	-56.6	*	+7.4	+26.9 (L)	+238.0
414-D-3	Q	II	P	2a	10	*	-56.7	*	+7.7	*	*
414-D-4	Q	II	P	2a	20	*	-56.6	*	+7.4	+28.1 (L)	+238.0
449-A-1	Q	II	P	1b ?	10 (L)	-15.0	*	-4.0	*	*	+230.1 (L)
449-A-2	Q	II	P	1b ?	10 (L)	*	*	-4.6	*	*	+188.5 (L)
449-A-3	Q	II	P	1b ?	10 (L)	-15.0	*	*	*	*	+238.6 (L)
449-A-4	Q	II	P	1b ?	8 (L)	-15.0	*	-3.6	*	*	+187.6 (L)
449-A-5	Q	II	P	1b ?	10 (L)	-27.8	*	*	*	*	+254.2 (L)
449-A-6	Q	II	P	1b ?	10 (L)	*	*	*	*	*	+221.1 (L)
449-A-7	Q	II	P	2c	10	*	*	*	*	*	+220.7 (H)
449-A-8	Q	II	P	2c	15	*	-56.7	*	+8.0	*	+255.2 (H)
449-A-9	Q	II	p	2c	10	*	-56.7	*	*	*	+245.6 (H)
474-A-1	Q	I	P	2a	40	*	-56.8	*	+8.3	+29.2 (L)	+291.0 (L)
474-A-2	Q	I	P	2a	20	*	-56.8	*	+8.2	+29.1 (L)	+291.0 (L)
474-A-3	Q	I	P	2a	20	*	-56.5	*	+8.2	+29.3 (L)	+280.0 (L)
474-A-4	Q	I	PS	2a	35	*	-56.8	*	+8.3	+29.3 (L)	+296.8 (H)
474-A-5	Q	I	PS	2a	30	*	-56.8	*	+8.3	+29.2 (L)	+297.2 (H)
474-A-6	Q	I	S	1b	1 (L)	-16.1	*	-2.9	*	*	+152.8 (L)
474-A-7	Q	I	S	1b	2 (L)	-16.1	*	-3.0	*	*	+148.9 (L)
474-A-8	Q	I	S	1b	2 (L)	*	*	*	*	*	+172.8 (L)
474-A-9	Q	I	S	1b	1 (L)	*	*	*	*	*	+170.1 (L)
474-A-10	Q	I	S	1b	1 (L)	*	*	*	*	*	+163.5 (L)
474-A-11	Q	I	S	1b	3 (L)	*	*	*	*	*	+189.9 (L)
474-A-12	Q	I	S	1b	2 (L)	-23.3	*	*	*	*	+160.2 (L)
474-A-13	Q	I	P	2c	60	*	-56.5	*	+8.2	*	*
474-A-14	Q	I	S	1b	2 (L)	-13.4	*	*	*	*	*
474-A-15	Q	I	P	2a	20	*	-56.5	*	+8.2	+29.4 (L)	+295.0 (L)

Sample No./ Chip/ Inclusion	Host	Para. Stage	Origin	Type	Vol. %	Te	Tm CO_2	Tm Ice	Tm Clath	Th CO_2	Th
494-A-1	Q	II	P	2a	40	•	-56.8	•	+8.1	+26.8 (L)	+268.6 (H)
494-A-2	Q	II	P	2b	65	•	•	•	+8.3	+23.8 (L)	•
494-A-3	Q	II	P	2a	30	•	-56.8	•	+8.3	+24.9 (L)	+253.0 (L)
494-A-4	Q	II	P	2a	20	•	-56.8	•	+8.2	+29.4 (L)	+255.2 (H)
494-A-5	Q	II	S	1b	2 (L)	-23.5	•	-4.3 ?	•	•	+186.5 (L)
494-A-6	Q	II	P	2a	40	•	•	•	+8.3	+24.2 (L)	+303.6 (H)
494-A-7	Q	II	PS	2b	65	•	-56.7	•	+8.3	+21.3 (L)	+308.0 (H)
494-A-8	Q	II	PS	1b	2 (L)	•	•	-4.3 ?	•	•	•
494-A-9	Q	II	P	2b	65	•	•	•	+8.3	•	•
494-B-1	Q	II	P	2a	20	•	-56.8	•	+8.3	+28.6 (L)	+240.3 (H)
494-B-2	Q	II	P	2a	10	•	-56.8	•	•	•	•
494-B-4	Q	II	P	2c	20	•	-56.7	•	+8.4	+28.5 (L)	+250.2 (H)
494-C-1	S	II	P	2a ?	30 ?	•	-57.5	•		•	+146.0
498-A-1	Q	II	PS	1a ?	8 (L)	-22.5	•	-4.4	•	•	+231.2 (L)
498-A-2	Q	II	PS	1a ?	10 (L)	-23.0	•	-4.3	•	•	•
498-A-3	Q	II	PS	1a ?	10 (L)	-23.4	•	•	•	•	•
498-A-4	Q	II	PS	1a ?	8 (L)	•	•	-4.2	•	•	+217.6 (L)
498-A-5	Q	II	PS	1a ?	10 (L)	-22.3	•	-4.3	•	•	+222.6 (L)
498-A-6	Q	II	PS	1a ?	10 (L)	-19.3	•	-4.2	•	•	+211.2 (L)
498-A-8	Q	II	PS	1a ?	8 (L)	•	•	-4.3	•	•	•
498-A-9	Q	II	PS	1a ?	10 (L)	-23.9	•	•	•	•	+220.8 (L)
498-A-10	Q	II	PS	2c	8	•	-56.4	•	•	•	+262.5 (H)
2650 Level											
728-A-1	Q	I	P	2a	30	•	-56.6	•	+8.3	•	+307.1 (H)
728-A-2	Q	I	S	1b	2 (L)	-22.0	•	•	•	•	+196.8 (L)
728-A-3	Q	I	P	2b	60	•	-56.8	•	+8.5	•	•
744-A-1	S	II	P	3	12 (L)	•	•	•	•	•	+211.5 (L)
776-A-1	Q	II	P	2a	40	•	-56.7	•	+9.0	+27.4 (L)	+284.6 (H)

Sample No./ Chip/ Inclusion	Host	Para. Stage	Origin	Type	Vol. %	Te	Tm CO_2	Tm Ice	Tm Clath	Th CO_2	Th
776-A-2	Q	II	P	2a	35	•	-56.4	•	+9.1	•	•
776-A-3	Q	II	P	2a	40	•	-56.6	•	+9.1	+28.7 (L)	+231.2 (H)
776-A-4	Q	II	P	2a	40	•	-56.6	•	+9.0	+28.7 (L)	+272.6 (H)
776-A-5	Q	II	P	2a	35	•	-56.8	•	+9.1	+29.4 (L)	+259.2 (H)
785-A-1	Q	I	P	2c	35	•	-56.6	•	+8.3	•	•
785-A-2	Q	I	P	2c	30	•	-56.6	•	•	•	+253.4 (H)
785-A-3	Q	I	P	2c	30	•	-56.7	•	+8.4	•	+248.6 (H)
785-A-4	Q	I	P	2c	30	•	-56.7	•	•	•	+252.7 (L)
785-A-5	Q	I	P	1b	20 (L)	-28.0	•	-4.2	•	•	+223.6 (L)
789-A-1	S	II	P	3	30 (L)	•	•	•	•	•	+208.8 (L)
789-A-2	S	II	P	2c ?	20	•	•	•	+7.0	+25.8 (V)	•
816-A-1	Q	I	S	1b	2 (L)	-26.8	•	+3.9 ?	•	•	•
816-A-4	Q	I	PS	2c	8	•	-56.7	•	•	•	•
816-A-5	Q	I	PS	2b	50	•	-56.8	•	+8.0	+28.4 (L)	+298.6 (H)
2600 Level											
1039-B-1	Q	II	PS	2c	5		•	•	+7.5	•	+204.3 (L)
1039-B-3	Q	II	P	1a	5 (L)	•	•	•	•	•	+216.4 (L)
1039-B-4	Q	II	P	2c	8	•	•	•	•	•	+205.5 (L)
1039-B-5	Q	II	PS	1a ?	8 (L)	-17.4	•	•	•	•	+201.4 (L)
1039-B-6	Q	II	P	1b	5 (L)	•	•	•	•	•	+180.6 (L)
1039-C-1	Q	II	P	2a	25	•	•	•	•	•	+249.0
1039-C-2	Q	II	S	1b	2 (L)	•	•	•	•	•	+197.6 (L)
1039-C-3	Q	II	P	2a	25	•	•	•	•	•	•
1039-C-4	Q	II	S	1b ?	5 (L)	•	•	•	•	•	+199.8 (L)
1041-A-1	Q	II	P	2a	10		-56.5	•	+7.8	+25.3 (L)	+255.1 (H)
1041-A-3	Q	II	P	2c	40	•	-56.5	•	+7.3	•	•
1041-A-4	Q	II	P	2c	20	•	-56.8	•	+7.7	•	+288.4 (H)

Sample No./ Chip/ Inclusion	Host	Para. Stage	Origin	Type	Vol. %	Te	Tm CO_2	Tm Ice	Tm Clath	Th CO_2	Th
1041-A-5	Q	II	S	1b	2 (L)	•	•	•	•	•	+213.5 (L)
1050-A-1	Q	I	PS	2a	30	•	-56.8	•	+8.4	+27.9 (L)	+282.0 (H)
1050-A-2	Q	I	PS	2a	30	•	-56.8	•	+8.4	+27.2 (L)	+248.7 (H)
1050-A-3	Q	I	PS	2a	15	•	-56.8	•	+8.5	+27.7 (L)	+284.5 (H)
1050-A-6	Q	I	S	1b	1 (L)	-15.2	•	•	•	•	+207.3 (L)
1063-A-1	Q	II	PS	1b	35	-15.2	•	-4.0	•	•	+172.0 (L)
1063-A-2	Q	II	PS	1b	3 (L)	•	•	-4.3	•	•	+153.2 (L)
1063-A-3	Q	II	P	2a	40	•	-56.7	•	+8.6	+28.8 (L)	+270.0 (H)
1088-A-1	Q	I	P	1a	10 (L)	-20.2	•	-4.0	•	•	•
1088-A-2	Q	I	P	1a	10 (L)	-20.2	•	•	•	•	•
1088-A-3	Q	I	P	2c	10	•	•	•	+8.6	•	•
1088-A-4	Q	I	P	1a	10 (L)	•	•	-2.6	•	•	+212.7 (L)
1088-A-5	Q	I	P	2c	10	•	-56.8	•	+8.6	•	•
1099-A-1	Q	I	P	2b	60	•	-56.9	•	+8.2	+26.6 (L)	+301.8 (H)
1099-A-2	Q	I	P	2b	60	•	-56.9	•	+8.2	+26.6 (L)	+300.4 (H)
1099-A-3	Q	I	S	1b	1 (L)	•	•	-2.0	•	•	+128.8 (L)
1099-A-4	Q	I	S	1b	2 (L)	•	•	-2.0	•	•	+196.8 (L)
1099-A-5	Q	I	P	2b	50	•	-57.0	•	+8.1	+28.7 (L)	+307.8 (H)
1099-A-6	Q	I	P	2b	50	•	-56.9	•	+8.1	+28.7 (L)	+305.6 (H)
1099-A-7	Q	I	P	2b	55	•	-56.8	•	+8.5	+27.9 (L)	+298.0 (H)
1099-A-8	Q	I	P	2b	50	•	-56.8	•	+8.5	+27.9 (L)	+298.0 (H)
1099-A-9	Q	I	P	2b	50	•	-56.8	•	+8.5	+27.9 (L)	+298.0 (H)
1099-A-10	Q	I	PS	2c	10		•	•	•	•	•
1099-A-11	Q	I	PS	2c	10	•	•	•	•	•	•
1099-B-1	Q	I	P	2c	25	•	-56.5	•	+8.1	•	+246.1 (H)
1099-B-2	Q	I	P	2b	50	•	•	•	+8.2	•	•
1099-B-3	Q	I	P	2c	70	•	-56.6	•	•	+27.5 (L) ?	•
1099-B-6	Q	I	S	1a ?	10 (L)	•	•	•	•	•	+204.8 (V)

Sample No./ Chip/ Inclusion	Host	Para. Stage	Origin	Type	Vol. %	Te	Tm CO_2	Tm Ice	Tm Clath	Th CO_2	Th
Other Veins											
Joe Petty											
JP-A-1	Q		P	2c	15		•	•	+7.6	•	+208.6 (H)
JP-A-2	Q		P	2c	10	•	•	•	•	•	+205.8 (H)
JP-A-3	Q		P	2c ?	10	•	•		•	•	+203.6 (H)
JP-A-4	Q		S	1b ?	5 (L)	-19.5	•	-4.3	•	•	+203.7 (L)
JP-A-5	Q		S	1b	5 (L)	•	•	-4.3	•	•	+166.9 (L)
JP-A-6	Q		S	1b	5 (L)	•	•	•	•	•	+192.4 (L)
JP-A-7	Q		S	1b	10 (L)	•	•	•	•	•	+206.8 (L)

Host mineral: Q=Quartz
S=Sphalerite

Para. Stage: Paragenetic Stage (Stage I or Stage II)

Origin: P=Primary
S=Secondary
PS=Pseudosecondary

Vol. %: (L)=volume percentage of CO_2 bubble in Type 2 inclusion or vapor bubble in Type 1 inclusion

$ThCO_2$: (L)=homogenized to liquid phase
(F)=faded near homogenization temperature

Th: (H)=homogenized to H_2O (Type 2 inclusions)
(F)=faded near homogenization temperature
(L)=homogenized to aqueous phase (Type 1 inclusions)
Bold numbers=decrepitation temperature

were done on several inclusions in sphalerite, temperature measurements were obtained from inclusions in only three chips (115-A,494-C,789-A).

Secondary inclusions in quartz often occur as flat, irregular shaped inclusions located in healed fractures cutting grain boundaries. Small (<5 μm) secondary fluid inclusions are generally oval in shape. Secondary inclusions in sphalerite are generally flat and irregular in shape.

Types of Inclusions

Two types of fluid inclusions were recognized, based on appearance at room temperature, and behavior during heating or cooling. Figure 5 shows representative drawings of each inclusion type. Figure 6 shows drawings of fluid inclusion fields from selected chips.

Type 1. Liquid-Vapor inclusions

Type 1 inclusions are characterized by two visible phases at room temperature (aqueous brine + vapor bubble). Neither solid CO_2 or CO_2 clathrate nucleated during freezing. Type 1 inclusions can be subdivided into two types:

Type 1a:

Liquid-vapor inclusions containing a vapor bubble which constitutes 5 to 40 percent of the total volume.

Type 1b:

Liquid-vapor inclusions containing a vapor bubble constituting less than 5 percent of the total inclusion volume. This type of inclusion is often secondary, irregular in shape, and flat.

Type 2. H_2O-CO_2 inclusions

Type 2 inclusions are characterized by the presence of CO_2. Type 2 inclusions can be divided into three types:

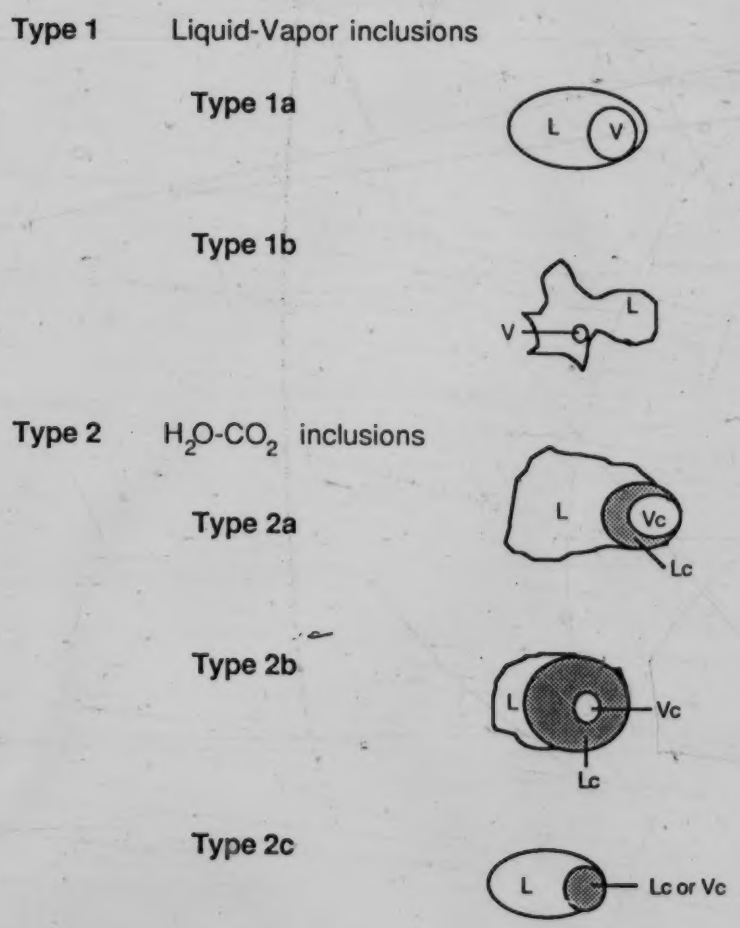

Figure 5. Types of fluid inclusions.

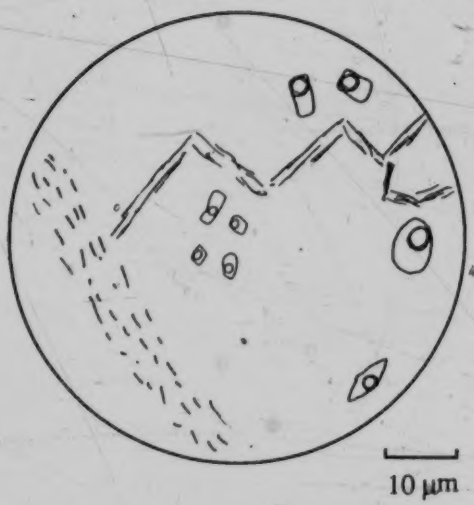

Chip 449 - consistent liquid-vapor ratio in primary Type 1 inclusions and Type 2c inclusions.

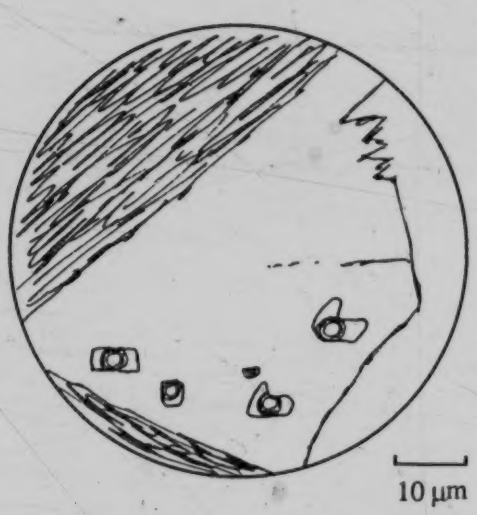

Chip 776 - consistent H_2O-CO_2 ratio in primary Type 2 inclusions

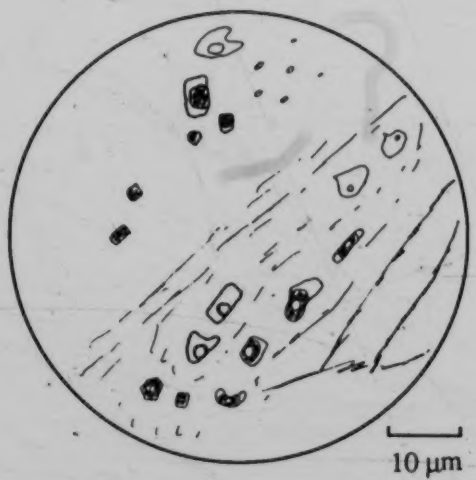

Chip 1099 - shows variable H_2O-CO_2 phase ratios in Type 2 inclusions. Also shows secondary Type 1a and Type 1b inclusions.

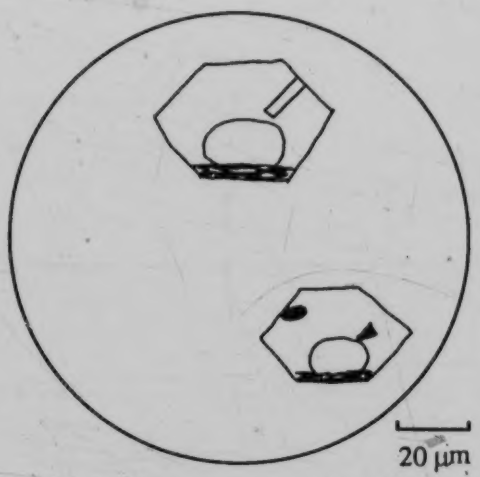

Close-up of sphalerite hosted inclusions with daughter crystals

Figure 6. Modes of occurrence for fluid inclusions.

Type 2a:

This type of inclusion contains three visible phases at room temperature (H_2O, CO_2 liquid and CO_2 vapor). The CO_2 vapor bubble constitutes less than 50 percent of the total inclusion volume (estimated visually).

Type 2b:

H_2O-CO_2 inclusions that contain a vapor bubble constituting greater than 50 volume percent CO_2 (estimated at room temperature).

Type 2c:

H_2O-CO_2 inclusions that appear to contain two phases at room temperature. A third phase (most often CO_2 vapor) may nucleate on cooling. The CO_2 vapor bubble constitutes 5 to 40 volume percent of the total inclusion.

Type 2a inclusions are volumetrically the most abundant type of inclusion. Type 1b inclusions are usually secondary inclusions, commonly located in healed fractures. Type 1a and Type 2c inclusions look very similiar at room temperature. If the vapor bubble contracted on cooling, and no CO_2 or CO_2 clathrate nucleated, then the inclusion was classified as a Type 1a (liquid-vapor inclusion). If a new vapor or liquid phase nucleated on cooling, or if $TmCO_2$ or TmClath was noted, then the inclusion was classified as Type 2 H_2O-CO_2.

No daughter crystals were found in any quartz hosted inclusions. Three sphalerite hosted inclusions (115-A-1,115-A-5,789-A-1) contained unidentified daughter crystals (Figure 6). The daughter crystals were black and either oval or triangular in shape. Rye and Sawkins (1974) describe similiar daughter crystals in sphalerite hosted inclusions from the Casapalca Ag-Pb-Zn-Cu deposit in Peru, and suggest that they might be tetrahedrite or chalcopyrite.

D. Phase Changes at Low Temperatures

Eutectic Temperature

Each fluid inclusion brine is characterized by a eutectic minimum, which can be used to estimate what ionic species are present in the fluid. The eutectic temperature of an inclusion is measured at the first appearance of liquid after complete freezing.

Measurement of Te was difficult to determine because of the small size of the inclusions being measured. Another difficulty was that the amount of melt formed at the eutectic temperature was generally very small. This is characteristic of low salinity fluids, when the bulk composition of the system lies far from the eutectic temperature (Crawford, 1981).

Twenty-eight values of Te were obtained from Type 1 liquid-vapor inclusions. A histogram of the results is shown in Figure 7. Most values were between -15 and -25°C. This is within the range for the eutectic temperature of -20.8°C for a pure H_2O-NaCl solution (Crawford, 1981). The addition of KCl to a H_2O-NaCl brine lowers the eutectic to -22.9°C (Crawford, 1981), which is also within the range of the measured Te values. The addition of $CaCl_2$ or $MgCl_2$ results in a much greater depression of the eutectic temperature (H_2O-$MgCl_2$=33.6 °C, H_2O-$CaCl_2$=49.5°C) than is indicated by the results.

Final Melting Temperature of CO_2

The melting point of CO_2 in Type 2 inclusions was measured to determine if CH_4 is present in the fluid. At room temperature, CO_2 and CO_2-CH_4 inclusions are indistinguishable. The presence of CH_4 can only be detected by observing the low temperature behavior of an inclusion. The addition of CH_4 lowers the melting point of CO_2 (-56.6°C) and extends the temperature interval over which $TmCO_2$ takes place (Burruss, 1981). The amount of reduction in $TmCO_2$ from -56.6°C gives only a semi-quantitative estimate of the bulk composition. CH_4 is strongly partitioned into the CO_2 vapor bubble, and the measured $TmCO_2$ relates only to the CH_4 depleted liquid phase (Burruss, 1981). To calculate the true

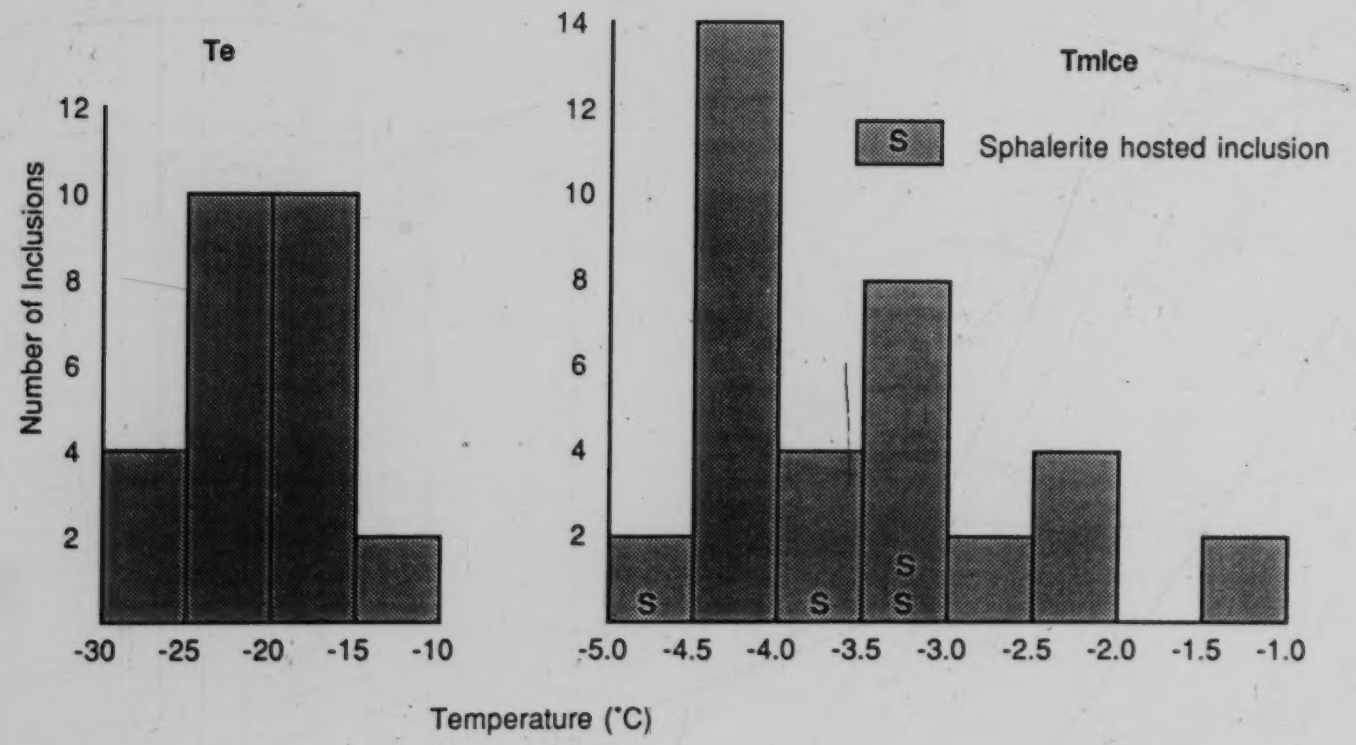

Figure 7. Te and Tmlce temperatures from Type 1 inclusions.

CH_4 content, the $ThCO_2$ must be measured and used in conjunction with $TmCO_2$. These values are compared with known P-V-T-X data for CO_2-CH_4 systems to obtain mole percent CH_4.

The recognition of CH_4 in inclusion fluids is particularly important when calculating salinities in the H_2O-CO_2-NaCl system. The effects of NaCl and CH_4 on salinity are opposite, so TmClath measurements alone cannot be used for calculating salinities if CH_4 is present in the fluid (Burruss, 1981).

Eighty-six values for $TmCO_2$ in Type 2 inclusions are plotted as a histogram in Figure 8. Most inclusions had $TmCO_2$ between -56.5°C and -57.0°C. The average $TmCO_2$ value is -56.8°C ± .55°C. Three inclusions (106-A-1,106-A-2,106-A-3) have a lower $TmCO_2$ (-58.5°C,-60.4°C,-60.8°C) compared to other Venus inclusions. For these three inclusions, the $TmCO_2$ results have to be compared with TmClath in order to verify the presence of CH_4 in the chip (see next section).

Final Melting Temperature for CO_2 Clathrate

Measurement of TmClath was attempted for all Type 2 inclusions. CO_2 clathrate forms as a result of interaction between the H_2O and CO_2 (liquid + vapor) components of an inclusion (Collins, 1979). Increasing the NaCl content decreases the chemical potential of the water, thereby lowering the temperature of formation of the clathrates (Burruss, 1981). Clathrates are solid compounds in which CO_2 gas molecules are encaged in cavities within a crystal lattice of water. Any salts or ions in solution such as NaCl are rejected from the clathrate lattice. TmIce measurements recorded in the presence of clathrates results in an overestimation of salinity due to the removal of water from the aqueous phase during clathration (Collins, 1979).

Collins (1979) describes the effect of clathration on salinity, and suggests using the final melting temperature of the clathrate to calculate salinity. A pure H_2O-CO_2 solution would show a TmClath of +10.0°C (Collins, 1979). However, with increasing salinity, the clathrate melting temperature is depressed, and the following formula from Bozzo *et al.*

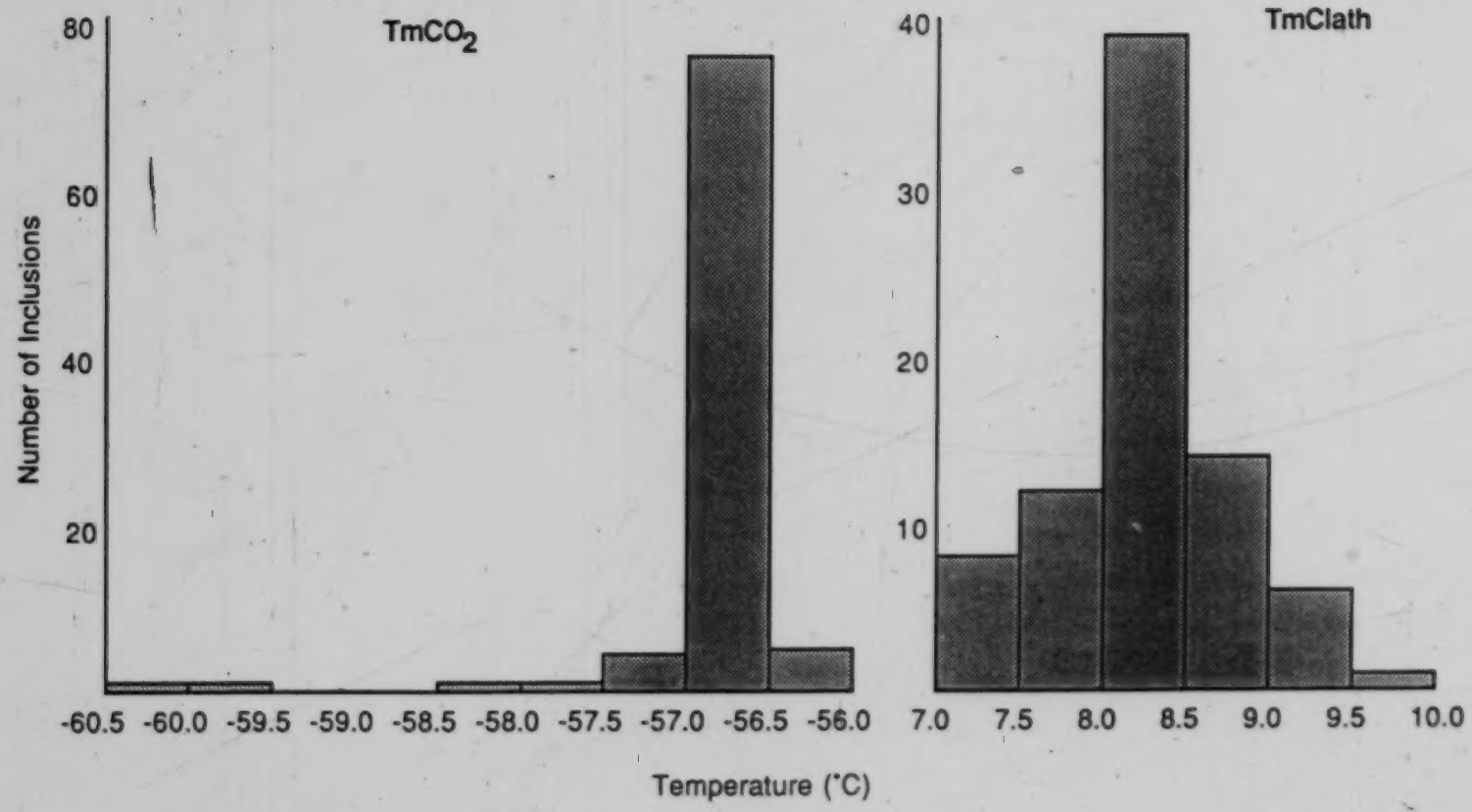

Figure 8. $TmCO_2$ and TmClath temperatures from Type 2 inclusions.

(1975) for H_2O-CO_2-NaCl solutions can be used:

$$W = 15.52023 - 1.02342(TmClath) - 0.05286(TmClath)^2$$

Where: W = weight percent NaCl in solution

TmClath = final melting temperature of CO_2 clathrate (°C)

The technique described by Collins (1979) for measuring TmClath was used in this study. The inclusion is warmed slowly until just prior to the suspected decomposition of the clathrate, then the inclusion is quickly cooled. If a clathrate is still present, it will renucleate on cooling and deform the interface between CO_2 and the aqueous fluid. The procedure is repeated at temperature increments of +0.1°C until the clathrate is completely decomposed and does not renucleate on cooling.

TmClath values are plotted as a histogram in Figure 8. Figure 9 is a histogram showing the weight percent NaCl equivalent values after the above formula is applied to the raw TmClath values. The average TmClath value is +8.2°C ± .48°C. which corresponds to an average salinity of 3.6 weight percent NaCl equivalent. There is a range in TmClath values from +7.0 to +9.6°C. Almost half (39 out of 80) of the values are between +8.0 and +8.5°C, which corresponds to a salinity of 3.0 to 4.0 weight percent NaCl. Except for chip 106-A (TmClath = +8.2 to +9.6), the TmClath values for any one chip are within a range of ± 5°C.

If CH_4 is present in the inclusion then TmClath cannnot be used to estimate salinity (Collins, 1979). CH_4 raises the upper temperature limit of CO_2 hydrate melting, thereby countering the effect of NaCl, which decreases the temperature limit of CO_2 clathrate. A TmClath value of over +10.0°C indicates another gas, such as CH_4, is present in the inclusion. There are no TmClath values above +10.0°C listed in Table 5. The highest two values are +9.3 and +9.6°C. The elevated TmClath values for these two inclusions corresponds to a depressed $TmCO_2$.

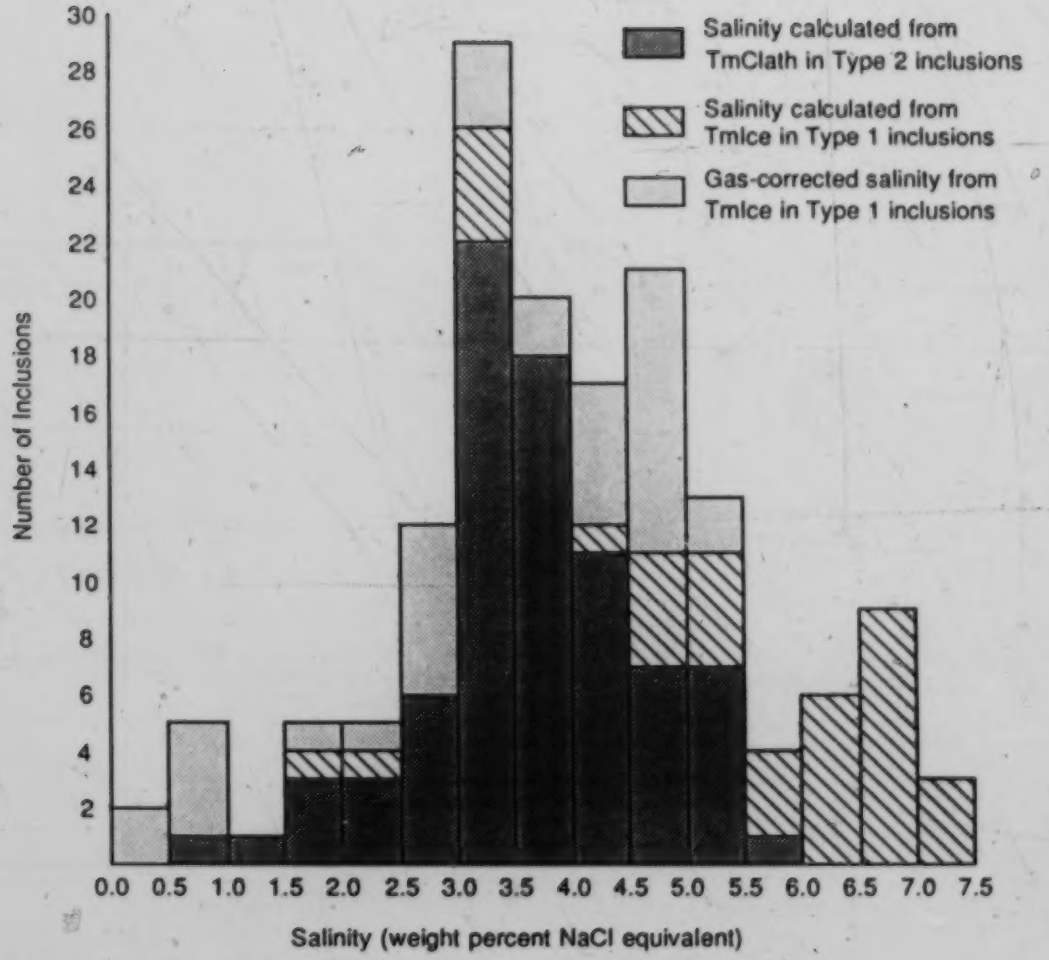

Figure 9. Salinity (weight percent NaCl equivalent) estimates for Type 1 and Type 2 inclusions.

The shifts in $TmCO_2$ and TmClath for inclusions 106-A-1 and 106-A-3 suggest that a small amount of methane may be present. Inclusion 106-A-2 from the same chip has a TmClath in the average range for Venus, therefore the evidence for the presence of methane in this chip is inconclusive.

Final Melting Temperature of Ice

The final melting temperature of ice was measured in Type 1 inclusions by supercooling the inclusion, then observing the TmIce on reheating. In the H_2O-NaCl system, the lowering of the freezing point of pure water is directly proportional to the amount of salt in solution. The final melting point of ice is measured instead of the freezing point of ice because most inclusions have to be supercooled in order to freeze (Crawford, 1981).

TmIce was difficult to measure in most inclusions. The technique described by Roedder (1984) was used to more easily recognize ice crystals. In this method, the inclusion is allowed to warm up to -10°C, then the heating rate is slowed to +0.3 to +0.4°C/min. The temperature is then held at several degrees below the suspected TmIce, in order to allow a large ice crystal to form.

The raw results are plotted as a histogram in Figure 7. TmIce ranged from -5.0 to -1.0°C, with most inclusions showing a TmIce of -3.0 to -4.5°C. The average TmIce value is -3.4 ± .93°C. There was no variation in TmIce between Type 1a and Type 1b inclusions, or between inclusions representative of Stage I quartz, and inclusions representative of Stage II quartz.

The TmIce results were converted to salinity using the following formula given by Potter *et al.* (1978).

$$W = 0.00 + 1.76957T - (4.2374 \times 10^{-2})T^2 + (5.2778 \times 10^{-4})T^3$$

Where W = weight percent NaCl equivalent in solution

T = freezing point depression in °C

The results are plotted as part of histogram on Figure 9. The measured salinity for Type 1 inclusions ranges from 1.5 to 7.5 weight percent NaCl equivalent. The average salinity is 5.5 weight percent NaCl equivalent. Figure 9 shows that the salinities calculated from TmIce are considerably higher than the salinities calculated using TmClath.

Hedenquist and Henley (1985), show that dissolved CO_2 in the H_2O-CO_2 system may result in the lowering of the ice melting temperature without the formation of visible CO_2 liquid or CO_2 clathrate on cooling. The dissolved CO_2 may escape detection during routine fluid inclusion studies, and yet may contribute up to -1.5°C to the depression of the melting point of dilute fluids. If CO_2 is present in small amounts in Type 1 inclusions, the apparent salinity (the salinity calculated using TmIce) will be higher than the actual salinity.

Gas corrected salinities range from 0 to 5.5 weight percent NaCl equivalent and average 3 to 5 weight percent NaCl equivalent (Figure 9). The gas corrected salinities more closely match the salinities calculated from TmClath, but the CO_2 correction may not be necessary. An increase in salinity (shown by the uncorrected TmIce values) would be expected due to vapor loss during sporadic phase separation (see next section). The increase in salinity exhibited in Figure 9 is therefore assumed to be real, and not a function of dissolved CO_2 in the aqueous phase.

E. Heating Measurements

Homogenization temperatures were determined using the "cycling" method for the U.S.G.S. heating/freezing stage. Final homogenization temperatures (Th) and CO_2 homogenization temperatures ($ThCO_2$) are listed in Table 5 and plotted as histograms in Figure 10 and Figure 11.

H_2O-CO_2 inclusions have high internal pressures which can exceed the strength of the walls of the host mineral, depending on the size (Leroy, 1979) and composition of the inclusion fluid (Burruss, 1981). Decrepitation of Type 2 inclusions was a problem during the study until fluid inclusion chips were made thicker and smaller inclusions were choosen for heating/freezing runs. Any inclusion that showed signs of leakage was ignored.

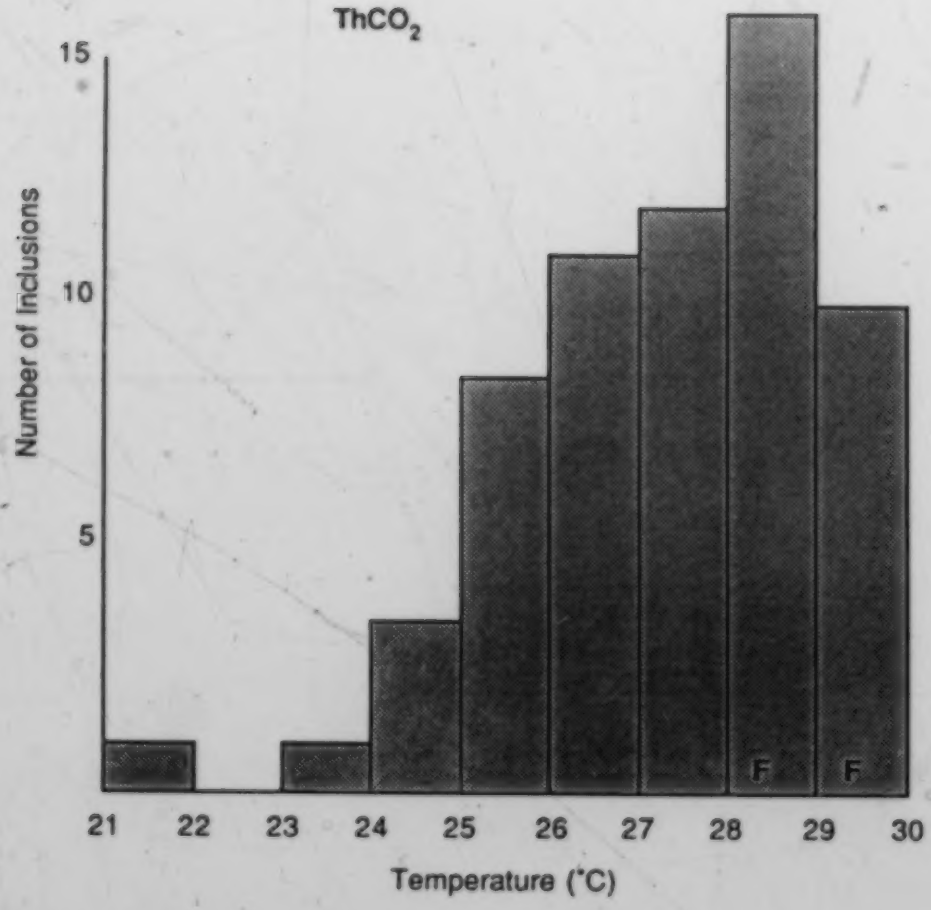

Figure 10. CO_2 homogenization temperatures. F = Fades

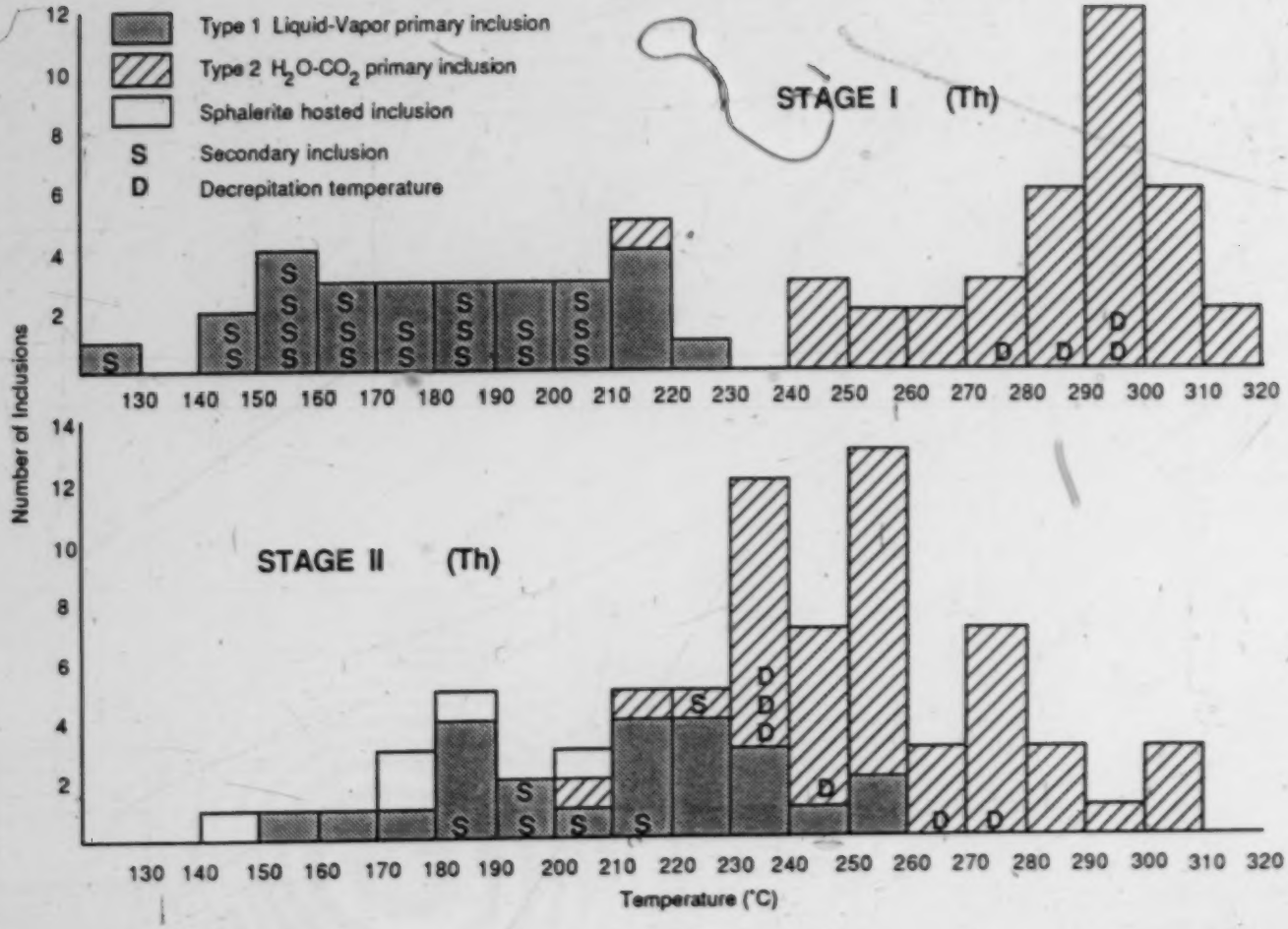

Figure 11. Homogenization and decrepitation temperatures.

The CO_2 phase in most Type 2 inclusions homogenized to the liquid phase. In one inclusion (789-A-2), the CO_2 homogenized to the vapor phase. Two inclusions (235-C-1,278-A-2) showed critical homogenization behavior (the boundary between the CO_2 vapor and CO_2 vapor faded) at temperatures near +31°C. The values for $ThCO_2$ range between +21°C and +30°C, with most values between +25°C and +30°C. The average $ThCO_2$ is +27.3°C. ± 1.7°C.

The densities and pressures of the CO_2 phase in Type 2 inclusions are calculated from the CO_2 homogenization temperatures, the modes of homogenization, and the equations for CO_2 densities and pressures given by Angus *et al.* (1976). The FORTRAN program CHNACL (Nicholls and Crawford, 1985) was used to calculate fluid compositions.

Calculated densities of the CO_2 phase are listed in Table 6 and range from 0.62 to 0.76 g/cm³. The average CO_2 density is 0.67 g/cm³.

Homogenization temperatures are plotted as a histogram in Figure 11. Temperatures of homogenization for primary Type 2 inclusions range from 210°C to 320°C in Stage I quartz, and 200°C to 310°C in Stage II quartz. The average homogenization temperature for Type 1 inclusions is 191°C ± 37.2 °C., and the average homogenization temperature for Type 2 inclusions is 266°C ± 26.9°C. The average homogenization temperature for Stage I primary Type 2 inclusions is 290°C, as opposed to 260°C for similiar Stage II inclusions. Decrepitation temperatures are lower (230°C to 280°C) in Stage II inclusions compared to Stage I inclusions (270°C to 300°C). Homogenization temperatures for sphalerite hosted inclusions range from 140°C to 210°C; however, these temperatures were difficult to measure and may be in error by up to ± 20°C.

Table 6. Fluid inclusion compositions, bulk densities, and pressures.

Sample No./ Chip/ Inclusion	Para. Stage	Vol %	Th	Salinity	Mole % H_2O	Mole % NaCl	Mole % CO_2	CO_2 Density	CO_2 Pressure	Inclusion Density	Molar Volume	Pressure
2850 Level												
38-A-1	II	10	+255.5 ?	4.0	0.96	0.01	0.03	0.64	69.7	0.98	19.6	250
38-B-1	II	30	+276.6 (H)	*	*	*	*	*	*	*	*	
89-A-1	I	40	+270.6 (H)	3.0	0.83	0.01	0.16	0.69	66.1	0.88	25.4	1800
89-B-1	I	25	+316.0 (F)	3.6	0.90	0.01	0.09	0.71	64.8	0.94	22.0	500
96-A-1	II	20	+242.7 (H)	2.8	0.93	0.01	0.06	0.66	68.3	0.94	21.2	800
96-A-2	II	20	+242.7 (H)	2.8	0.93	0.01	0.06	0.66	68.3	0.94	21.2	
97-A-1	II	15	*	3.6	0.94	0.01	0.05	0.68	67.3	0.97	20.3	
97-A-5	II	15	*	3.6	0.94	0.01	0.05	0.69	66.1	0.97	20.3	
106-A-2	II	20	+252.1 (H)	3.6	0.92	0.01	0.07	0.70	65.2	0.95	21.1	650
122-B-1	I	25	+280.0 (F)	2.8	0.90	0.01	0.09	0.70	65.4	0.93	22.0	650
122-B-2	I	25	+290.6 (H)	3.0	0.90	0.01	0.09	0.69	66.1	0.93	22.0	600
122-B-3	I	20	+212.3 (H)	*	*	*	*	*	*	*	*	
2800 Level												
217-A-5	II	30	+271.6 (H)	4.1	0.89	0.01	0.10	0.64	70.1	0.90	23.3	950
235-C-1	I	30	+270.2 (H)	2.2	0.89	0.01	0.10	0.65	69.2	0.90	23.2	850
262-A-1	II	15	+255.5 (H)	5.0	0.94	0.02	0.04	0.66	68.9	0.97	20.4	250
262-A-4	II	30	+251.9 (H)	4.7	0.87	0.01	0.11	0.72	63.6	0.93	23.0	1500
262-A-5	II	25	+235.2 (H)	4.5	0.90	0.01	0.08	0.67	67.8	0.94	22.1	
262-A-6	II	20	*	4.9	0.92	0.01	0.07	0.69	66.7	0.96	21.2	
262-A-7	II	15	+232.6 (H)	4.3	0.94	0.01	0.04	0.64	70.0	0.96	20.4	300
278-A-2	II	15	+306.8 (H)	5.4	0.93	0.02	0.04	0.63	70.6	0.97	20.4	300
2700 Level												
435-A-1	I	30	+291.9 (H)	*	*	0.01	*	*	*	*	*	
435-A-3	I	25	+284.3 (H)	3.6	0.90	0.01	0.09	0.70	65.5	0.94	22.0	700
435-B-2	I	50	+266.7 (H)	4.1	0.77	0.01	0.22	0.70	65.8	0.86	28.2	2700
435-B-5	I	35	+265.6 (H)	4.0	0.85	0.01	0.13	0.70	65.2	0.91	24.1	1350
414-A-1	II	30	*	*	*	*	*	*	*	*	*	

Sample No./ Chip/ Inclusion	Para. Stage	Vol %	Th	Salinity	Mole % H_2O	Mole % NaCl	Mole % CO_2	CO_2 Density	CO_2 Pressure	Inclusion Density	Molar Volume	Pressure
414-B-1	II	10	*	*	*	*	*	*	*	*	*	
414-C-1	II	20	*	4.1	0.93	0.01	0.06	0.64	70.0	0.94	21.3	
414-D-1	II	20	*	5.0	0.92	0.02	0.07	0.68	67.2	0.96	21.2	
414-D-4	II	20	*	5.0	0.92	0.02	0.06	0.65	69.0	0.95	21.2	
474-A-1	I	40	+291.0 (H)	3.4	0.84	0.01	0.15	0.62	70.8	0.86	25.8	1400
474-A-2	I	20	+291.0 (H)	3.6	0.93	0.01	0.06	0.63	70.6	0.94	21.3	300
474-A-3	I	20	+280.0 (H)	3.6	0.93	0.01	0.06	0.62	70.9	0.94	21.3	400
474-A-4	I	35	+296.8 (H)	3.4	0.87	0.01	0.12	0.62	70.9	0.88	24.5	1000
474-A-5	I	30	+297.2 (H)	3.4	0.89	0.01	0.10	0.62	70.8	0.90	23.3	750
474-A-15	I	20	+295.0 (H)	3.6	0.93	0.01	0.06	0.62	71.1	0.94	21.3	400
494-A-1	II	40	+268.6 (H)	3.8	0.83	0.01	0.16	0.68	67.0	0.88	25.4	1800
494-A-2	II	65	*	3.4	0.64	0.01	0.36	0.73	62.6	0.83	33.3	
494-A-3	II	30	+253.1 (H)	3.4	0.88	0.01	0.11	0.71	64.2	0.92	23.0	1250
494-A-6	II	40	+303.6 (H)	3.4	0.82	0.01	0.16	0.72	63.1	0.90	25.2	1500
494-A-7	II	65	+308.0 (H)	3.4	0.62	0.01	0.37	0.76	59.0	0.85	32.8	
494-B-1	II	20	+240.3 (H)	3.4	0.93	0.01	0.06	0.64	69.8	0.94	21.2	600
494-B-4	II	20	+250.2 (H)	3.2	0.93	0.01	0.06	0.64	69.7	0.94	21.3	500
2650 Level												
776-A-1	II	40	+284.6 (H)	2.0	0.84	0.01	0.16	0.67	67.9	0.87	25.5	1650
776-A-3	II	40	+231.2 (H)	1.8	0.84	0	0.15	0.64	70.0	0.86	25.7	
776-A-4	II	40	+272.6 (H)	2.0	0.84	0.01	0.15	0.64	70.0	0.86	25.7	1700
776-A-5	II	35	+259.2 (H)	1.8	0.87	0.01	0.12	0.62	71.1	0.87	24.5	1300
789-A-2	II	20	*	5.8	0.92	0.02	0.07	0.70	65.5	0.97	21.1	
816-A-5	I	50	+298.6 (H)	4.0	0.78	0	0.21	0.65	69.5	0.83	28.6	2500
2600 Level												
1041-A-1	II	10	+255.1 (H)	4.3	0.96	0.01	0.03	0.71	64.8	0.99	19.5	255
1050-A-1	I	30	+282.0 (H)	3.2	0.89	0.01	0.10	0.66	68.7	0.91	23.2	800
1050-A-2	I	30	+248.7 (H)	3.2	0.89	0.01	0.11	0.67	67.6	0.91	23.1	1750
1050-A-3	I	15	+284.5 (H)	3.0	0.94	0.01	0.46	0.66	68.4	0.96	20.3	

Sample No./ Chip/ Inclusion	Para. Stage	Vol %	Th	Salinity	Mole % H_2O	Mole % NaCl	Mole % CO_2	CO_2 Density	CO_2 Pressure	Inclusion Density	Molar Volume	Pressure
1063-A-3	II	40	+270.0 (H)	2.8	0.84	0.01	0.15	0.64	70.1	0.86	25.7	1700
1099-A-1	I	60	+301.8 (H)	3.6	0.69	0.01	0.30	0.69	66.7	0.82	31.8	
1099-A-2	I	60	+300.4 (H)	3.6	0.69	0.01	0.30	0.69	66.7	0.82	31.8	
1099-A-5	I	50	+307.8 (H)	3.8	0.78	0.01	0.21	0.64	70.0	0.83	28.7	2100
1099-A-6	I	50	+305.6 (H)	3.8	0.78	0.01	0.21	0.64	70.0	0.83	28.7	
1099-A-7	I	55	+298.0 (H)	3.0	0.74	0.01	0.25	0.66	68.7	0.82	30.3	2700
1099-A-8	I	50	+298.0 (H)	3.0	0.74	0.01	0.25	0.66	68.7	0.82	30.3	
1099-A-9	I	50	+298.0 (H)	3.0	0.74	0.01	0.25	0.66	68.7	0.82	30.3	

Para. Stage: Paragenetic Stage (Stage I or Stage II)

Vol. %: Volume percentage of CO_2 in inclusion

Th: (H)=homogenized to H_2O phase
(F)=faded near homogenization temperature

Salinity: Weight percent NaCl equivalent

CO_2 density: g/cm^3

CO_2 pressure: bars

Molar volume: moles/l

Pressure: bars

F. Fluid Composition and Bulk Density

The bulk density of a fluid inclusion may be calculated from the phase ratios of H_2O and CO_2 at 40°C, and the temperatures and pressures of various phase changes in the inclusion. Once the composition and bulk density are known, lines of constant density, or molar volume may be constructed on a P-T diagram.

Any estimation of bulk density is based on a number of assumptions (Burruss, 1981), which are:

1. At 40°C, the coexisting CO_2 and H_2O phases are pure endmembers.
2. The bulk molar volume of an inclusion is a linear combination of the end-member components.
3. Up to 40°C, the H_2O phase is incompressible, and therefore the pressure within a given inclusion is fixed by the isochore for the one phase CO_2 fluid at 40°C.

Bodnar *et al.* (1985) point out that the first assumption may be in error for inclusions with low CO_2 contents or low internal pressures.

The major source of error in any estimate of the mole fraction CO_2 and bulk density is the volume estimate of the CO_2 phase in the inclusion at 40°C. In this study, the diagrams of Roedder (1984), and Shepherd *et al.* (1985), which illustrate various volume percentages and degrees of fill for different shapes of inclusions, were used. Also, the dimensions of each fluid inclusion, and the diameter of the vapor bubble were measured using a micrometer ocular.

An attempt was made to use Bodnar's (1983) method of calculating volumes and densities for irregular shaped inclusions. The method depends on the precision of measuring the vapor bubble diameter. Most vapor bubble diameters at Venus are less than 5 μm. Bodnar (1983) showed that the error generated when using such small vapor bubble diameters is large,

so the method was not used.

The mole fractions, salinities, bulk compositions, and molar volumes for Type 2 inclusions are listed in Table 6. The average mole fraction CO_2 content is .13 ± .09. Table 7 is a summary of the average fluid composition.

G. Discussion

Evidence for Phase Separation

Boiling of high temperature, low pressure fluids has been cited as a possible mechanism for precious metal precipitation in epithermal systems (Drummond and Ohmoto, 1985; Bodnar *et al.*, 1985). In hydrothermal ore fluids containing CO_2 or other dissolved gases, effervescence has been suggested as a mechanism for gold precipitation (Kerrich and Fyfe, 1981; Kay and Strong, 1983). Both boiling and effervescence are simply examples of phase separation. Recognition of phase separation in the fluid is important because of the possible effect on gold precipitation and accompanying changes in fluid chemistry.

Fluid inclusions trapped from a heterogeneous fluid may look similiar to inclusions trapped during the later separation of an originally homogeneous one. The constancy of phase ratios in a number of inclusions can be used to distinguish between the two situations. Roedder (1984) suggests looking for widely variable H_2O-CO_2 ratios as evidence of phase separation from an originally homogeneous fluid, although he cautions that variable H_2O-CO_2 ratios can be caused by trapping at different times from fluids under different pressure-temperature conditions. The CO_2 volume content in Venus inclusions ranges from 5% to 60% and averages 20% to 30%. Some fields of view (Chip 776-A; Figure 6) contain inclusions with consistent H_2O-CO_2 ratios which indicate that phase separation was not taking place when the inclusions were trapped. Other chips contain primary inclusions with variable H_2O-CO_2 ratios (Chip 1099-A). It is possible that the chips with consistent H_2O-CO_2 ratios represent the original, earlier homogeneous fluid. A similiar distribution of H_2O-CO_2 phase ratios was noted by Wood *et al.*, (1986) in the Hollinger-McIntyre gold deposit.

Table 7. Average fluid inclusion composition.

	Stage I	Stage II	Average
Molar Fraction CO_2	.17	0.10	0.13
Salinity (weight percent NaCl equivalent)	3.4	3.7	3.6
Bulk Density (g/cm^3)	0.88	0.93	0.91
Molar Volume (moles/l)	25.3	22.9	24.0
Homogenization Temperature (°C)	290	260	275
Pressure (bars) -calculated using average fluid composition	1750	1000	1250
Pressure (bars) -calculated using average pressure from individual fluid compositions	1300	1100	1150

Examination of homogenization temperatures in Figure 11 shows that primary Type 1 inclusions have lower homogenization temperatures (150°C to 260°C) than primary Type 2 inclusions (200°C to 320°C). Most secondary inclusions (Th=150°C to 210°C) are Type 1 inclusions. Secondary liquid-vapor inclusions were noted in samples from both Stage I and Stage II. The existence of CO_2 free, liquid-vapor inclusions was noted in samples from both Stage I and Stage II quartz. Liquid-vapor Type 1 inclusions homogenize at lower temperatures than Type 2 inclusions. A plot of mole % CO_2 vs Th (Figure 12) indicates a slight depletion of CO_2 in Stage II inclusions relative to Stage I inclusions. Lower temperature, primary Type 1 inclusions, most of which are in Stage II, are completely depleted in CO_2, as are secondary liquid-vapor inclusions present in both stages. The plot suggests that sporadic CO_2 separation (or effervescence) took place between 200°C and 260°C, leaving a residual CO_2 free fluid.

Although there is no conclusive evidence for H_2O-CO_2 immiscibility at the time of trapping, the above section presents evidence that sporadic phase separation probably occurred during the later stages of mineral deposition.

Pressure and Depth Estimates

A plot of pressure vs mole % CO_2 (Figure 13) is used in conjunction with homogenization temperatures to graphically obtain the minimum pressure of trapping, assuming the coexistence of a CO_2 phase. Figure 13 has been constructed using the diagrams of Parry (1986) for the 6 weight percent NaCl isotherm, and diagrams from Takenouchi and Kennedy (1964) for the 0 weight percent NaCl isotherm. The 3 weight percent NaCl isotherm in Figure 13 has been extrapolated from the 0 and 6 weight percent NaCl isotherms. The average salinity of Venus fluid is 3.6 weight percent NaCl equivalent, which corresponds closely to the 3 weight percent NaCl isotherms on Figure 13.

The average inclusion fluid from Venus (Table 7) has a mole fraction CO_2 content of $0.13 \pm .09$, and a homogenization temperature of 275°C. This corresponds to a pressure (using Figure 13) of about 1250 bars assuming that the inclusions were trapped in the two

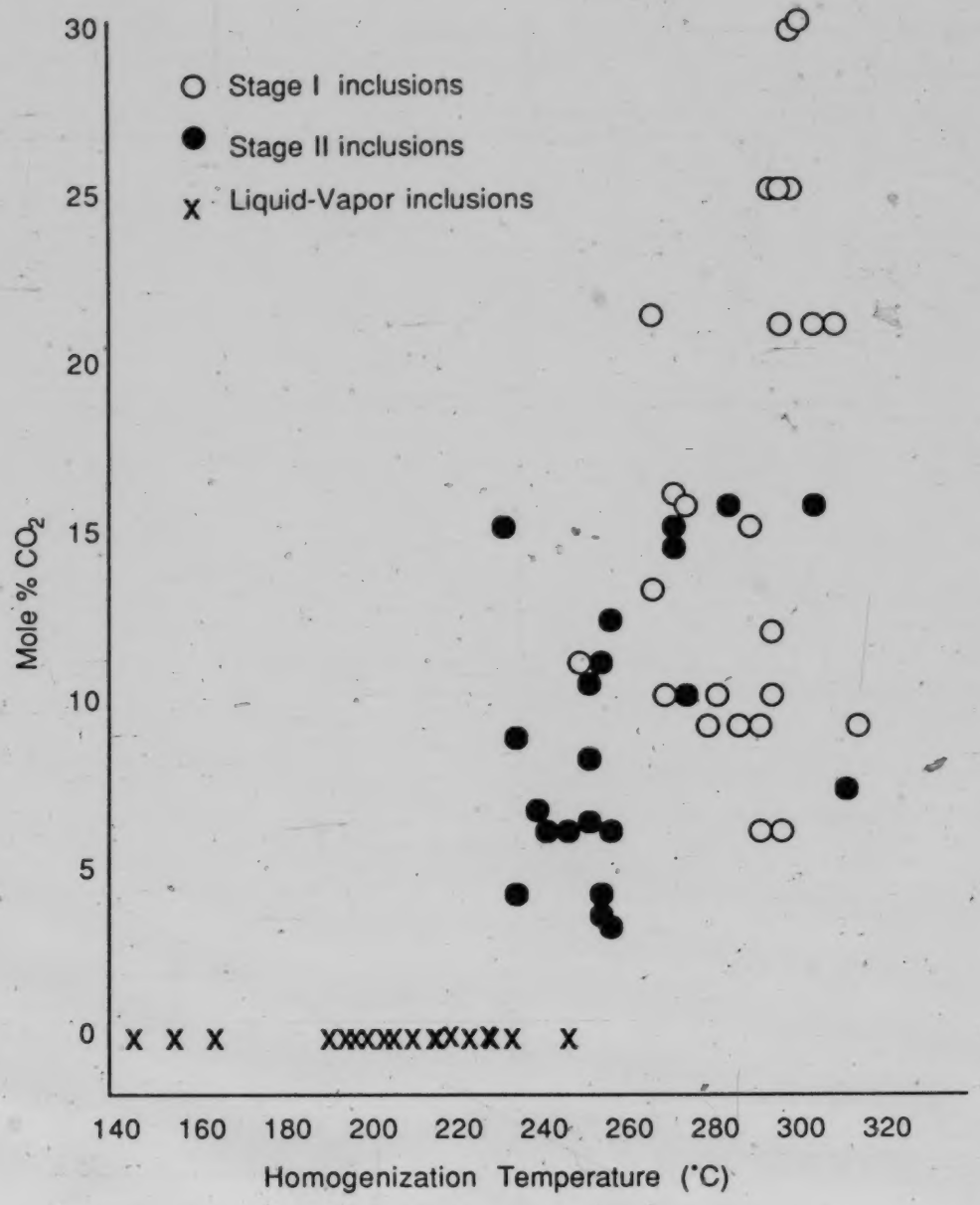

Figure 12. Mole % CO_2 vs. Th

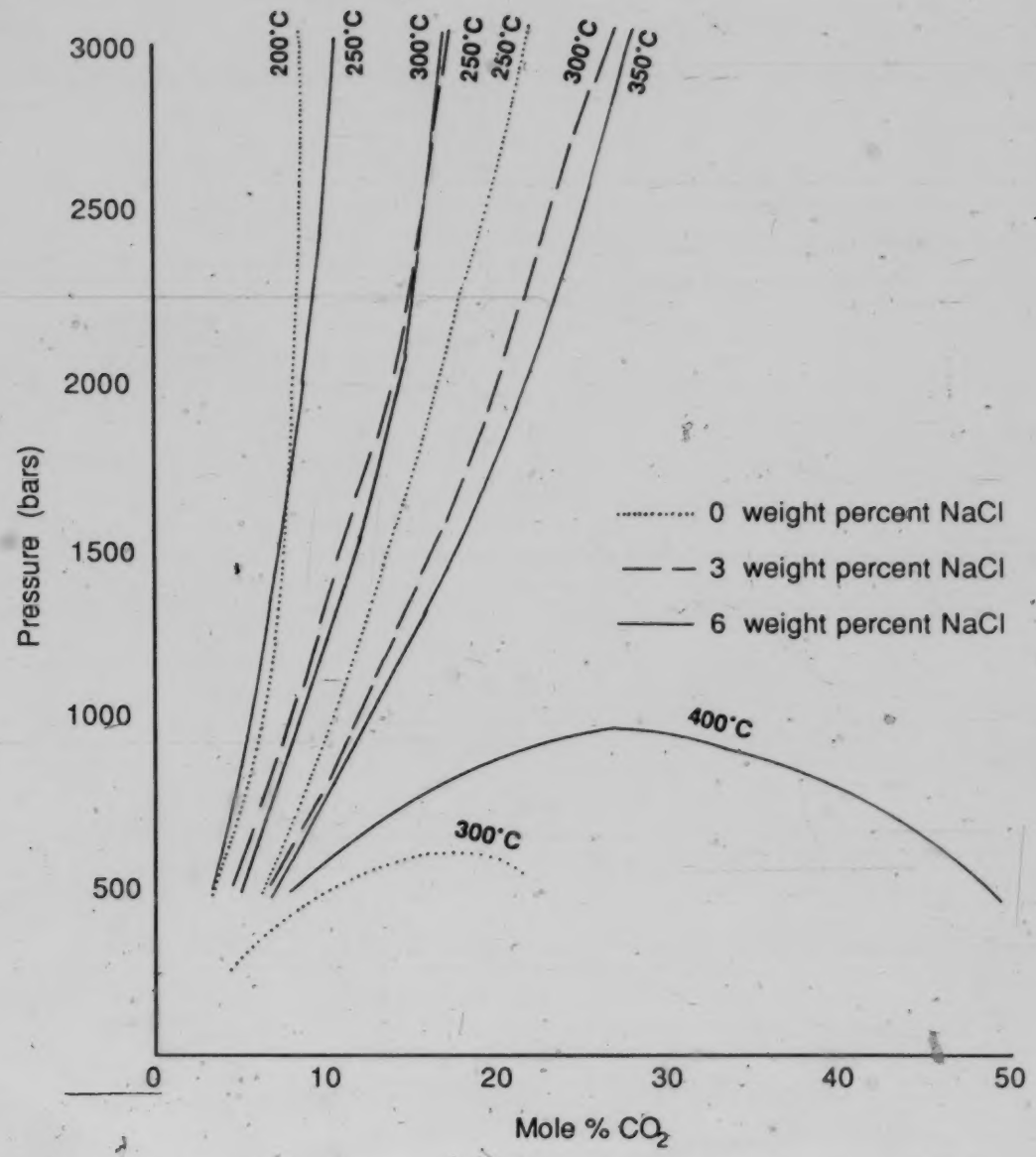

Figure 13. Pressure vs. mole % CO_2 (modified after Takenouchi and Kennedy (1964) and Parry (1986).

phase field. Stage I mineralizing fluids have a higher mole fraction CO_2 (0.17) and a higher average homogenization temperature (290°C), which corresponds to a pressure of 1750 bars. Lower temperature (260°C) and CO_2 depleted Stage II inclusions have an average pressure of about 1000 bars.

The pressures mentioned above were estimated by assuming an average fluid composition (Table 7) for the quartz depositing fluid. However, the fluid in individual inclusions most likely has a composition that differs from the average fluid composition. Figure 13 shows that even a slight variation in the CO_2 content, for instance, will drastically affect the pressure estimate for any one particular inclusion. Pressures were calculated for each individual inclusion (Table 6). An average pressure was then calculated from the individual fluid inclusion pressures. The pressures range from 250 to 2700 bars. The pressure estimate for Stage I inclusions is 1300 bars. Stage II inclusions have an average pressure of 1100 bars, and the average pressure for the system is about 1150 bars. The average pressure calculated by using the combined pressures for each inclusion is lower than the pressure range calculated using average fluid composition. The pressure calculated using individual inclusions probably most accurately reflects the true fluid pressure.

A large amount of uncertainty in pressure estimates is due to errors in estimating the fluid composition and hence its P-V-T characteristics. Bowers and Helgeson (1983a,b) have calculated P-V-T-X relationships in the system H_2O-CO_2-NaCl. Any estimate of fluid composition, including CO_2 content, is very dependent on volume estimates. The effect of an error in the volume estimate of CO_2 on pressure is illustrated by inclusion 474-A-4. The inclusion has a volume percentage of CO_2 of 35% CO_2, corresponding to a mole fraction CO_2 of 0.12. The homogenization temperature is 298.8°C, and the salinity is 3.4 weight percent NaCl equivalent. Assuming a Th of 300°C, and a salinity of 3.0 weight percent NaCl equivalent, the pressure is about 1000 bars. If the volume estimate is in error by ±10%, then the corresponding pressure estimates would be 500 bars for a volume of 25% CO_2 and 1700 bars for a volume of 45% CO_2.

An increase or decrease in salinity also affects the position of the boundary between the one and two phase fields. Ellis and Golding (1963) showed that when NaCl is added to the pure H_2O-CO_2 system, the solubility of CO_2 decreases, and the miscibility gap is widened. Takenouchi and Kennedy (1964) showed that even for a solution containing 6 weight percent NaCl, the solubility of CO_2 is reduced to about half the value for pure water at the same temperature and pressure. The effect of increasing NaCl content is shown in Figure 13. An inclusion with 15 mole percent CO_2, 3 weight percent NaCl, and a Th of 300°C, will have a minimum pressure of about 1300 bars. If 6 weight percent instead of 3 weight percent NaCl is assumed, then the pressure would be 2500 bars.

The homogenization temperatures and pressures in Table 7 may represent minimum pressures and temperatures of entrapment. If the pressure on the fluid at the time of entrapment was greater than the vapor pressure of the fluid in the inclusion at the Th, then the CO_2 and H_2O will homogenize at a temperature below that at which the inclusion formed. In this case, the temperature difference (i.e. "pressure correction") between the homogenization temperature and the trapping temperature must be added to the homogenization temperature to obtain the true trapping temperature (Roedder and Bodnar, 1980). If the inclusion was trapped when the fluid was effervescing, then the homogenization temperature may represent the true trapping temperature, and no pressure correction is needed. The previous section outlined evidence for a late stage phase separation when the temperature of the fluids dropped below 260°C.

The average pressure in the Venus system is about 1000 to 1300 bars but individual inclusions may have pressures far greater or lower than the calculated averages. The formation of inclusions at an average pressure of about 1000 bars requires a formation depth of about 3 to 4 km assuming lithostatic pressures, and about 10 km assuming hydrostatic pressures.

H. Summary

The following constraints on the nature of the quartz depositing fluid at Venus were determined using fluid inclusion analyses:

1. The initial Stage I fluid is characterized by homogenization temperatures averaging 290°C, a moderate CO_2 content (.17 mole fraction) and low salinities (3 to 4 weight percent NaCl equivalent).
2. Stage II fluid is characterized by homogenization temperatures averaging 260°C, low CO_2 contents and slightly higher salinities (up to 7.5 weight percent NaCl equivalent) relative to Stage I.
3. Sporadic effervescence of the CO_2 phase is indicated by widely variable H_2O-CO_2 phase ratios in some groups of inclusions.
4. The average pressure in the Venus system is about 1000 to 1300 bars, but individual inclusions may have pressures far greater or lower than the calculated average.

VI. STABLE ISOTOPE STUDY

A. Introduction

A preliminary study (Zhang *pers. comm.*, 1985) of the $\delta^{18}O$ values of quartz samples from the Venus vein revealed an unusual enrichment in ^{18}O relative to epithermal precious metal vein deposits hosted in young volcanic rocks (Field and Fifarek, 1985). The aim of the present study was to confirm the ^{18}O enrichment, and to better define the isotopic nature of the fluid responsible for formation of the Venus vein.

Quartz samples for the preliminary study, done by Zhang, were taken from ore shoots and low grade areas within the vein structure. All andesitic hostrock samples were taken from underground, and have therefore undergone hydrothermal alteration. A sample location map is shown in Appendix 3.

For the present study, quartz samples from Stage I and Stage II were selected for analysis. Each sample of vein quartz selected for isotopic analysis was also included in the fluid inclusion study. A sample of banded, chalcedony float found along the surface trace of the Venus vein, and a sample of chalcedony found in outcrop were also analyzed. Seven samples from other vein systems on Montana Mountain were also included in the study.

B. Analytical Technique

Oxygen Isotopes

All quartz samples were fine to medium grained, massive to crystalline vein materal. The samples were hand crushed to -40 mesh, and then soaked in aqua regia for 24 hours to remove soluble impurities. A small amount of hydrogen peroxide was added to the aqua regia to dissolve trace amounts of sulphides attached to the quartz grains. The clean samples were hand picked to further purify the final product.

Oxygen was liberated from the samples by reaction with BrF_5 for 12-14 hours at 650°C (Clayton and Mayeda, 1963). The derived oxygen was reacted with a platinum treated carbon

rod at approximately 850°C to produce CO_2 gas. The CO_2 gas was analyzed by mass spectrometry to determine the $\delta^{18}O$ value of the samples. All oxygen isotope analyses were performed by Dr. K. Muehlenbachs and Mrs. E. Toth at the University of Alberta. The analytical error is estimated to be ± 1‰ for oxygen and ±10‰ for deuterium.

Hydrogen Isotopes

An attempt was made to extract the fluid contained in fluid inclusions. The method used involved crushing clean quartz samples to a grain size of about 0.5 to 1.0 mm in diameter. The quartz samples were placed in a quartz tube and heated to 250°C to drive off water vapor. The tube was evacuated for 12 to 20 hours. The sample tube was then heated very slowly up to 600°C. The fluid from all inclusions which decrepitated at temperatures above 250°C was collected for two hours in a liquid nitrogen trap. A dry ice trap was then used to separate CO_2 and water vapor. The fluid vapor was sent to Global Geochemistry Laboratory for hydrogen isotopic analysis.

Despite numerous attempts at fluid extraction, only two samples of inclusion waters were collected. One of the samples leaked and was subsequently discarded. Each time the sample tube was heated to 600°C, the sample tube exploded in the furnace. Various attempts to correct the problem were made (annealing the sample tube, changing from quartz to a Vycor sample tube, slowing the rate of heating, changing the grain size of the quartz). It is possible that during final heating, the pressure inside the tube built up and the tube exploded due to the release of CO_2 gas from primary Type 2 fluid inclusions.

C. Results of Isotopic Analysis

The $\delta^{18}O$ results from both the preliminary study and the present study are listed in Table 8. The isotopic compositions of the samples are listed in the δ notation in permil (‰) deviation from Standard Mean Ocean Water (Craig, 1961).

The eighteen quartz samples from the Venus mine had $\delta^{18}O$ values of +10.2 to +13.7‰. The average $\delta^{18}O$ value for quartz is +12.1‰ ± 1‰. Five samples of Stage I

Table 8. Oxygen isotope data.

Sample Number	Elevation (ft.)	Paragenetic Stage	$\delta^{18}O$ Value (SMOW)	Parent Fluid $\delta^{18}O$ Value
Venus Mine Quartz Samples				
12	2850	II	+13.7	+5.9
122	2850	I	+11.7	+3.9
217	2800	II	+10.2	+2.4
235	2800	I	+11.0	+3.2
435	2700	I	+13.6	+5.8
498	2700	II	+12.8	+5.0
728	2650	I	+11.3	+3.5
776	2650	II	+12.5	+4.7
1039	2600	II	+12.2	+4.4
1099	2600	I	+11.5	+3.7
10	2850		*+11.1*	*+3.3*
15	2850		*+13.1*	*+5.3*
117	2850		*+11.5*	*+3.7*
233	2800		*+13.0*	*+5.2*
268	2800		*+13.3*	*+5.5*
521	2800		*+12.2*	*+4.4*
1032	2600		*+12.7*	*+4.9*
1077	2600		*+11.0*	*+3.2*
Venus Vein Surface Samples				
5009	3400		+14.2	+6.4
5059	2950		+10.5	+2.7
5068	3250		+11.8	+4.0
Chalcedony	Float		-3.0	-20.2
Chalcedony	Outcrop		-1.3	-18.5
Altered Wallrock				
9	2850		*+10.0*	
30	2850		*+6.2*	
294	2800		*+8.6*	
475	2700		*+10.5*	
1011	2600		*+5.9*	
1031	2600		*+10.0*	
Intensely Altered Wallrock				
60	2850		*+3.2*	
213	2800		*+6.6*	
432	2700		*+1.6*	

Sample Number	Elevation (ft.)	Paragenetic Stage	$\delta^{18}O$ Value (SMOW)	Parent Fluid $\delta^{18}O$ Value
Montana Mountain Au-Ag Veins				
Ruby Silver	4250		+14.2	+2.6
Uranus Pit	4600		+14.6	+3.0
Uranus Adit	4600		+10.7	-0.9
			+10.2	
Peerless	5000		+10.7	-0.9
			+10.1	
Joe Petty	5500		+16.9	+5.3
Aurora	5600		+14.4	+2.8
Arctic	5700		+14.5	+2.9

NBS-28=9.6‰ SMOW
$1000 \ln\alpha = 3.34(10^6/T^2) - 3.31$ (Matsuhisa et al., 1979)
Italicized values are from Zhang, 1985 (pers. comm.)

Parent fluid temperatures: Venus vein=275°C
Chalcedony (arbitrary temperature)=130°C (Fournier, 1985)
Montana Mountain Au-Ag veins=200°C (based on fluid inclusion temperatures from Uranus Adit and Joe Petty

quartz have an average $\delta^{18}O$ value of +11.8‰. Five samples of Stage II quartz have an average $\delta^{18}O$ value of +12.3‰. The three samples taken from suspected Venus vein outcrop have an average $\delta^{18}O$ value of +12.2‰. The two chalcedony samples have $\delta^{18}O$ values of -1.3 and -3.0‰.

Isotopic analyses of altered andesitic wallrocks shows a wide range in $\delta^{18}O$ values. Typical hydrothermally altered wallrock samples have a range of +5.9 to 10.0‰, averaging +8.5‰. Two samples of intensely altered wallrock from the clay alteration zone have values of +3.2 to +6.6‰. The sample of "fresher" wallrock has a $\delta^{18}O$ value of +1.6‰.

The one successful water extraction was from a quartz sample (#122) from the 2850 level of the mine. This sample had a δD value of -159‰ relative to SMOW.

Seven quartz samples from other veins on Montana Mountain had $\delta^{18}O$ values for quartz ranging from +10.7‰ (Uranus Adit, Peerless) to +16.9‰ (Joe Petty).

The $\delta^{18}O$ values of the parent hydrothermal ore fluid can be calculated by using the oxygen isotope fractionation equation given by (Matsuhisa *et al.*, 1979):

$$1000\ln\alpha = 3.34(10^6/T^2) - 3.31$$

Where T = °K

The temperatures used in the equation are obtained from fluid inclusion analysis. An average homogenization temperature of 275°C is assumed for all Venus quartz vein samples. A temperature of 275°C was also used for samples of Venus vein quartz from surface exposures. Fournier (1985) states that chalcedony is stable only at temperatures below 180°C, so an arbitrary temperature of 130°C was assumed for the chalcedony. Homogenization temperatures of 180°C and 200°C were determined for fluid inclusions from the Uranus Adit and Joe Petty veins, therefore a minimum temperature of 200°C was assumed for the other precious metal veins on Montana Mountain.

The calculated $\delta^{18}O$ values for the quartz depositing fluid are listed in Table 8. The parent ore fluid for Venus vein quartz has a range in $\delta^{18}O$ values of +2.4 to + 5.9‰. The average $\delta^{18}O$ value for the Venus vein parent fluid is +4.3‰ ± 1‰. Quartz from the surface trace of the Venus vein has parent fluid values averaging +4.4‰. The chalcedony samples have $\delta^{18}O$ values of -18.5 and -20.2‰ for the fluid, assuming an arbitrary temperature of 130°C. If the lower limit of 80°C is used (Fournier, 1985) then the chalcedony fluid value would be -22.2‰ to -26.5‰. If the upper limit of +180°C is used, then the chalcedony fluid values are -14.3‰ and -16.0‰. Other veins on Montana Mountain have a range of $\delta^{18}O$ fluid values of -0.9 to +5.3‰.

Any upwards adjustment of the temperature as a result of a pressure correction would be reflected in higher $\delta^{18}O$ values for the quartz depositing fluid.

D. Discussion

The location of the meteoric water line and Standard Mean Ocean Water (SMOW) are shown on a plot of δD vs $\delta^{18}O$ (Figure 14). The meteoric water line on the plot is a function of the systematic variation in $\delta^{18}O$ and δD as shown by most present day meteoric water (Craig, 1961; Taylor, 1974). The higher the latitude or elevation, the lower are the δD values and the $\delta^{18}O$ values of the water with respect to ocean water (SMOW). The Yukon is in an ideal geographic location for distinguishing between different types of waters, based on the δD and $\delta^{18}O$ composition of the fluid. The δD and $\delta^{18}O$ of present day, pristine groundwater in the Yukon should be about -150 to -170‰ for δD, and between -17.5 to -20‰ for $\delta^{18}O$ (Taylor, 1979). Dagenais (1984) measured the $\delta^{18}O$ value of well water from the Dezdeash map area near Beloud Post, Yukon. He showed that the $\delta^{18}O$ value of -21.4‰ is consistent with the expected $\delta^{18}O$ value from Taylor (1979). Another sample of meteoric water sampled near the Yukon-N.W.T. southern border has a $\delta^{18}O$ value of -23.1‰ (Bowman and Covent, 1983).

The meteoric water line is used as a point of reference when interpreting the isotopic composition of fossil hydrothermal systems, therefore it is important to determine whether

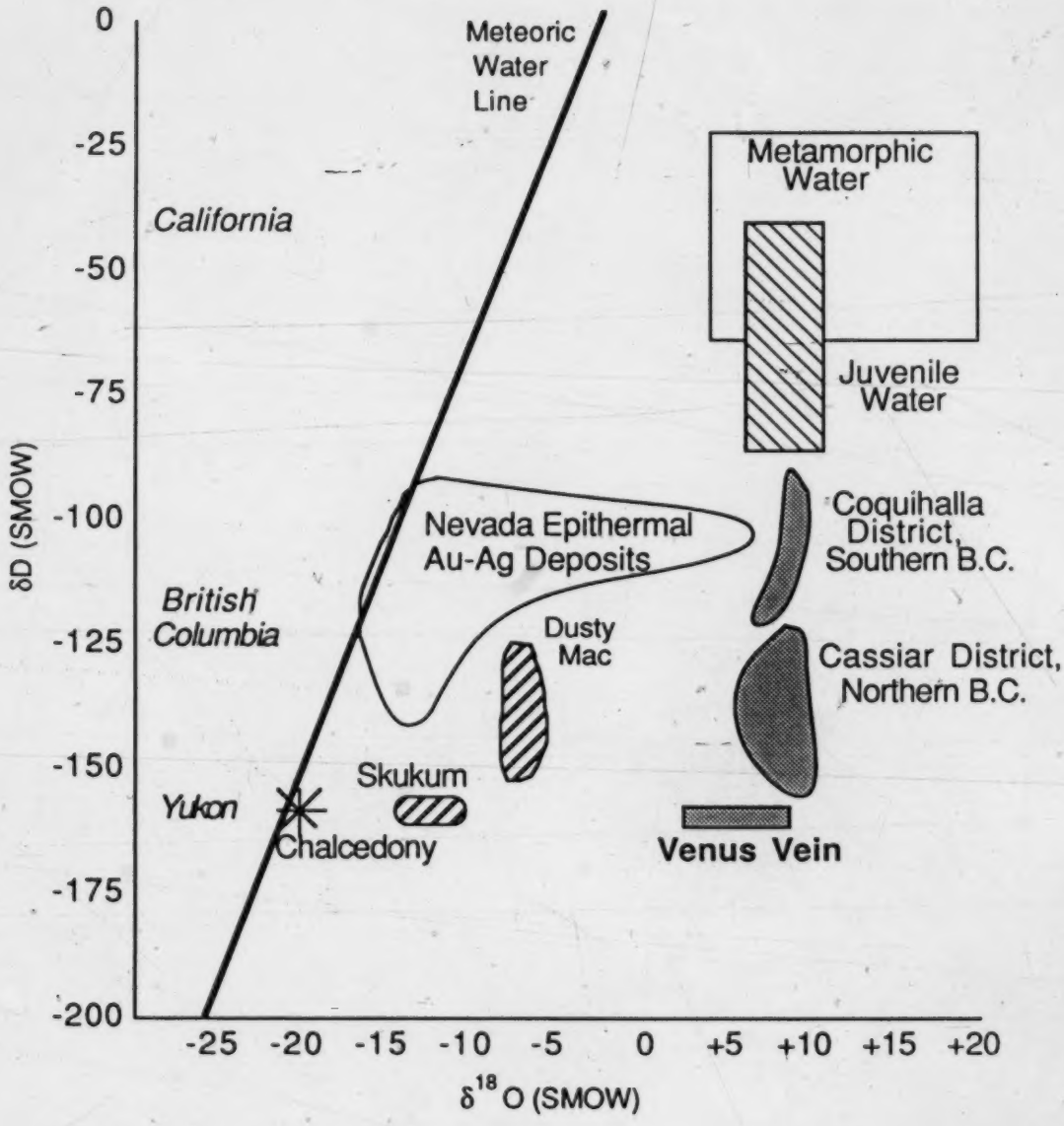

Figure 14. Results of Venus isotope study on a plot of δD vs. $\delta^{18}O$

the isotopic composition of surface waters has stayed constant with time. Although the exact age of the Venus deposit is not known, it is hosted in Late Cretaceous volcanic rocks, and is therefore Late Cretaceous or younger in age. Taylor (1979) showed that the meteoric water line for North America has remained essentially unchanged since early Cretaceous. Dagenais (1984) suggested a $\delta^{18}O$ value of -16‰ for Cretaceous to Tertiary meteoric water in the Whitehorse Trough. Magaritz and Taylor (1976) used the δD values of those rocks that have exchanged with large amounts of meteoric water to estimate that early Tertiary meteoric water in the Skagway-Carcross area had a δD value of -120‰.

Figure 14 shows the range of $\delta^{18}O$ fluid values for Venus (+2.4 to +6.4‰). The results show little variation in $\delta^{18}O$ between Stage I fluids and Stage II fluids, and between $\delta^{18}O$ values for quartz depositing fluid from different elevations in the mine. The lack of spatial or temporal gradients in the $\delta^{18}O$ values of the quartz depositing fluid at Venus indicates that a homogeneous fluid (with respect to isotopic composition) was responsible for mineral deposition. Multiple fluid types have been identified, based on isotopic composition, in several hydrothermal vein deposits. Creede, Colorado (Bethke and Rye, 1979), Sunnyside (Casadevall and Ohmoto, 1977), and Finlandia (Kamalli and Ohmoto, 1977) are examples of deposits formed from isotopically variable fluids. Mixing between hot hydrothermal fluids with enriched ^{18}O, and dilute, relatively exchanged meteoric water has been suggested as a mechanism for ore deposition in the Southern Amethyst vein system, Colorado (Robinson and Norman, 1984) and in the Kushikino epithermal gold-silver mine, Japan (Matsuhisa *et al.*, 1985). The fluid inclusion study and the consistent $\delta^{18}O$ fluid values show that mixing between isotopically and chemically distinct fluids did not occur at Venus, although there is a broad decrease in temperature and loss of CO_2 with time.

The $\delta^{18}O$ fluid values for Venus fall within a narrow range despite a broad temperature decrease with time and a indicated loss of CO_2 (see Chapter 5). A decrease in temperature is generally reflected by an increase in the $\delta^{18}O$ values for quartz. Higgins and Kerrich (1982) suggest that an accompanying $\delta^{18}O$ increase with time of the $\delta^{18}O$ of the fluid

in equilibrium with quartz would act to oppose the larger quartz-water fractionations accompanying a temperature decrease, therefore the $\delta^{18}O$ quartz value would remain relatively constant.

Figure 14 shows that the Venus ore fluid is highly enriched in $\delta^{18}O$ relative to pristine surface water. Assuming a meteoric-hydrothermal fluid with a δD of -160‰, then the corresponding equilibrium $\delta^{18}O$ fluid value would be -19‰. The average $\delta^{18}O$ fluid value for Venus is +4.3‰. The enrichment in the $\delta^{18}O$ of the ore fluid is at least 23‰. The originial $\delta^{18}O$ value of meteoric water generally undergoes a shift in ^{18}O away from its initial value. This is because rocks contain about 50 percent by weight oxygen, and will exchange oxygen with the fluid during water-rock interaction. In contrast, rocks contain little hydrogen compared to the fluid, therefore the fluid will control the D/H ratio of the system. For this reason, δD values for meteoric-hydrothermal fluids are generally constant (relative to $\delta^{18}O$ values) and, in places like the Yukon, serve to distinguish between fluids of different origin. If a average δD value close to -160‰ for the Venus system is assumed (sample 122), then the Venus ore fluid can be defined as a dilute, CO_2 bearing, high ^{18}O meteoric-hydrothermal fluid.

The size of the ^{18}O shift depends on the exchangeability of oxygen in the host rocks, the temperature of isotopic exchange, the initial isotopic composition of the phases, and the chemistry of the ore fluid (Sheppard, 1986; Field and Fifarek, 1985).

Fluid inclusion analysis shows a depletion of CO_2 with time in the Venus fluid, which is probably the result of CO_2 immiscibility at temperatures of 200 to 260°C, in response to decreasing temperatures and pressures in the system. Higgins and Kerrich (1982) show that in the Grey River Tungsten deposit, up to 7‰ depletion in the $\delta^{18}O$ of a residual aqueous fluid may occur as a result of effervescence and subsequent loss of 40 mole percent CO_2 from the hydrothermal fluid. The depletion occurs because CO_2 is preferentially enriched in $\delta^{18}O$ relative to H_2O. A loss of CO_2 would result in a lowering of the $\delta^{18}O$ composition of the residual CO_2 depleted fluid. Also, the amount of CO_2 in the Venus vein system (average 13

mole percent) is not as large as the 40 mole percent reported by Higgins and Kerrich (1982), therefore, the effect of effervescence on the isotopic composition of Venus ore fluid is likely to be minimal.

Compared to other gold vein deposits hosted in young volcanic rocks, the $\delta^{18}O$ values for the Venus ore fluid are unusual (Field and Fifarek, 1985). The Skukum epithermal gold vein, located 35 km northeast of the Venus mine (see Chapter 2), has fluid $\delta^{18}O$ values of -14 to -11‰, (Nesbitt *et al.*, 1986). The Dusty Mac epithermal gold deposit in southern British Columbia has a calculated $\delta^{18}O$ of the fluid of -7 to -9‰ based on fluid inclusion temperatures of 240°C (Zhang, 1986). The Blackdome epithermal gold deposit in British Columbia has $\delta^{18}O$ fluid values of -7.5 to -9.0‰ (Schroeter, 1987). The three deposits have been classified as epithermal based on similiar geology and geochemistry to generally accepted Cordilleran epithermal models (Panteleyev, 1986). Nesbitt *et al.* (1986) have shown that Cordilleran epithermal gold-silver veins are deposited from shallow circulating, relatively unexchanged, meteoric water with $\delta^{18}O$ fluid values of -14 to -7‰, and δD values of -160‰. Field and Fifarek (1985) summarize $\delta^{18}O$ and δD values for epithermal gold deposits in the United States. The results compare favorably with values from Nesbitt *et al.* (1986) for Canadian epithermal gold deposits.

The Venus quartz depositing fluid is obviously greatly enriched in ^{18}O relative to Cordilleran epithermal gold-silver deposits. The exact mechanism and fluid history that would generate such a large shift can only be defined by a more detailed isotopic study of the Venus vein and surrounding country rocks; however, similiar extreme ^{18}O shifts in meteoric-hydrothermal fluids have been noted in Canadian mesothermal gold deposits (Nesbitt *et al.*, 1986), and in Korean Au-Ag vein deposits (Shelton, 1986). In both models, the mechanism for such an extreme shift has been ascribed to extensive water-rock interaction. In the model described by Nesbitt *et al.* (1986) for mesothermal gold deposits in the Canadian Cordillera, the meteoric fluid evolves by deep circulation near major strike-slip fault zones, where extensive water-rock interaction at high temperatures raise the ^{18}O and CO_2

content of the fluid. The highly evolved, low salinity meteoric-hydrothermal fluid cools as it rises through faults related to major strike-slip faults and subsequently deposits minerals in steep normal or reverse fault zones. The resulting fluid is highly enriched in ^{18}O, but retains its low δD value. Nesbitt *et al.* (1986) list the calculated $\delta^{18}O$ values for the parent ore fluid for several lode gold deposits in the Canadian Cordillera, including Coquihalla, Cassiar, and Cariboo. The $\delta^{18}O$ values for the fluids range from +5 to +9‰. The average $\delta^{18}O$ value for Venus is +4.3‰. slightly lower than that for the deposits listed by Nesbitt *et al.* (1986). This may be due to water-rock interaction with volcanic host rocks, as opposed to the high ^{18}O carbonate rocks and serpentinites listed as host rocks for Cordilleran mesothermal deposits by Nesbitt *et al.* (1986). Zhang (1986) also found high $\delta^{18}O$, low δD fluid values for the Oro Fino and Fairview vein in southern British Columbia, and concluded that they were mesothermal veins of the type described by Nesbitt *et al.* (1986), based on isotopic signature and geochemical similiarities.

Shelton (1986), studied Au-Ag veins in Korea associated with granites. The granites differ in their levels of emplacement. The meteoric-hydrothermal fluids responsible for vein deposition show an increase in $\delta^{18}O$ of the fluid, and therefore greater water-rock interaction, with increasing depth of emplacement of the associated granitic pluton. The vein fluid associated with the deeper pluton would be affected by greater depths (higher water-rock interaction), higher temperatures, and would show a higher $\delta^{18}O$ shift than the fluids associated with the shallower pluton.

The $\delta^{18}O$ values for the two chalcedony samples are especially interesting. One sample of chalcedony was found as float on the surface trace of the Venus vein and one sample was taken from a chalcedony vein located at a higher elevation than the Venus vein. The calculated $\delta^{18}O$ fluid values for the chalcedony plot on the meteoric water line (Figure 16). The chalcedony is therefore interpreted to have been precipitated from pristine, unexchanged near surface meteoric water. The Venus vein and the chalcedony samples have drastically different $\delta^{18}O$ values (a difference in the $\delta^{18}O$ of the fluid of about 25‰), which indicates they belong to separate hydrothermal systems.

Regional Considerations

A regional survey of whole rock isotope compositions is beyond the scope of this study; however, limited analyses from Zhang's preliminary investigation of the Venus mine host rocks are listed in Table 8.

The altered volcanic host rocks have $\delta^{18}O$ values ranging from +1.6 to +10.5‰. The lower values are depleted in $\delta^{18}O$ relative to the average whole rock $\delta^{18}O$ value for andesite, which is +6.5‰ (Taylor, 1974). Sample 60 ($\delta^{18}O = +3.2$‰) is from a clay alteration zone on the 2850 ft. level of the mine. Sample 432 from the 2700 ft. level of the mine has a $\delta^{18}O$ value of +1.6‰. The quartz depositing fluid at Venus was highly enriched in ^{18}O, and could not have been responsible for the ^{18}O depletion in wallrock samples 60 and 432. The presence of a separate hydrothermal system has been indicated by low $\delta^{18}O$ values for chalcedony found in the volcanic complex. Heated groundwater from such a system may have interacted with upper level Venus wallrock, especially in the clay alteration zones.

Summary

A limited number of isotopic analyses has proved to be surprisingly useful in defining constraints on the nature of the fluid responsible for mineral deposition.

1. Lack of spatial or temporal variations in the $\delta^{18}O$ value of the Venus fluid suggests one quartz depositing fluid of constant isotopic composition was responsible for mineral deposition.
2. Chalcedony previously believed to be part of the Venus vein system has a $\delta^{18}O$ signature 25‰ lower than Venus, and is therefore deduced to be a separate event.
3. The calculated $\delta^{18}O$ values for the Venus ore fluid are surprisingly enriched in $\delta^{18}O$ despite retaining a low δD value of -160‰. This suggests the ore fluid was a dilute CO_2 bearing, ^{18}O enriched meteoric-hydrothermal fluid.

VII. DISCUSSION AND MODEL

A. Summary

The Venus Au-Ag-Pb-Zn vein is a simple fissure filling hosted by Late Cretaceous, intermediate volcanic rocks. Vein development can be divided into two stages (Figure 15). The initial hydrothermal ore fluid (Stage I) is characterized by low salinities, high CO_2 contents and homogenization temperatures averaging 290°C. Quartz, arsenopyrite and pyrite were deposited during this stage. Stage II fluid is characterized by slightly higher salinities, moderate CO_2 contents and homogenization temperatures averaging 260°C. Quartz, sphalerite, galena and gold were deposited from the Stage II fluid. Gold precipitation was restricted to wider parts of the vein where Stage II fluid was in direct contact with earlier deposited arsenopyrite and pyrite. Stable isotope analysis of vein quartz indicates the mineralizing fluid was of meteoric-hydrothermal origin, and was highly enriched in ^{18}O.

B. Environment of Ore Deposition

The exact depth of formation of the Venus vein is not known, but Roots (1982) concluded that the Venus vein was preserved from erosion by subsidence of the Montana Mountain complex, and that the part of the vein exposed today must have been emplaced at depths lower than the present day erosion level. He suggests that a large amount of erosion has taken place (greater than 1000 m). The age of the vein is not known, but would be useful in estimating the amount of erosion.

Textures exhibited by the Venus vein lack the delicate crustiform banding, chalcedonic quartz, and banded botryoidal quartz typical of epithermal environments (Bodnar *et al.*, 1985). The massive, crudely banded nature of the vein resembles textures described by Lindgren (1933) for mesothermal type gold deposits. Bodnar *et al.* (1985) described microscopic textures found in deeper, hotter hydrothermal environments which resemble features seen in the Venus vein. These include the presence of numerous, wispy, shear zones outlined by secondary, small fluid inclusions and the absence of growth zones in quartz.

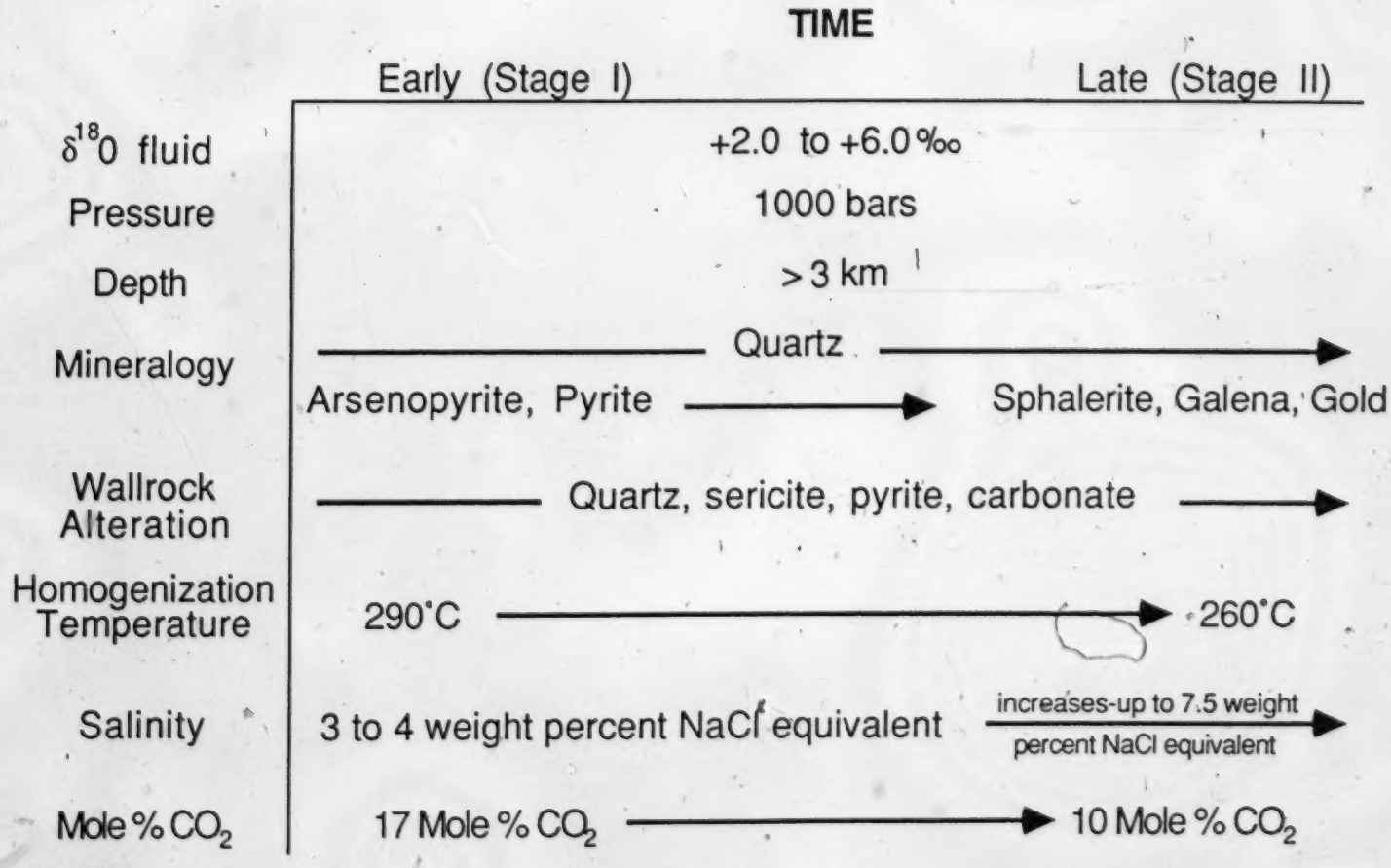

Figure 15. Changes in fluid chemistry and mineralogy with time at the Venus deposit.

Fluid inclusions in Venus vein quartz commonly contain CO_2 and three visible phases (Type 2a inclusions) at room temperature. Visible CO_2 is not found in fluid inclusions trapped under low temperature and pressure conditions (Bodnar *et al.*, 1985). Pressure estimates for the Venus system indicate the deposit formed at depths of at least 3 km. The pressures and depths indicated by the fluid inclusion study are inconsistent with an epithermal, shallow-seated model (Bodnar *et al.*, 1985). A deeper model correlates with interpretation of the $\delta^{18}O$ values for the Venus ore fluid. A deep, hot environment would be conducive to extensive water-rock exchange and subsequent ^{18}O enrichment of the ore fluid.

C. Controls on Ore Shoot Formation

Location of Ore Shoots

Although there is no reliable method of visually distinguishing ore shoots within the vein structure from low grade parts of the vein, two general observations on ore shoot character were noted during fieldwork. One was that ore shoots tend to occur in wider parts of the vein, relative to the average vein width for that particular elevation. The second observation was that ore shoots generally consist of quartz, arsenopyrite, pyrite, sphalerite and galena. This is in contrast to the more common Venus vein filling of quartz, arsenopyrite and pyrite.

The location of ore shoots along the vein structure is dependent on availability of open space for passage of Stage II fluid. The walls of the Venus vein, like most other veins formed at depth, are not smooth, but have an undulatory nature. Stage I quartz-arsenopyrite-pyrite deposition would seal narrower parts of the vein. Slickensides and clay gouge indicate that movement along the vein has taken place. The timing and amount of movement along the vein is uncertain. If fault movement occurred during deposition of Stage I and Stage II minerals, narrow parts of the vein previously filled by quartz, arsenopyrite and pyrite would be reopened. Variation in strike and dip of the curved fault surfaces of the vein could generate an increase in the width of the vein. The type of opening could be a function

of the type of fault movement; for instance, open space would develop in the steeply dipping parts of a normal fault, and in the shallow dipping parts of a reverse fault. Structural controls on ore shoot formation and the effect of fault movement are discussed in detail by Newhouse (1942). Mine geologists at Venus (Carlyle *pers. comm.*, 1984) have noted this type of situation on the 2850 ft. level of the mine. On this level, ore shoots were found in the shallower dipping parts of the vein. Statistical analysis of the relationship between gold grades, strike, dip, and vein width should better define the relationship between ore shoots and vein structure. If fault movement was not a factor in generating open space, then ore shoots simply developed in wider parts of the vein that had not completely infilled after deposition of Stage I mineral phases.

Gold Precipitation

Assay data shows that gold distribution in ore shoots is not consistent. Although the structure in a given portion of the vein may be favorable for ore shoot location, the actual precipitation of gold is dependent on two processes:

1. Prior deposition of arsenopyrite and pyrite.
2. Infiltration or replacement of arsenopyrite and pyrite by Stage II sphalerite and galena.

Even though gold and galena are paragenetically related in Stage II, massive quartz-sphalerite-galena parts of the vein are depleted in gold relative to quartz-arsenopyrite-pyrite parts of the vein that have been infiltrated by Stage II fluids. This may be a function of how gold is transported, and the physical-chemical conditions associated with gold precipitation. The transport and deposition of gold in hydrothermal systems was summarized by Seward (1984). Gold precipitation can be triggered by changes in fluid temperature, pressure, oxidation potential, pH and fluid composition. The fluid composition, temperature and pressure in the Venus hydrothermal ore fluid have been determined by fluid inclusion studies, and the relationship of gold to other mineral phases has been determined from petrographic studies. The following observations may help define the method of transport of gold in the system:

1. Salinity may have increased (up to 7.5 weight percent NaCl equivalent) in Stage II fluids relative to Stage I fluids.
2. The hydrothermal fluid contains a significant amount of base metals.
3. Gold precipitation occurred later than or contemporaneously with late stage base metals.
4. Precipitation of sphalerite, galena and gold are linked to a cooling hydrothermal ore fluid that may have effervesced, although the exact timing of the effervescence in relation to gold precipitation is not known.

Stage I mineral deposition at Venus involved precipitation of arsenopyrite and pyrite, which removed a large amount of aqueous sulphide from the fluid. Fluid inclusion analysis of Stage II inclusions at Venus has shown evidence of H_2O-CO_2 immiscibility, at least in some parts of the vein. The loss of CO_2 causes the pH of the system to increase. Base metal chloride complexes break down, and precipitation of sphalerite and then galena further decreases the availability of reduced sulphur in the system. As a result of the decrease in activity of aqueous sulphide in the fluid due to loss of H_2S, and precipitation of sulphides, $Au(HS)_2^-$ complexes are destroyed and gold precipitates. Reed and Spycher (1985) discuss the above model in relation to epithermal deposits, and state that an aqueous sulphide deficiency is more likely to prevail in a base metal rich fluid.

The above model explains the late stage association of gold with base metal sulphides seen in many lode gold deposits (Schwartz, 1944). The possible role of As complexes in the Venus system is not known.

Kay and Strong (1984) suggest that in the Moretons Harbor arsenopyrite-gold vein system, gold is transported as a chloride complex and precipitates as a result of decreasing temperature and instability of gold-chloride complexes as a result of effervescence. A similiar mechanism is proposed for the Lass Ag-Pb-Zn vein system in B.C. (Godwin *et al.*, 1986). The gold in both of these systems is assumed to have been deposited early; based on element zonation studies. Venus shows a similiar zonation, with a strong Au-As correlation, and a weak Au-Pb correlation, yet a detailed petrographic study showed that the gold is among the last minerals to be deposited, instead of the first.

Site controls on Gold Precipitation

Although gold precipitates from Stage II fluid, it does not precipitate in massive sphalerite-galena parts of the vein, or in barren quartz parts of the vein. There must be a mechanism operating by which gold is preferentially precipitated from Stage II fluid when the fluid is in contact with arsenopyrite and pyrite. Colvine *et al.* (1984) noted that in Archean gold deposits, the breakdown of $Au(HS)_2^-$ complexes due to changes in the physical-chemical nature of the ore fluid did not account for the common spatial association of gold with earlier deposited sulphides. They suggest that electrochemical interaction between charged pyrite grain surfaces and the hydrothermal ore fluid induces gold to preferentially precipitate in sulphide fractures and on pyrite grain surfaces. Electrochemical interaction between sulphides and ore fluid has been studied experimentally by Jean and Bancroft (1985); Sakharov and Lobacheva (1978) and Mironov *et al.* (1981). Pyrite acts as a semi-conductor with variable conductive properties (Smith, 1942), and is favored as a depositional site compared to other sulphides. Arsenopyrite is also a favorable host for infiltration of Stage II fluid because of its brittleness and susceptibility to microfracturing. It is possible that in the Venus vein system, prior deposition of arsenopyrite and pyrite set up a microgalvanic system.

Heinrich and Eadington (1986) discuss the behavior of As complexes in hydrothermal solutions at high temperature and pressure. They suggest that in arsenopyrite-pyrite-quartz deposits where the gold is associated with later base metal sulphides, minor dissolution of arsenopyrite could act as an oxidation-reduction trap for later gold precipitation, a process which could have occurred at Venus.

D. Model for Ore Deposition

The available data on the Venus vein deposit are compatible with a model involving two stages of ore paragenesis, according to the following sequence of events:

1. Late Cretaceous, calc-alkaline magmas intrude Mesozoic rocks of the Whitehorse Trough and Paleozoic Atlin Terrane metabasalts. Extrusions of the calc-alkaline magma build a volcano that reaches a height of over 1 km before partial collapse opens subsidence faults

in the volcanic complex (Roots, 1982). The magma becomes more granitic and intrudes the pre-existing volcanic pile at 63.4 Ma (Morrison *et al.*, 1979). Arching of the volcanic pile opens fissures in the complex into which felsic dykes intrude.

2. Hot hydrothermal fluids move through fault fissures in the volcanic complex. The fluid has an average $\delta^{18}O$ value of +4.3‰ and a δD value of -159‰, which indicates it is of meteoric hydrothermal origin. The enrichment of $\delta^{18}O$ in the system is probably a function of extensive water-rock interaction at high temperatures and pressures. Pressure estimates from fluid inclusion analysis indicate a depth of formation of 3 km assuming lithostatic pressures and 10 km assuming hydrostatic pressures. The initial Stage I fluid is characterized by homogenization temperatures averaging 290°C, low salinities (3 to 4 weight percent NaCl equivalent), and an average CO_2 content of 17 mole percent. Quartz, arsenopyrite and pyrite precipitate during Stage I (Figure 16). The andesitic to felsic wallrocks alter to a quartz-sericite-pyrite-carbonate assemblage.
3. Syndepositional movement along the vein in response to structural adjustments occurs during vein development. A layer of fault gouge forms between the vein and the wallrock.
4. The hydrothermal ore fluid cools with time. Stage II fluid is characterized by lower homogenization temperatures (averaging 260°C), and less CO_2 (average 10 mole percent) relative to Stage I. Salinity estimates (uncorrected for CO_2) calculated from TmIce in residual liquid-vapor inclusions indicate the Stage II fluid has higher salinities (up to 7.5 weight percent NaCl equivalent) relative to Stage I. Prior deposition of arsenopyrite and pyrite has removed aqueous sulphide from the system. Base metals carried by chloride complexes break down in response to decreasing temperature and sporadic phase separation. Precipitation of base metals is restricted to those parts of the vein wide enough to allow passage of Stage II fluid. Phase separation and subsequent loss of H_2S into the vapor phase reduces the availability of aqueous sulphide. Continued precipitation of sphalerite and galena in available open space also reduces availability of aqueous sulphide. The mineralizing fluid is now sulphide deficient and $Au(HS)_2$ complexes begin to break down.

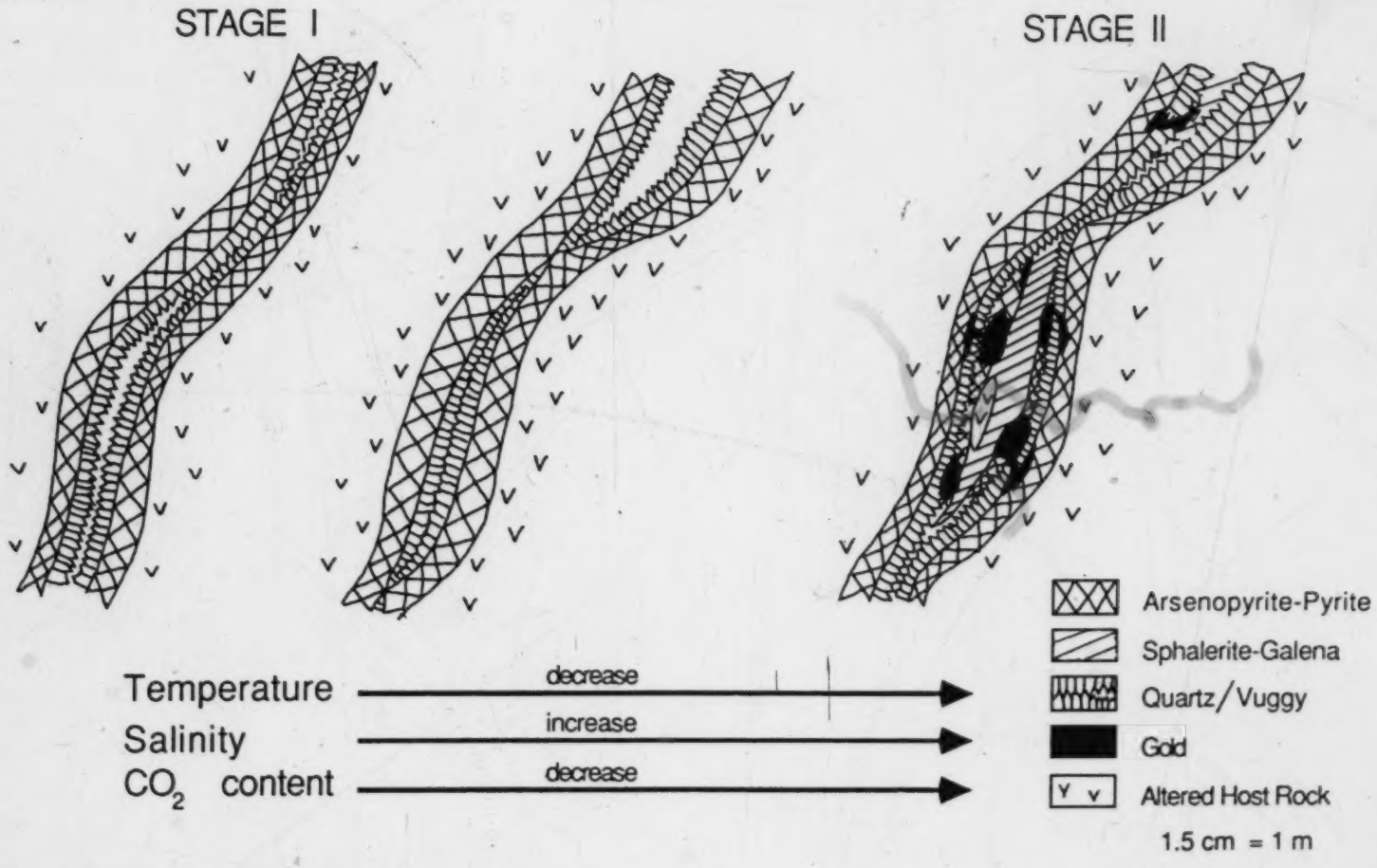

Figure 16. Idealized model of ore shoot formation.

5. Gold precipitation with late stage galena or tetrahedrite is enhanced when the sulphide deficient fluid is in contact with earlier deposited arsenopyrite and pyrite. Arsenopyrite is a favorable host for infiltration of Stage II fluid due to its abundance and brittleness. Microgalvanic systems set up by the electrochemical interaction of sulphide grain surfaces with the ore fluid, and oxidation-reduction reactions near arsenopyrite grain surfaces, may help induce gold precipitation. Gold enrichment occurs where there has been extensive interaction between Stage I and Stage II phases. Separate arsenoyrite-pyrite and sphalerite-galena parts of the vein will not be as enriched in gold compared to parts of the vein that contain all four sulphide phases.
6. During or after gold precipitation, clay alteration zones develop and late stage carbonate veinlets infiltrate into the wallrock. The vein is preserved from erosion by down dropping of the volcanic host block. Supergene weathering oxidizes upper vein workings. Low $\delta^{18}O$ values of chalcedony veins in the volcanic complex indicate the presence of a separate low $\delta^{18}O$ fluid.

E. Regional Considerations

The Venus vein exhibits a well defined paragenetic sequence of arsenopyrite, followed by pyrite, sphalerite, galena and gold. The Uranus vein and South Aurora veins, also hosted in the Montana Mountain volcanic complex, contain arsenopyrite and pyrite. Silver rich veins such as the Ruby Silver and Joe Petty are generally situated at higher elevations. Fluid inclusion and stable isotope analyses in this study indicate that all the veins sampled in the Montana Mountain area were deposited from a single ^{18}O enriched ore fluid. The varying mineralogy and Au:Ag ratios of precious metal veins on Montana Mountain may reflect a change from deep seated, high temperature, arsenopyrite-pyrite-quartz veins to a cooler base metal rich zone (Stage I and Stage II at Venus) and finally to silver rich veins.

Documentation of the late stage association of gold and galena is not new. Recent studies on Archean gold deposits describe the affinity of gold for earlier deposited sulphides (Colvine, *et al.*, 1984). The same galena-gold association was noted by Schwartz (1944) but

was previously unrecognized at Venus. The galena-gold relationship at Venus is masked by the action of pre-existing arsenopyrite and pyrite acting as site controls for later gold-galena precipitation. Gasparrini (1983) notes that there is a tendency to among geologists to assume that gold is genetically associated with arsenopyrite in solid solution when dealing with quartz-arsenopyrite-pyrite veins. This is true in some gold deposits, but recognition of a late galena-gold association is particularly important when planning extraction processes for the ore, because ores containing galena with refractory arsenopyrite and pyrite are especially difficult to work with (Gasparrini, 1983).

In a review of 115 deposits containing native gold, Schwartz (1944) found that gold most frequently occurs with pyrite, arsenopyrite and galena. He suggests that, in many deposits, galena is not abundant, but forms at about the same time as gold and may be a good indicator mineral. The association between gold and base metal sulphides appears to be ubiqitous in Cordilleran mesothermal gold deposits (Nesbitt *et al.*, 1986). Examples of such occur at the Cassiar, Cariboo, and Bralorne-Pioneer Mine, where gold and late base metals fill fractures in earlier deposited sulphides (Nesbitt *pers. comm.*, 1986).

There are numerous quartz-arsenopyrite-pyrite-base metal sulphide veins in southwestern Yukon and northwestern British Columbia (Schroeter, 1986). Gold enrichment is predicted in these veins where later base metal sulphides crosscut or infiltrate earlier deposited arsenopyrite and pyrite.

References

Angus, S., Armstrong, B., de Reuck, K.M., Altunin, V.V., Gadetskii, O.G., Chapela,G.A. and Rowlinson, J.S., 1976, International thermodynamic tables of the fluid state, volume 3, Carbon dioxide: New York, Pergamon Press, 385 pp.

Bethke, P.M. and Rye, R.O., 1979, Environment of ore deposition in the Creede mining district, San Juan Mountains, Colorado-Part IV, Source of fluids from oxygen, hydrogen, and carbon isotope studies: Economic Geology, v. 74, p. 1832-1851.

Bodnar, R.J., 1983, A method of calculating fluid inclusion volumes based on vapor bubble diameters and P-V-T-X properties of inclusion fluids: Economic Geology, v. 78, p. 535-542.

Bodnar, R.J., Reynolds, T.J. and Kuehn, C.A., 1985, Fluid inclusion systematics in epithermal systems *in* Geology and geochemistry of epithermal systems, Berger, B.R. and Bethke, P.M. (eds.), Society of Economic Geologists, Reviews in Economic Geology, v. 2, Published by the Economic Geology Publishing Company, El Paso, Texas, p. 73-97.

Bostock, H.S., 1936, Carmacks District, Yukon: Geological Survey of Canada Memoir 189, 67 pp.

Bostock, H.S. and Lees, E.J., 1938, Laberge Map-area, Yukon: Geological Survey of Canada Memoir 217, 32 pp.

Bowers, T.S. and Helgeson, H.C., 1983a, Calculation of the thermodynamic and geochemical consequences of nonideal mixing in the system H_2O-CO_2-NaCl on phase relations in geologic systems. Equation of state for H_2O-CO_2-NaCl fluids at high pressures and temperatures: Geochimica et Cosmochimica Acta, v. 47, p. 1247-1275.

Bowers, T.S. and Helgeson, H.C., 1983b, Calculation of the thermodynamic and geochemical consequences of nonideal mixing in the system H_2O-CO_2-NaCl on phase relations in geologic systems: metamorphic equilibria at high pressures and temperatures: American Mineralogist, v. 68, p. 1059-1075.

Bowman, J.R. and Covent, J., 1983, Hydrogen, carbon and oxygen isotope studies of the CanTung scheelite skarn, Tungsten, N.W.T., Canada: Program with Abstracts, Geological Association of Canada and Mineralogical Association of Canada, v. 8, p. A7.

Bozzo, A.T., Chen, H-S, Kass, J.R. and Barduhn, A.J., 1975, The properties of the hydrates of chlorine and carbon dioxide: Desalination, v. 16, p. 303-320.

Burruss, R.C., 1981, Analysis of phase equilibria in C-O-H-S fluid inclusions *in* Fluid inclusions: Applications to petrology, Hollister, L.S. and Crawford, M.L. (eds.), Mineralogical Association of Canada, Short Course Handbook, v. 6, Calgary, p. 39-74.

Cairnes, D.D., 1907, Exploration in a portion of the Yukon south of Whitehorse: Geological Survey of Canada, Summary Report for 1906, p. 22-30.

Cairnes, D.D., 1908, Reports on a portion of the Conrad and Whitehorse mining districts, Yukon: Geological Survey of Canada, Department of Mines, Publication 982, p 14-18.

Cairnes, D.D., 1912, Wheaton District, Yukon Territory: Geological Survey of Canada

Memoir 31,

Cairnes, D.D., 1917, Lode mining in the Windy Arm portion, Conrad mining district, Southern Yukon: Geological Survey of Canada, Summary Report for 1916, p. 34-44.

Carlyle, L., 1984, Private company report.

Casadevall, T. and Ohmoto, H., 1977, Sunnyside mine, Eureka mining district, San Juan County, Colorado-Geochemistry of gold and base-metal ore deposition in a volcanic environment: Economic Geology, v. 72, p. 1285-1320.

Clayton, R.N. and Mayeda, T.K., 1963, The use of bromine pentafluoride in the extraction of oxygen from oxides and silicates for isotopic analysis: Geochimica et Cosmochimica Acta, v. 27, p. 43-52.

Cockfield, W.E. and Bell, A.H., 1926, Whitehorse District, Yukon: Geological Survey of Canada Memoir 150, 63 pp.

Collins, P.L.F., 1979, Gas hydrates in CO_2-bearing fluid inclusions and the use of freezing data for estimation of salinity: Economic Geology, v. 74, p. 1435-1444.

Colvine, A.C., Andrews, A.J., Cherry, M.E., Durocher, M.E., Fyon, A.J., Lavigne, M.J., Jr., Macdonald, A.J., Marmont, S., Poulsen, K.H., Springer, J.S. and Troop, D.G., 1984, An integrated model for the origin of the Archean lode gold deposits: Ontario Geological Survey, Open-File Report 5524, 99 pp.

Craig, H., 1961, Standard for reporting concentrations of deuterium and oxygen-18 in natural waters: Science, v. 133, p. 1833-1834.

Crawford, M.L., 1981, Phase equilibria in aqueous fluid inclusions *in* Fluid inclusions: Applications to petrology, Hollister, L.S. and Crawford, M.L. (eds.), Mineralogical Association of Canada, Short Course Handbook, v. 6, Calgary, p. 75-100.

Criss, R.E. and Taylor, H.P., Jr., 1986, Meteoric-hydrothermal systems *in* Stable isotopes in high temperature geological processes, Valley, J.W., Taylor, H.P., Jr. and O'Neil, J.R. (eds.): Mineralogical Society of America, Reviews in Mineralogy, v. 16, p. 373-424.

Dagenais, G.R., 1984, The oxygen isotope geochemistry of granitoid rocks from the southern and central Yukon: Unpublished M.Sc. thesis, University of Alberta, 168 pp.

Drummond, S.E. and Ohmoto, H., 1985, Chemical evolution and mineral deposition in boiling hydrothermal systems: Economic Geology, v. 80, p. 126-147.

Ellis, A.J. and Golding, R.M., 1963, The solubility of carbon dioxide above 100°C in water and in sodium chloride solutions: American Journal of Science, v. 261, p. 47-60.

Field, C.W. and Fifarek, R.H., 1985, Light stable isotope systematics in the epithermal environment *in* Geology and geochemistry of epithermal systems, Berger, B.R. and Bethke, P.M. (eds.), Society of Economic Geologists, Reviews in Economic Geology, v. 2, Published by the Economic Geology Publishing Company, El Paso, Texas, p. 99-128.

Findlay, D.C., 1967, The mineral industry of Yukon Territory and southwestern District of MacKenzie, 1966: Geological Survey of Canada, Paper 67-40, p. 46-50.

Findlay, D.C., 1969a, The mineral industry of Yukon Territory and southwestern District of MacKenzie: Geological Survey of Canada Paper 68-68, p. 62-64.

Findlay, D.C., 1969b, The mineral industry of Yukon Territory and southwestern District of MacKenzie: Geological Survey of Canada Paper 69-55, p. 37-38.

Fournier, R.O., 1985, The behavior of silica in hydrothermal solutions *in* Geology and geochemistry of epithermal systems, Berger, B.R. and Bethke, P.M. (eds.), Society of Economic Geologists, Reviews in Economic Geology, v. 2, Published by the Economic Geology Publishing Company, El Paso, Texas, p. 45-61.

Gasparrini, C., 1983, The mineralogy of gold and its significance in metal extraction: Canadian Institute of Mining and Metallurgy Bulletin, v. 76, n. 851, p. 144-151.

Godwin, C.I., Watson, P.H. and Shen, K., 1986, Genesis of the Lass vein system, Beaverdell silver camp, south-central British Columbia: Canadian Journal of Earth Sciences, v. 23, p. 1615-1626.

Grond, H.C., Churchill, S.J., Armstrong, R.L., Harakal, J.E. and Nixon, G.T., 1984, Late Cretaceous age of the Hutshi, Mount Nansen, and Carmacks groups, southwestern Yukon Territory and northwestern British Columbia: Canadian Journal of Earth Sciences, v. 21, p. 554-558.

Hedenquist, J.W. and Henley, R.W., 1985, The importance of CO_2 on freezing point measurements of fluid inclusions: Evidence from active geothermal systems and implications for epithermal ore deposition: Economic Geology, v. 80, p. 1379-1406.

Heinrich, C.A. and Eadington, P.J., 1986, Thermodynamic predictions of the hydrothermal chemistry of arsenic, and their significance for the paragenetic sequence of some cassiterite-arsenopyrite-base metal sulfide deposits: Economic Geology, v. 81, p. 511-529.

Higgins, N.C. and Kerrich, R., 1982, Progressive ^{18}O depletion during CO_2 separation from a carbon dioxide rich hydrothermal fluid: Evidence from the Grey River tungsten deposit, Newfoundland: Canadian Journal of Earth Sciences, v. 19, p. 2247-2257.

Jean, G.E. and Bancroft, G.M., 1985, An XPS and SEM study of gold deposition at low temperatures on sulphide mineral surfaces: Concentration of gold by adsorption/reduction: Geochimica et Cosmochimica Acta, v. 49, p. 979-987.

Kamilli, R.J. and Ohmoto, H., 1977, Paragenesis, zoning, fluid inclusion and isotopic studies of the Finlandia Vein, Colqui District, Central Peru: Economic Geology, v. 72, p. 950-982.

Kay, A. and Strong, D.F., 1983, Geologic and fluid controls on As-Sb-Au mineralization in the Moretons Harbour area, Newfoundland: Economic Geology, v. 78, p. 1590-1604.

Kerrich, R. and Fyfe, W.S., 1981, The gold-carbonate association: Source of CO_2 and CO_2 fixation reactions in Archean lode deposits: Chemical Geology, v. 33, p. 265-294.

Lambert, M.B., 1974, The Bennett Lake cauldron subsidence complex, British Columbia and Yukon Territory: Geological Survey of Canada Bulletin 227, 213 pp.

Lindgren, W.L., 1933, Mineral Deposits, McGraw-Hill Book Company, Inc., New York, New York, 930 pp.

MacDonald, A.J., 1967, Private company report.

MacDonald, C.H., 1971, Private company report.

MacLean, T.A., 1914, Windy Arm district: Lode mining in Yukon: an investigation of quartz deposits in the Klondike division: Canadian Mines Branch Publication 222, p. 188-200.

Magaritz, M. and Taylor, H.P., Jr., 1976, Isotopic evidence for meteoric-hydrothermal alteration of plutonic igneous rocks in the Yakutat Bay and Skagway areas, Alaska: Earth and Planetary Science Letters, v. 30, p. 179-190.

Matsuhisa, Y., Goldsmith, J.R. and Clayton, R.N., 1979, Oxygen isotopic fractionation in the system quartz-albite-anorthite-water: Geochimica et Cosmochimica Acta, v. 43, p. 1131-1140.

Matsuhisa, Y., Morishita, Y. and Sato, T., 1985, Oxygen and carbon isotope variations in gold-bearing hydrothermal veins in the Kushikino mining area, southern Kyushu, Japan: Economic Geology, v. 80, p. 283-293.

McConnell, R.G., 1906, Windy Arm district, northwestern B.C.: Geological Survey of Canada, Summary Report for 1905, p. 30-32.

McDonald, B.W.R., Stewart, E.B. and Godwin, C.I., 1986, Geology of the Mount Skukum Tertiary epithermal gold-silver vein deposits, southwestern Yukon Territory: Program with Abstracts, GeoExpo/86-Exploration in the North American Cordillera, p. 57.

Mironov, A.G., Zhmodik, S.M. and Maksimova, E.A., 1981, An experimental investigation of the sorption of gold by pyrites with different thermoelectric properties: Geochemistry International, v. 18, n. 2, p. 153-160.

Monger, J.W.H., 1975, Upper Paleozoic rocks of the Atlin Terrane, northwestern B.C. and south-central Yukon: Geological Survey of Canada Paper 74-47, 63 pp.

Monger, J.W.H., Price, R.A. and Tempelman-Kluit, D.J., 1982, Tectonic accretion and the origin of the two major metamorphic and plutonic welts in the Canadian Cordillera: Geology, v. 10, p. 70-75.

Morin, J.A., 1981, Element distribution in Yukon gold-silver deposits *in* Yukon Geology and Exploration 1979-1980; Geology Section, Department of Indian and Northern Affairs, Whitehorse, p. 68-84.

Morin, J.A. and Downing, D.A., 1984, Gold-Silver Deposits and Occurrences in Yukon: Exploration and Geological Services Division, Yukon, Indian and Northern Affairs Canada Open File, 22 pp.

Morrison, G.W., Godwin, C.I. and Armstrong, R.L., 1979, Interpretation of isotopic ages and $^{87}Sr/^{86}Sr$ initial ratios for plutonic rocks in the Whitehorse map area, Yukon: Canadian Journal of Earth Sciences, v. 16, p. 1988-1997.

Nesbitt, B.E., Murowchick, J.B. and Muehlenbachs, K., 1986, Dual origins of lode gold deposits in the Canadian Cordillera: Geology, v. 14, p. 506-509.

Newhouse, W.H. (ed.), 1942, Ore deposits as related to structural features: Princeton University Press, Princeton, New Jersey, 280 pp.

Nicholls, J. and Crawford, M.L., 1985, FORTRAN programs for calculation of fluid properties from microthermometric data on fluid inclusions: Computers Geoscience, v. 11, p. 619-645.

Ohmoto, H., 1986, Stable isotope geochemistry of ore deposits *in* Stable isotopes in high temperature geological processes, Valley, J.W., Taylor, H.P., Jr. and O'Neil, J.R. (eds.): Mineralogical Society of America, Reviews in Mineralogy, v. 16, p. 491-559.

Panteleyev, A, 1986, Ore deposits, #10. A Canadian cordilleran model for epithermal gold-silver deposits: Geoscience Canada, v. 13, n. 2, p. 101-111.

Parry, W.T., 1986, Estimation of $X(CO_2)$, P, and fluid inclusion volume from fluid inclusion temperature measurements in the system $NaCl-CO_2-H_2O$: Economic Geology, v. 81, p. 1009-1013.

Potter, R.W., II, Clynne, M.A. and Brown, D.L., 1978, Freezing point depression of aqueous sodium chloride solutions: Economic Geology, v. 73, p. 284-285.

Pride, M.J., 1983, Interlayered sedimentary-volcanic sequence of the Mt. Skukum volcanic complex *in* Yukon exploration and geology 1983, Geology Section, Department of Indian and Northern Affairs, Whitehorse, p. 94-104.

Pride, M.J. and Clark, G.S., 1985, An Eocene Rb-Sr isochron for rhyolite plugs, Skukum area, Yukon Territory: Canadian Journal of Earth Sciences, v. 22, p. 1747-1753.

Prince, D.R., 1984a, Private company report.

Prince, D.R., 1984b, Private company report.

Ralfs, K., 1975, A study of the mineralogy, paragenesis, zoning and wallrock alteration, Venus vein, Montana Mountain, S.W. Yukon: Unpublished B.Sc. thesis, University of British Columbia, 48 pp.

Reed, M.H. and Spycher, N., 1985, Boiling, cooling and oxidation in epithermal systems: a numerical modeling approach *in* Geology and geochemistry of epithermal systems, Berger, B.R. and Bethke, P.M. (eds.), Society of Economic Geologists, Reviews in Economic Geology, v. 2, Published by the Economic Geology Publishing Company, El Paso, Texas, p. 249-272.

Robinson, R.W. and Norman, D.I., 1984, Mineralogy and fluid inclusion study of the Southern Amethyst vein system, Creede Mining District, Colorado: Economic Geology, v. 79, p. 439-447.

Roedder, E., 1984, Fluid inclusions: Mineralogical Society of America, Reviews in Mineralogy, v. 12, 644 pp.

Roedder, E. and Bodnar, R.J., 1980, Geologic pressure determinations from fluid inclusion studies: Annual Review of Earth and Planetary Sciences, v. 8, p. 263-301.

Roots, C.F., 1981, Geological setting of gold-silver veins on Montana Mountain *in* Yukon Geology and Exploration 1979-1980; Geology Section, Department of Indian and Northern Affairs, Whitehorse., p. 116-122.

Roots, C.F., 1982, Geology of the Montana Mountain area, Yukon: Unpublished M.Sc. thesis, Carleton University, 127 pp.

Rye, R.O. and Sawkins, F.J., 1974, Fluid inclusion and stable isotope studies on the Casapalca Ag-Pb-Zn-Cu deposit, Central Andes, Peru: Economic Geology, v. 69, p. 181-205.

Sakharova, M.S. and Lobacheva, I.K., 1978, Microgalvanic systems involving sulfides and gold-bearing solutions, and characteristics of gold deposition: Geochemistry International, v. 15, n. 6, p. 152-157.

Schroeter, T.G., 1986, Bennett Project (104M): British Columbia Ministry of Energy, Mines and Petroleum Resources, Geological Fieldwork, 1985, Paper 1986-1., p. 185-189.

Schroeter, T.G., 1987, Brief studies of selected gold deposits in southern British Columbia: British Columbia Ministry of Energy, Mines and Resources, Geological Fieldwork, 1986, Paper 1987-1, p. 15-22.

Schwartz, G.M., 1944, The host minerals of native gold: Economic Geology, v. 39, p. 371-411.

Scott, J.D., 1974, Private company report.

Seward, T.M., 1984, The transport and deposition of gold in hydrothermal systems *in* The geology, geochemistry and genesis of gold deposits, Foster, R.P. (ed.), Gold '82, Geological Society of Zimbabwe, Special Publication No. 1., p. 165-181.

Shelton, K.L., 1986, Geochemical and stable isotope evidence of progressive meteoric water interaction in vein-type gold-silver deposits, Republic of Korea: Program with Abstracts, Geological Association of Canada and Mineralogical Association of Canada, v. 11, p. 127.

Shepherd, T.J., Rankin, A.H. and Alderton, D.H.M., 1985, A practical guide to fluid inclusion studies: Chapman and Hall in association with Methuen, Inc., New York, 239 pp.

Sheppard, S.M.F., 1986, Characterization and isotopic variations in natural waters *in* Stable isotopes in high temperature geological processes, Valley, J.W., Taylor, H.P., Jr. and O'Neil, J.R. (eds.): Mineralogical Society of America, Reviews in Mineralogy, v. 16, p. 165-183.

Smith, F.G., 1942, Variation in the properties of pyrite: American Mineralogist, v. 27, p. 1-19.

Takenouchi, S. and Kennedy, G.C., 1964, The binary system H_2O-CO_2 at high temperatures and pressures: American Journal of Science, v. 262, p. 1055-1074.

Taylor, H.P., Jr., 1974, The application of oxygen and hydrogen isotope studies to problems of hydrothermal alteration and ore deposition: Economic Geology, v. 69, p. 843-883.

Taylor, H.P., Jr., 1979, Oxygen and hydrogen isotope relationships in hydrothermal mineral deposits *in* Geochemistry of hydrothermal ore deposits, second edition, Barnes, H.L. (ed.), John Wiley and Sons, Inc., New York, p. 236-277.

Tempelman-Kluit, D.J., 1978, Reconnaissance geology, Laberge map-area, Yukon: Geological Survey of Canada Paper 78-1A, p. 61-66.

Tempelman-Kluit, D.J., 1979, Transported cataclasite, ophiolite and granodiorite in Yukon: evidence of arc-continent collision: Geological Survey of Canada Paper 79-14, 27 pp.

Tempelman-Kluit, D.J., 1980, Highlights of field work in the Laberge and Carmacks map-areas, Yukon: Geological Survey of Canada Paper 80-1A, p. 357-362.

Walton, L., 1984, Private company report.

Watson, K.W., 1979, Private company report.

Wheeler, J.O., 1961, Whitehorse map-area, Yukon Territory: Geological Survey of Canada Memoir 312, 156 pp.

Wood, P.C., Burrows, D.R., Thomas, A.V. and Spooner, E.T.C., 1986, The Hollinger-McIntyre Au-Quartz vein system, Timmins, Ontario, Canada; geologic characteristics, fluid properties and light stable isotope geochemistry *in* Gold '86, Toronto, p. 56-80.

Zhang, X., 1986, Fluid inclusion and stable isotope studies of the gold deposits in Okanagan Valley, British Columbia: Unpublished M.Sc. thesis, University of Alberta, 101 pp.

	Elevation (ft.)	Structure	Mineralogy, Texture	Host Rock
Uranus Vein	4600	Vein strikes north and dips 30° to 40° W. Traced for 400 m. Vein width up to 1 m.	Resembles Venus vein. Crudely banded quartz, arsenopyrite, pyrite and minor galena. Also get scorodite, limonite and Mn coating.	Silicified volcanic flow rocks and breccias. Weathers brown, rust and creme. Minor vesicules.
Ruby Silver	4250	Vein strikes north and dips 35° to 40° W. Up to 50 cm width. 15 cm strike length.	White to greyish quartz with disseminated galena and unidentified sulphides.	Rhyolite and intermediate volcanic flow rock
Joe Petty	5500	Vein strikes E-W and dips 60° N, Strike length of 200 m. Up to 30 cm wide.	White to grey quartz with disseminated sulphides, including tetrahedrite and galena.	Intermediate volcanic flow rocks and breccias.
Aurora	5600	Vein strikes approximately NE-SW and dips 80° N. Up to 15 cm wide	Quartz and calcite with minor arsenopyrite, galena, tetrahedrite, malachite and azurite. Banded in places. South Aurora vein resembles Venus.	Intermediate volcanic flow rocks and breccias
Arctic	5700	Vein strikes NE-SW and dips 30° NW into the hill. Up to 4 m wide.	Quartz vein with arsenopyrite, pyrite, chalcopyrite and galena.	'Carcross' pluton-granite, granodiorite.
Peerless	5000	Small quartz veins	Bluish grey quartz with pyrite, and arsenopyrite in host rocks.	'Carcross' pluton-Granite.

LOCATION MAP (VENUS MINE)
Fluid Inclusion Samples

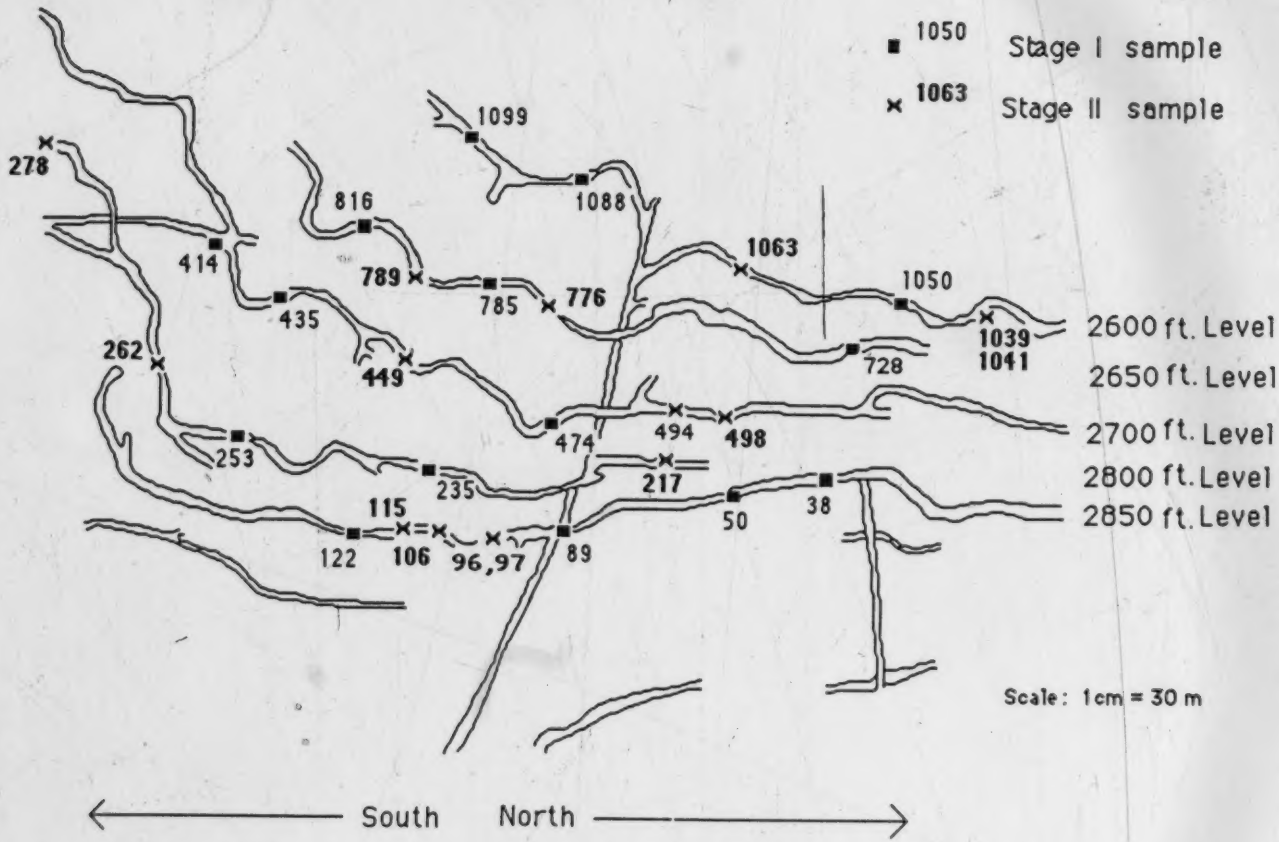

LOCATION MAP (VENUS MINE)
Stable Isotope Samples